AD-A130 914 PHASE-SLIP CENTERS AND THEIR INTERACTIONS(U) HARVARD UNIV CAMBRIDGE MA DIV OF APPLIED SCIENCES J M APONTE JUN 83 TR-21 N00014-77-C-0085 1/2

UNCLASSIFIED F/G 20/3 NL

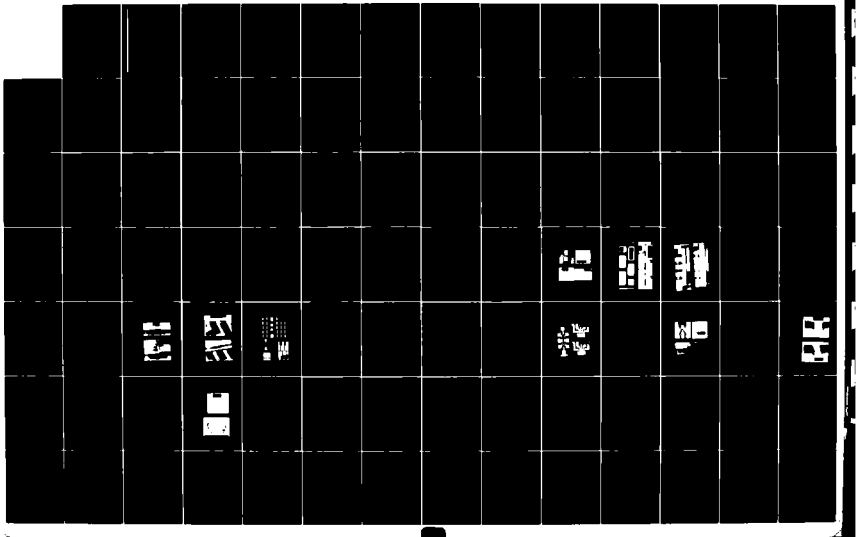

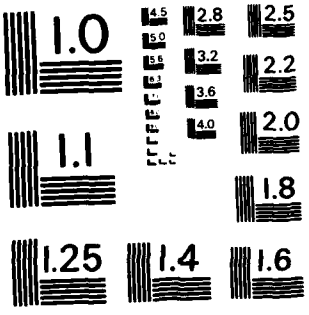

(12)

Office of Naval Research
Contract N00014-77-C-0005 NR-319-118
Contract N00014-75-C-0648 NR-372-012
National Science Foundation Grant DMR79-04155

PHASE-SLIP CENTERS AND THEIR INTERACTIONS

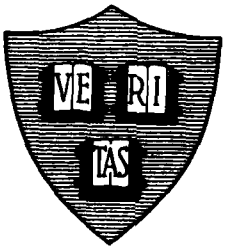

By

Juan M. Aponte

JUNE 1983

Technical Report No. 21

Division of Applied Sciences
Harvard University Cambridge, Massachusetts

Unclassified

SECURITY CLASSIFICATION OF THIS PAGE (When Data Entered)

REPORT DOCUMENTATION PAGE		READ INSTRUCTIONS BEFORE COMPLETING FORM
1. REPORT NUMBER Technical Report No. 21	2. GOVT ACCESSION NO. AD-A130 114	3. RECIPIENT'S CATALOG NUMBER
4. TITLE (and Subtitle) PHASE-SLIP CENTERS AND THEIR INTERACTIONS		5. TYPE OF REPORT & PERIOD COVERED Interim Report 6. PERFORMING ORG. REPORT NUMBER
7. AUTHOR(s) Juan M. Aponte		8. CONTRACT OR GRANT NUMBER(s) N00014-77-C-0085 N00014-75-C-0648 NSF DMR79-04155
9. PERFORMING ORGANIZATION NAME AND ADDRESS		10. PROGRAM ELEMENT, PROJECT, TASK AREA & WORK UNIT NUMBERS
11. CONTROLLING OFFICE NAME AND ADDRESS Division of Applied Sciences Harvard University Cambridge, Mass. 02138		12. REPORT DATE June 1983 13. NUMBER OF PAGES 123
14. MONITORING AGENCY NAME & ADDRESS(if different from Controlling Office)		15. SECURITY CLASS. (of this report) Unclassified 15a. DECLASSIFICATION/DOWNGRADING SCHEDULE

16. DISTRIBUTION STATEMENT (of this Report)

Reproduction in whole or in part is permitted for any purpose of the United States Government. Approved for public release; distribution unlimited.

17. DISTRIBUTION STATEMENT (of the abstract entered in Block 20, if different from Report)

18. SUPPLEMENTARY NOTES

19. KEY WORDS (Continue on reverse side if necessary and identify by block number)

Phase-slippage
Quasiparticle current
Diffusion length
Microwave radiation

20. ABSTRACT (Continue on reverse side if necessary and identify by block number)

We have performed a series of different experiments in order to measure the diffusion length Λ_{Q^*} of the quasiparticle charge generated in a phase-slip center (PSC) and to detect the oscillations of the supercurrent in the PSC. Three different types of samples were fabricated photolithographically: samples of type S, samples of type T and samples of type M..

In samples of type S, consisting of long tin microbridges (40μm × 1μm × 0.1μm) with four side probes, we measured the effects of the quasiparticle current generated in one PSC on the appearance of other PSCs in the same microbridge. The

DD FORM 1 JAN 73 1473 EDITION OF 1 NOV 65 IS OBSOLETE
S/N 0102-014-6601

Unclassified
SECURITY CLASSIFICATION OF THIS PAGE (When Data Entered)

20. Abstract continued

geometry of these samples was such that the nucleation of PSCs in different locations was controlled by applying current through the side probes to different segments of the microbridge. In that way the interaction effects could be measured as a function of the distance between the two interacting PSCs. We separated heating effects from diffusive current effects and we observed the exponential decay of the quasiparticle current with the distance from the PSC source. We found that the characteristic decay length corresponds to a relaxation time $\tau_{Q*} = (7 \pm 2) \times 10^{-10}$ sec at $T = 0.99T_c$. From the heating effect data we determined that the heat transfer coefficient is $\alpha = 1.5$ watt/K cm^2 for our samples on glass substrates and in direct contact with the liquid He bath.

In samples of type T, consisting of long tin microbridges (40μm × 1μm × 0.1μm) with four normal tunnel junction probes, we measured the quasiparticle potential. We found that this potential decays exponentially from the center of the PSC and that the characteristic decay length diverges tat the critical temperature T_c corresponding to a relaxation time $\tau_{Q*}(T) = (0.7 \pm 0.2) \times 10^{-10}$ sec $(1 - T/T_c)^{1/2}$. We also measured the nonequilibrium potential induced by a normal current injected through one of the probes and the effect of that normal current on the appearance of the first PSC in the microbridge. From those injection experiments we also obtained a value of Λ_{Q*}, which agrees with our previous results on the same samples. From the experimental magnitude of τ_{Q*} in samples of type S and of type T, we determined the inelastic phonon scattering time τ_E and found that close to T_c, $\tau_E = (1.6 \pm 0.4) \times 10^{-10}$ sec in tin.

Samples of type M consist of tin microbridges of various lengths. The effect of microwave radiation on the I-V curves of these samples was investigated. We observed Josephson steps in some of those samples, proving the presence of oscillations of the supercurrent in the core of the PSC. Unfortunately, we have not been able to identify a systematic explanation for the observability of steps in only a fraction of samples of similar dimensions. A quantitative analysis of the power dependence of the magnitude of the steps was impeded by the presence of other effects such as the Wyatt-Dayem effect and heating effects.

Office of Naval Research

Contract N00014-77-C-0085 NR-319-116
Contract N00014-75-C-0648 NR-372-012
National Science Foundation Grant DMR79-04155

PHASE-SLIP CENTERS AND THEIR INTERACTIONS

By

Juan M. Aponte

Technical Report No. 21

June 1983

The research reported in this document was made possible through support extended the Division of Applied Sciences, Harvard University, by the Office of Naval Research, under Contract N00014-77-C-0085, Contract N00014-75-C-0648 and by the National Science Foundation under Grant DMR79-04155.

Division of Applied Sciences

Harvard University · Cambridge, Massachusetts

TABLE OF CONTENTS

CHAPTER		PAGE
	TABLE OF CONTENTS	iii
	LIST OF FIGURES	v
	LIST OF TABLES	viii
I	INTRODUCTION	1
II	THEORIES AND EXPERIMENTS ON PHASE-SLIP CENTERS	
	II.1.Definition of phase-slippage	7
	II.2.Pre-SBT models of phase-slip centers	9
	II.3.SBT model of a phase-slip center	10
	II.4.Post-SBT models of phase-slip centers	15
	II.5.Previous experiments on phase-slip centers	31
III	EXPERIMENTAL TECHNIQUES	
	III.1.Fabrication of the samples	39
	III.1.1.Substrate cleaning procedure	43
	III.1.2.Preparation of the photoresist stencil	44
	III.1.3.Fabrication of masks	50
	III.1.4.Evaporation of the samples	53
	III.1.5.Other methods of fabrication	55
	III.2.Measurement techniques	59

IV RESULTS AND DISCUSSION

IV.1.Samples of type S: interacting phase-slip centers..... 66

IV.2.Samples of type T:

IV.2.1.Measurements of the nonequilibrium potential..... 79

IV.2.2.Injection experiments..... 90

IV.3.Samples of type M: effects of microwaves on phase-slip centers..... 95

V CONCLUDING SUMMARY..... 102

REFERENCES..... 105

ACKNOWLEDGMENTS..... 111

LIST OF FIGURES

FIGURE		PAGE
I.1.	Current-voltage characteristics of tin whisker at various temperatures obtained by Meyer and Minnigerode (reference 2). $\Delta T=T_c-T$.	3
II.1.	Time averages of (a) electrochemical potentials and (b) supercurrent and normal current in a long microbridge with a single phase-slip center according to SBT (reference 3).	14
II.2.	Spatial dependence of the normal current at a certain time according to the KSS model (reference 10). In this figure the total applied current is $I=I_c$ and $\Lambda_{a.c.}=\Lambda_{Q^*}/8$.	16
II.3.	Theoretical set of I-V curves calculated by Kramer and Watts-Tobin (reference 28) for $\gamma=10$ and $\gamma=20$. The shaded region indicates the range of current for which Kramer and Baratoff (reference 27) found phase-slip oscillations. d is the spatial period of the periodic array of PSCs.	20
II.4.	Theoretical I-V curves calculated by Tinkham (reference 34) for filaments of various lengths L and for $I_{exc}=0.5I_c$.	25
II.5.	Approximate analytic solution of the dynamics equations corresponding to the phase slippage process obtained by Ivlev and Kopnin (reference 38).	28
II.6.	Experimental measurements of the energy gap along a tin microbridge obtained by Skocpol and Jackel (reference 41).	34
III.1.	SEM pictures of samples (a) M-29, (b) M-15, (c) M-30 and (d) M-25. Sample M-25 was made with the same mask used to make samples of type T, but doing a single evaporation. The microbridge is the horizontal strip.	40
III.2.	SEM pictures of samples (a) S-1 and (b) S-2. In S-2 it is possible to see the contour of the heat front propagating from the burnt-out segment.	41
III.3.	SEM pictures of samples (a) TN-1 and (b) TN-2. The middle segment of TN-2 burnt out.	42
III.4.	SEM pictures of photoresist stencils ready to be used to prepare (a) a sample of type M and (b) a sample of type T.	47
III.5.	Close-up of two stencils used to prepared samples of type T. We can see the difference between a bad (a) and a good (b) contact printing. Both pictures were taken at the same magnification.	48

III.6.(a) Micrograph of the entire mask used to make samples of type M and samples of type S and close-up of the masks used to make samples of type S (d) and samples of type M (b)(c). 49

III.7.Diagram of the oblique evaporation technique. $w=a-h\tan\theta$. 51

III.8.(a) Micrograph of one mask used to make samples of type T. (b)(c) Close-up of the central part of the masks. 54

III.9.Microbridges fabricated using the diamond knife technique. (a) Sample MD-2. 56

III.10.SEM pictures of stencils of AZ1350J photoresist treated with chlorobenzene. 58

III.11.Schematic diagram of the experimental set-up used to measure I-V curves. 61

III.12.SEM pictures of burnt-out microbridges. The fiber in (b) is a whisker crystal that grew out of the film which had been stored for more than a year before this picture was taken. 62

IV.1.I-V characteristics of each one of the five segments of sample S-1. Variations in I_c along the bridge are due to imperfections such as nonuniform width. The inset shows the sample geometry. 67

IV.2.I-V characteristics of the segment CL of the sample S-1 taken for different fixed values of the current through the segment LD. (+) or (-) correspond to the cases when the current in the two segments flow in the same or in opposite directions, respectively. 69

IV.3.Symmetric ΔI_c^s and antisymmetric ΔI_c^a parts of the change of the critical current of CL of the sample S-1 as a function of the quasiparticle current in the center of the phase-slip center in LD. The inset shows the linear temperature rise at CL as a function of the power dissipated in LD. 71

IV.4.I-V characteristic of the segment CL of sample S-1 taken for different values of the current through DM. (+) or (-) correspond to the cases when the current in the two segments flow in the same or in opposite directions, respectively. 73

IV.5.Decay with distance from the source of the surviving fraction of quasiparticle current generated in phase-slip centers in the sample S-1. 74

IV.6. Set of I-V curves of sample TN-2. The current is applied between the ends of the microbridge (A and B) and the voltage is measured between A and each one of the normal probes C, L, D and M and also between A and B. 80

IV.7. μ_n/e versus tunnel probe position for sample TN-2. The circles represent the raw data. The triangles represent the data after the geometrical correction was made. Reference potential is μ_s to the rigth of the PSC location. 81

IV.8. Semilog plot of the normalized quasiparticle potential versus tunnel probe position in sample TN-2. v(x) is defined in the text. 83

IV.9. Semilog plot of the normalized quasiparticle potential versus tunnel probe position in sample TN-1. 84

IV.10. Semilog plot of the normalized quasiparticle potential versus tunnel probe position in samples TU-1. 85

IV.11. Temperature dependence of the quasiparticle diffusion length in sample TN-2. The best fit (full line) for n=0.28 is compared to the expected $(1-T/T_c)^{-1/4}$ divergence (dashed line). 87

IV.12. Effect of the supercurrent on the relaxation of the quasiparticle charge. The dashed line is $(1-T/T_c)^{-1/4}$. The full line is $[(1-T/T_c)(1+1/\beta(T))]^{-1/4}$. 91

IV.13. Set of I-V curves taken in sample TN-1 for different fixed values of the current injected through D. 92

IV.14. I-V curves of sample M-29 at various levels of microwave power. 97

IV.15. I-V curves of sample M-29 at various levels of microwave power. 98

IV.16. Length versus width of samples of type M normalized to their respective temperature-dependent coherence length. The thick black lines indicate where Josephson steps were observed. According to Likharev, the upper left region corresponds to one-dimensional filaments. 101

LIST OF TABLES

PAGE

III.1. Some physical properties of samples of type S and samples of type T..... 64

III.2. Some physical properties of samples of type M..... 65

IV.1. Experimental values of quasiparticle charge diffusion length Λ_{Q^*} and relaxation time τ_{Q^*}..... 88

IV.2. Best values of n and $\Lambda'_{Q^*}(0)$ for fit of our data to $\Lambda_{Q^*}(T) = \Lambda'_{Q^*}(0)(1-T/T_c)^{-n}$..... 88

CHAPTER I

INTRODUCTION

The current-induced transition to the normal state of one-dimensional superconducting filaments (ODSF) is one of the most interesting problems in nonequilibrium superconductivity. The term one-dimensional is used for samples with transverse dimensions small with respect to the Ginzburg-Landau (GL) coherence length $\xi(T)$ and to the London penetration length $\lambda(T)$, and with length large compared with those parameters. In this situation, any spatial dependence of the superconducting properties of the sample is assumed to occur only along the filament.

Experimentally, the resistive transition of a superconducting filament can be studied when a constant current is applied to the sample and the voltage across the sample is measured as a function of the temperature (V versus T curves, also called R vs. T curves). Conversely, the temperature can be kept fixed and the voltage across the sample measured as a function of the current applied (V versus I curves, commonly called I-V curves).

For temperatures close, but not too close, to the "mean-field" critical temperature T_c of the sample, that is, for $0.1 \gtrsim 1-T/T_c \gtrsim 0.001$, the onset of resistance is characterized by the appearance of reproducible regular voltage steps occurring at specific values of temperature and current. This structure was first observed in 1968 by Webb and Warburton[1] in the R vs. T curve of whisker crystals of tin with cross-sectional areas smaller than 1 $(\mu m)^2$.

A few years later, Meyer and Minnigerode[2] published their experi-

mental results on the resistive transition of tin whiskers. They observed voltage steps in the V vs. T curves for current intensities larger than 35 μA and found that the height of the voltage steps increased linearly with the current applied. They also measured the I-V curves at fixed temperatures and observed voltage steps followed by a plateau of constant differential resistance. Figure I.1 shows a set of I-V curves taken from reference 2. These are the first published set of I-V curves showing the step-like structure and for that reason were chosen to be the first figure in this thesis.

Similar I-V curves have been measured in long microbridges of tin[3], aluminum[4], indium[5] and niobium[6], and also in indium whiskers[7].

Two very important features of those I-V curves are, firstly, the changes in differential resistance at all the steps in a given curve have the same magnitude, and secondly, the presence of an excess current, meaning that the extrapolation to zero voltage of the linear part of the steps intercepts the current axis at a finite positive value, I_{exc}.

Skocpol, Beasley and Tinkham[3] developed a model, known as the SBT model, to explain those features in the I-V curves of superconducting filaments. According to SBT, each voltage step corresponds to the appearance of a spatially localized "phase-slip center" (PSC) which, in simple terms, can be described as a dissipative unit that is able to carry a finite supercurrent. Each unit consists of a region of length $\approx \xi(T)$ where the GL order parameter undergoes a relaxation oscillation at a Josephson frequency determined by the voltage across the PSC. This voltage is determined by the relaxation of the nonequilibrium potential

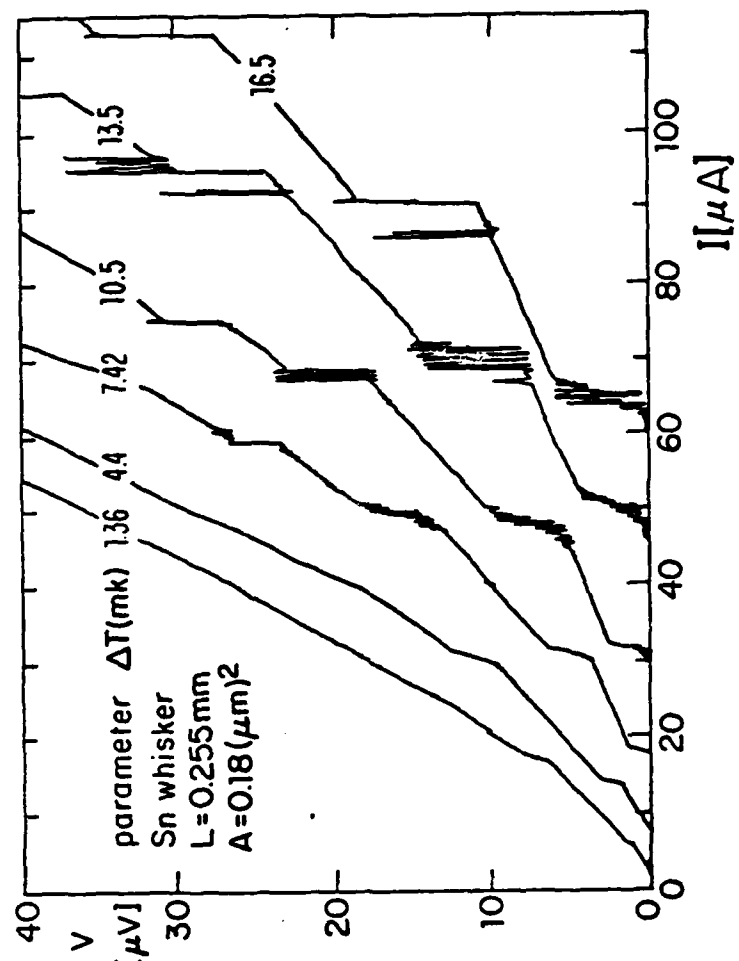

Figure I.1. Current-voltage characteristics of a tin whisker at various temperatures obtained by Meyer and Minnigerode (reference 2). $\Delta T = T_c - T$.

which occurs in a longer length scale corresponding to the diffusion length of the quasiparticle charge, namely, Λ_{Q^*}.

In order to explain the significance of the SBT model, it is necessary to provide a historical review. For that reason, the next chapter is organized chronologically. Starting with the origins of the concept of phase slippage, I will discuss briefly the models of PSCs proposed by different authors before and after SBT. A general view of the most relevant experiments on PSCs will be also presented.

As it will be shown in the next chapter, all the models agree in the explanation of the voltage steps in the I-V curves of ODSF in terms of the appearance of PSCs. However, the interpretation of the quasiparticle diffusion length Λ_{Q^*} has been a subject of controversy over the last few years. For that reason we have performed a series of experiments[8] in order to measure the decay with distance from the center of the PSC of the quasiparticle current and the nonequilibrium potential and we have compared our results with the existing theories and with the experimental results obtained by other authors.

In one experiment we have measured the effect that the quasiparticle current generated in one PSC has on the appearance of other PSCs in the same microbridge. The geometry of these samples was such that the nucleation of PSCs in different locations was controlled by applying current through side probes to differents segments of the microbridge (I will refer to these samples as samples of type S). In that way the interaction effects could be measured as a function of the distance between the two interacting PSCs. We have separated heating effects from

diffusive current effects in the same fashion as Jillie[9] did is his work on interacting short microbridges. We have observed that the quasiparticle diffusion current decays exponentially with distance and that for a temperature $T= 0.99T_c$, the magnitude of the characteristic decay length is $\Lambda_{Q^*}= (6 \pm 1)\mu m$, corresponding to a relaxation time of $\tau_{Q^*}= (7 \pm 2)\times10^{-10}$ sec for our tin microbridges. The temperature rise of the microbridge caused by the PSC corresponds to a heat transfer coefficient $\alpha = 1.5$ watt/K cm^2 for our tin samples on glass substrates and in direct contact with the liquid He bath. No voltage locking was observed, presumably due to the relatively long distance between PSCs compared to the decay length of the a.c. nonequilibrium currents $\Lambda_{a.c.}$ ($\Lambda_{a.c.} \approx 0.6\ \Lambda_{Q^*}$ for tin at $T= 0.99T_c$)[10].

In a different type of experiment we have measured directly the exponential decay of the quasiparticle potential. We have fabricated tin microbridges with normal tunnel junction probes, similar to the samples used in the Dolan and Jackel[11] experiment (I will refer to these samples as samples of type T). We have proved that the decay of the quasiparticle potential is, in fact, exponential and that the characteristic decay length Λ_{Q^*} diverges at the critical temperature as $\Lambda_{Q^*} \propto (1 - T/T_c)^{-1/4}$ which corresponds to a relaxation time $\tau_{Q^*}(T)= (0.7 \pm 0.2)\times10^{-10}\text{sec}(1 - T/T_c)^{-1/2}$, which agrees very well with the result of our previous experiment.

We have also injected normal current in the microbridge through the normal probes in samples of type T. The induced nonequilibrium potential was measured at other points of the bridge and we observed the

decay of this potential with the distance from the injection site. The effect of that injected nonequilibrium current on the appearance of the first PSC in the microbridge was also measured and we observed the decay of this effect with the distance between the injection site and the PSC. The magnitude of the decay length obtained in these experiments also agrees with the results of the other experiments[8].

We have not found any conclusive evidence of the existence of the "matching region", proposed by Baratoff[12], where the decay of the nonequilibrium potential is non-exponential.

According to the theory[13,14,15] very close to T_c, τ_{Q^*} can be written as $\tau_{Q^*} = 0.73\, \tau_E\, \Delta(0)/\Delta(T)$. Using this relation, we have found that the inelastic phonon scattering time τ_E in our tin samples at T_c is $\tau_E = (1.6 \pm 0.4) \times 10^{-10}$ sec.

The last part of this work consists of the detection of the oscillations of the supercurrent in the core of the PSC. We have fabricated tin microbridges of various lengths, from short microbridges ($L \simeq 1\,\mu m$) to long microbridges ($L \simeq 40\,\mu m$) and the effect of an external microwave field on the I-V curves of those microbridges was investigated. We have observed well defined Josephson steps in microbridges up to $10\,\mu m$ long.

CHAPTER II

THEORIES AND EXPERIMENTS ON PHASE-SLIP CENTERS.

II.1 DEFINITION OF PHASE-SLIPPAGE

The concept of a phase-slip event was developed by Langer and Ambegaokar (LA)[16] and it is based on an idea proposed by Little[17]. According to LA, if V_{12} is the voltage difference between points x_1 and x_2 at each end of the filament and

$$\psi(x) = |\psi(x)| e^{i\varphi(x)} \tag{II.1}$$

is the GL order parameter, then the phase difference between those two points evolves in time following the Josephson relation

$$\frac{d}{dt} (\varphi(x_2) - \varphi(x_1)) = \frac{2eV_{12}}{\hbar} \tag{II.2}$$

According to the GL theory, the magnitude of the supercurrent in the filament is

$$J_s(x) = \frac{2e}{m^*} |\psi(x)|^2 \hbar \left(\frac{d\varphi}{dx} - \frac{2eA}{c} x \right) \tag{II.3}$$

In a one dimensional filament, the magnetic field can be neglected and we assume $A_x = 0$. Then

$$J_s(x) = \frac{2e\hbar}{m^*} |\psi(x)|^2 \frac{d\varphi}{dx} \tag{II.4}$$

From equations (II.2) and (II.4) it follows that in the presence of a voltage difference, the supercurrent along the filament will increase continually without limit. Therefore, in order to achieve a steady state situation, thermal fluctuations in the interior of the superconductor

must occur in order to reduce the phase difference at the same rate as the voltage increases it. According to LA, when the supercurrent J_s reaches a critical value J_c, the phase coherence is broken at a certain point in the filament, and the GL order parameter vanishes briefly, allowing the phase to slip by 2π before the coherence is reestablished.

LA found that fluctuations of the order parameter that allow phase slippage are most likely to occur over a length $\xi(T)$, the GL coherence length. A greater or lesser length is energetically less favorable. The LA theory, with the correction introduced by McCumber and Halperin[18], describes very well the onset of resistance in one-dimensional superconducting filaments (ODSFs) in the limit of low current density and temperatures very close to T_c, i. e. $1-T/T_c \lesssim 0.001$.

II.2 PRE-SBT MODELS OF PHASE-SLIP CENTERS

The first model intended to explain the voltage steps observed in the resistive transition of ODSFs was proposed by Fink[19,20] in 1973 and for the first time, the expression "phase-slip center" was used.

According to Fink, when the total current along the filament exceeds the critical current, the order parameter becomes zero at some points in the filament, permitting the phase of the order parameter to change in time at those points. In this model, the modulus of the order parameter is time-independent but spatially periodic. The phase is a time-dependent quantity and its evolution is described in terms of the time dependent Ginzburg-Landau (TDGL) theory.

The voltage across each PSC is an integer fraction of the total voltage across the filament. Fink calculated the I-V curves and compared them to the experimental results of Meyer et al.[2]. The qualitative agreement is only fair, the main discrepancy being related to the existence of an excess current. The I-V curves calculated by Fink extrapolate to the origin and he suggested that the offset in the experimental I-V curves was caused by a recorder drift.

Skocpol et al.[3] also tried, unsuccessfully, to fit their data to Fink's model.

II.3 SBT MODEL OF A PHASE-SLIP CENTER

According to Skocpol, Beasley and Tinkham (SBT)[3], when the current along a ODSF exceeds the critical current of the weakest point, the filament jumps into a dissipative state with periodic phase-slip events occurring in that weakest point at a Josephson frequency set by the total voltage between the ends of the filament.

SBT considered a two-fluid picture to describe the current through the phase-slip center. One part of the current is carried by quasiparticles, the dynamics of which is determined by a normal electrochemical potential μ_n; the other part of the current is carried by the condensate with which a superconducting electrochemical potential μ_s is associated.

Using the results of the GL theory, SBT wrote the supercurrent density as

$$J_s(x) = \frac{2e\hbar}{m^*}|\psi(x)|^2 \frac{d\varphi}{dx} \qquad (II.4)$$

and from the Josephson relation

$$\hbar \frac{d\varphi}{dt} = -2\mu_s \qquad (II.5)$$

Combining those two equations, one obtains

$$\frac{dJ_s}{dt} = -\frac{4e}{m^*}|\psi(x)|^2 \frac{d\mu_s}{dx} \qquad (II.6)$$

An important SBT assumption is that the normal current density is given by

$$J_n = -\frac{1}{\rho e} \frac{d\mu_n}{dx} \qquad (II.7)$$

where ρ is approximately the normal resistivity of the filament.

As we mentioned before, in order for a phase-slip event to occur, the order parameter $|\psi(x)|$ must vanish. The difference with Fink's model is that, according to SBT, $|\psi(x)|$ vanishes only momentarily, driving J_s to zero, with the total current being carried by normal electrons, before $|\psi(x)|$ regains its maximum value to collapse again in the next phase-slip event. This process is just a relaxation oscillation of the supercurrent like in the model of Notarys and Mercereau[21] of the dynamic behaviour of non-tunneling type weak links.

SBT calculated the time average of the supercurrent at the center of the PSC by using current-carrying solutions of the GL equations, so that equation (II.4) can be written in the form

$$J_s = J_o q \xi (1 - q^2 \xi^2) \qquad \text{(II.8)}$$

where $q = d\varphi/dx$. When the average is taking between $q=0$ and $q=1/\xi$, the result is

$$J_s = \frac{3\sqrt{3}}{8} J_c = 0.65\, J_c$$

where J_c is the critical current density $J_c = 2\, J_o/3\sqrt{3}$.

According to the SBT model, the oscillations of the order parameter occur in a length of the order of $\xi(T)$ (this region is called the core of the PSC) as proposed by Langer and Ambegaokar[16]. However, the conversion of normal current into supercurrent occurs in a length scale which is determined by the quasiparticle diffusion length Λ_{Q^*}, usually much larger than $\xi(T)$. This region is called the wings of the PSC in the most recent literature[22]. The quasiparticle diffusion length can be

written as

$$\Lambda_{Q^*} = \left(\frac{1}{3} v_F \ell \tau_{Q^*}\right)^{1/2} \qquad \text{(II.9)}$$

where v_F is the Fermi velocity, ℓ is the mean free path and τ_{Q^*} is the relaxation time for the processes which lead to the relaxation of the difference $\bar{\mu}_n - \bar{\mu}_s$. The interpretation of the time τ_{Q^*} will be discussed in section II.5.

SBT also calculated the spatial dependence of the time average of the pair potential μ_s and the normal potential μ_n. They found that μ_s is constant at each side of the core and it changes discontinuosly at the center of the PSC. On the other hand, $\bar{\mu}_n - \bar{\mu}_s$ changes more gradually

$$\bar{\mu}_n - \bar{\mu}_s = -e\rho\Lambda_{Q^*}(J - \bar{J}_s(x_1))\sinh\left(\frac{x-x_o}{\Lambda_{Q^*}}\right) \Big/ \cosh\left(\frac{x_1-x_o}{\Lambda_{Q^*}}\right) \qquad \text{(II.10)}$$

x_o is a point where $\bar{\mu}_n = \bar{\mu}_s$ like at the ends of the filament, where it makes contact with the banks, and x_1 is the position of the center of the PSC where $J_s(x_1) = 0.65\ J_c$. For a very long filament ($L \gg \Lambda_{Q^*}$), with bias current going from left to right, equation (II.10) reduces to

$$\bar{\mu}_n - \bar{\mu}_s = -e\rho\Lambda_{Q^*}(J - \bar{J}_s(x_1))\exp\left[-\left(\frac{x_1-x}{\Lambda_{Q^*}}\right)\right] \qquad \text{(II.11)}$$

for points to the left of the core $x < x_1$, and

$$\bar{\mu}_n - \bar{\mu}_s = e\rho\Lambda_{Q^*}(J - \bar{J}_s(x_1))\exp\left[-\left(\frac{x-x_1}{\Lambda_{Q^*}}\right)\right] \qquad \text{(II.12)}$$

for points to the right of the core $x > x_1$.

From (I.7), the time average of the normal current is

$$\overline{J_n}(x)=(J-\overline{J_s}(x_1))\exp\left(-\frac{|x_1-x|}{\Lambda_{Q^*}}\right) \qquad \text{(II.13)}$$

Figure II.1 shows the time average of the electrochemical potentials and currents as a function of the coordinate along the filament (from reference 3). The total voltage drop across the filament is:

$$V=2\rho\Lambda_{Q^*}\left(\frac{I-\overline{I_s}(x_1)}{wd}\right) \qquad \text{(II.14)}$$

and the differential resistance associated with the PSC is

$$\frac{dV}{dI}=\rho\frac{2\Lambda_{Q^*}}{wd} \qquad \text{(II.15)}$$

where wd is the cross-sectional area of the filament. Equation (II.15) is one of the most important results of the SBT model. It equates the differential resistance of a PSC with the resistance of a normal segment of length $2\Lambda_{Q^*}$.

Insofar as these results of the simple model are correct, the magnitude of Λ_{Q^*} and the value of $I_s(x_1)$ can be inferred directly from the experimental I-V curves.

Now, I will discuss briefly some of the models of PSCs developed by other authors.

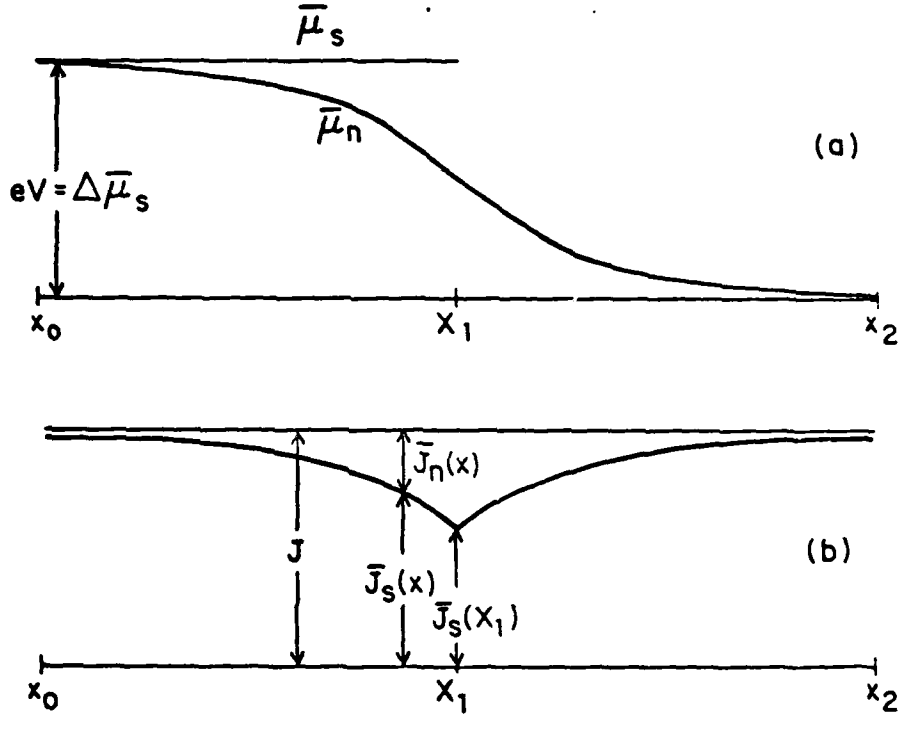

Figure II.1.Time averages of (a) electrochemical potentials and (b) supercurrent and normal current in a long microbridge with a single phase-slip center according to SBT (reference 3)

II.4 POST-SBT MODELS OF PHASE-SLIP CENTERS

In order to deal with the time-dependent character of the PSC, Kadin, Smith and Skocpol (KSS)[10] developed a clever model in which a PSC can be visualized as a Josephson oscillator, of zero length and negligible resistance connected to a transmission line. If the total current through the PSC is constant, the normal current injected in the transmission line will have an a.c. character because of the a.c. supercurrent generated in the Josephson element. This a.c. normal current decays more rapidly than its d.c. component. Figure II.2 shows the spatial dependence of the normal current at a certain time. The time average of the current and potentials reduce to the results of the SBT model.

KSS[10] also found that the differential resistance of the PSC is given by equation (II.15) and that the extrapolated excess current I_{exc} is

$$I_{exc} = \overline{I_s}(x_1) = \langle f \rangle I_c \qquad \text{(II.16)}$$

where $\langle f \rangle$ is the average of the current-phase relation of the Josephson element

$$\langle f \rangle = \frac{1}{2\pi}\int_0^{2\pi} f(\Delta\theta)\,d(\Delta\theta)$$

$$I_s = I_c f(\Delta\theta(t)) \qquad \text{(II.17)}$$

$\Delta\theta$ is the phase difference across the core. Equations (II.16) and (II.17) are valid if the voltage across the Josephson element is constant so that the phase difference $\Delta\theta$ increases linearly in time. This assumption is correct at the high voltage limit of the I-V curve where

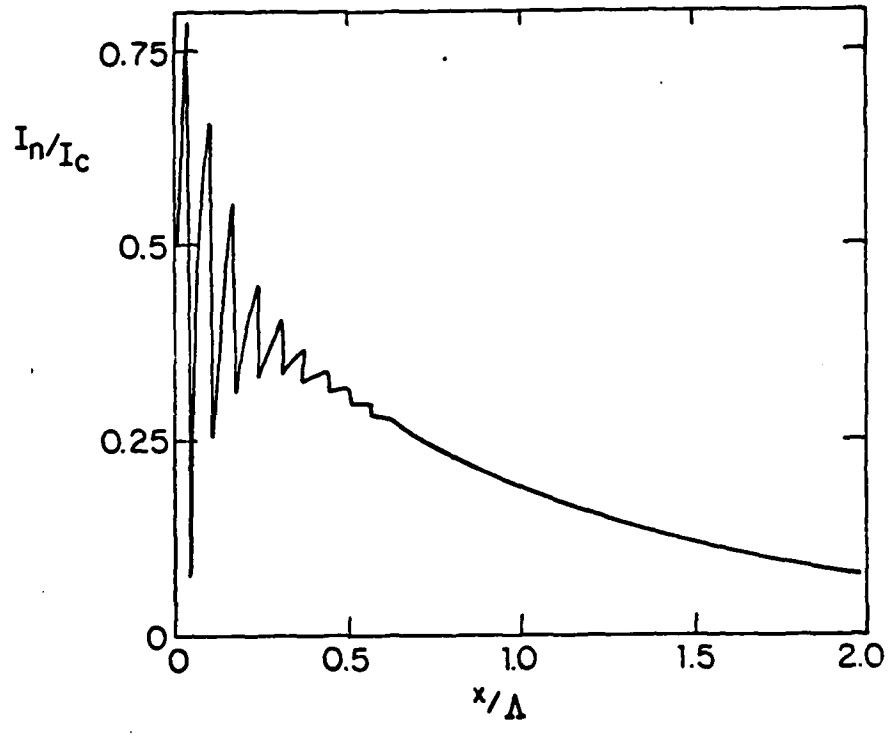

Figure II.2. Spatial dependence of the normal current at a certain time according to the KSS model (reference 10). In this figure the total applied current is $I=I_c$ and $\Lambda_{a.c.} = \Lambda_{Q^*}/8$.

the oscillations of the normal current are small compared to the total current. For a linear current-phase relation, equations (II.16) and (II.17) give $I_{exc}=I_c/2$.

A different approach has been taken by other authors.

In a series of papers[23,24,25], Galaiko has developed a model based on the microscopic theory for the resistive state of ODSFs in the range of current $j_c < j < j_{c2}$ and very close to T_c. j_c is the critical current determined by the dependence of the number of superconducting electrons on the velocity of the condensate (pair breaking current) and j_{c2} is the current below which superconductivity pairing develops in the normal state. In Galaiko's model, the resistive state of a superconducting channel consists of a dynamic structure of normal and superconducting regions alternating along the channel, like in Fink's model[19,20]. In the presence of an electric field, this state is characterized by discontinuities of the phase of the complex order parameter in the regions where $\Delta=0$. Galaiko calls those regions "centers of singularity". Galaiko solved the kinetic equations, derived in a previous paper[26] based on the BCS theory, for a dirty superconductor of infinite length and for temperatures very close to T_c where the Joule heating can be neglected. The spatial period of the structure of normal and superconducting regions in the filament was found by maximizing Δ for a given current.

As j increases approaching j_{c2} , the spatial period increases because of the size of the normal regions increasing. As j decreases, the spatial period decreases until the superconducting regions reach a

size $\xi(T)$ and then increases again because of the increase of the size of the superconducting regions.

As j gets closer to j_c, the resistive state is determined by the penetration of the electric field ℓ_E from the normal regions into the superconducting regions. Galaiko calculated the shape of the I-V curve with j in the vicinity of j_c and j_{c2} and an excess current was found in both limits. For $j \approx j_c$ the excess current is associated with the addition of a superconducting current while at $j \approx j_{c2}$ it is associated with the increase of the normal conductivity. Galaiko's model is valid only for infinite samples; however, he suggests that for samples of finite length, "centers of singularity" should appear and that the voltage steps observed experimentally in the I-V curves of ODSFs are related to the penetration of new centers into the sample, but no numerical results for the magnitude of those jumps are derived in his papers.

Kramer and Baratoff[27] have solved numerically the time-dependent Ginzburg-Landau (TDGL) equations for homogeneous ODSFs. They found that for a limited range of current $j_{min} < j < j_c$, localized phase-slip oscillations occur in which $|\psi|$ goes to zero at one point and the phase changes by 2π .In Kramer's nomenclature, the experimental critical current at which a voltage first appears is j_{max} which corresponds to the GL value for J_c used in the SBT model. j_{min} is the current below which the state is pure superconducting. j_c is the critical current above which the superconducting state becomes globally unstable or below which the normal state is globally unstable. As j decreases toward j_{min}

the period of the oscillation goes to infinity. Above j_c the order parameter performs oscillations with decreasing amplitude between phase-slip events. Eventually, an expanding normal domain develops. j_{max}= 0.385, j_c= 0.335 and j_{min}=0.326 in units of $j_o = hc^2/8e\pi\lambda^2\xi$

Later, Kramer and Watts-Tobin[28] found that phase-slip oscillations are possible for a larger range of currents. They solved generalized TDGL equations derived[29] from microscopic theory and taking into account the effect of a nonequilibrium quasiparticle distribution.

For $\gamma \rightarrow 0$, where $\gamma = 2\tau_E\Delta_o/\hbar$, their equations become the simple TDGL equations derived in reference 27. τ_E is the inelastic scattering time and Δ_o is the temperature-dependent value of the equilibrium order parameter. Kramer and Watts-Tobin found that the range of current where phase-slip oscillations occur increases as γ increases and for $j > j_{max}$, a periodic array of phase-slip centers can exists. Thus, the dissipative states observed experimentally corresponds to the appearance of successive PSCs. They found that the linear portion of the I-V is equivalent to that of a segment of filament of length Λ through which a time-averaged normal current of magnitude $j - \beta j_{max}$ flows. The magnitude of the excess current depends on γ but is independent of the spatial period of the periodic array of PSCs. e.g. β =0.46 for γ =20, β=0.6 for γ =10). On the other hand, $\Lambda \approx 7.5\,\xi(T)$ independent of the spatial period of the periodic array and independent of γ. Figure II.3 shows a set of I-V curves calculated by Kramer and Watts-Tobin.

Deriving the theoretical existence of an array of PSCs by means of

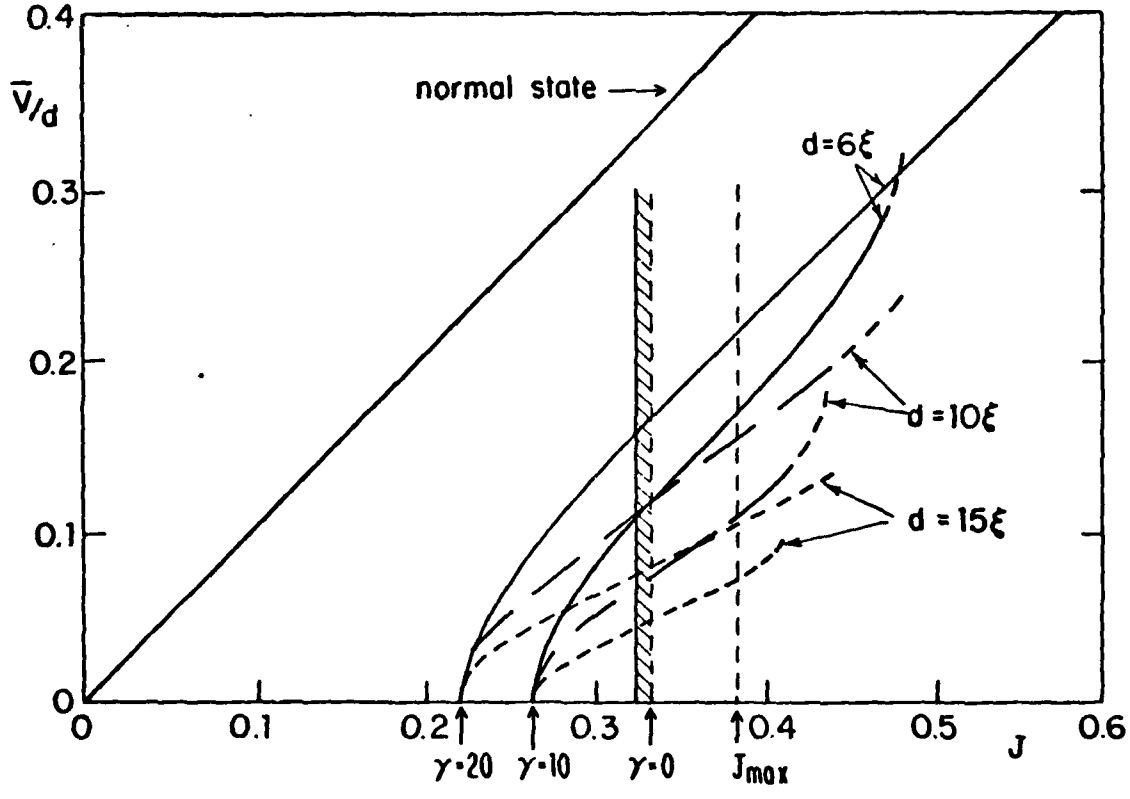

Figure II.3. Theoretical set of I-V curves calculated by Kramer and Watts-Tobin (reference 28) for γ =10 and γ =20. The shaded region indicates the range of current for which Kramer and Baratoff (reference 27) found phase-slip oscillations. d is the spatial period of the periodic array of PSCs.

a theory such as TDGL is a big advance in the understanding of the features in the I-V curves of ODSFs. However, the Kramer and Watts-Tobin equations are only valid if $\xi(T) \gg (D\,\tau_E)^{1/2}$, that is, in the limit of local equilibrium or slowly varying distribution. In tin, for example, this limit is true at $1-T/T_c \ll 0.003$, but the range of temperature in which voltage steps are observed is much wider. Furthermore, this model was developed for infinite samples, so the I-V curves are determined by the separation between PSCs and not by the total number of PSCs activated.

One important qualitative result of Kramer's work[27,28,29] is that during the phase-slip oscillations, the magnitude of the order parameter is depressed during the whole cycle and the time average of $|\psi|$ is much smaller than the equilibrium value. This result, which was not anticipated in the SBT model, has been observed experimentally as will be mentioned in section II.5.

Octavio and Skocpol[30] solved numerically the Kramer and Watts-Tobin equation for a finite sample ,modified by inclusion of a damping term proportional to the time derivative of the nonequilibrium potential. They also found that the order parameter is depressed throughout the cycle, and moreover that the oscillations of J_s, J_n and $\mu_n - \mu_s$ at the center of the PSC propagate like damped and dispersive waves, just as in the KSS model[10].

Kulik[31] has developed an elegant model for the penetration of an electric field in a superconductor. His model, like the SBT model, is based in the dynamic equations of the two-fluid model, namely

$$\rho_s + \rho_n = 0$$
$$\text{div}\,\rho_n + \text{div}\,\rho_s = 0 \qquad \text{(II.18)}$$

and the gauge invariant formulation of superconductivity:

$$\vec{v}_s = \frac{1}{2m}(\hbar\vec{\nabla}\varphi - \frac{2e\vec{A}}{c})$$
$$\mu = \frac{1}{2}(\hbar\frac{d\varphi}{dt} + 2e\Phi) \qquad \text{(II.19)}$$

where μ is the invariant potential of the superconductor and is equivalent to $\mu_n - \mu_s$ in the SBT model. Φ is the scalar potential of the electric field. Kulik calculates the electron distribution function using the Boltzmann kinetic equation, neglecting the effect of the gap, but taking into account the scattering of the normal excitations by the collective oscillations of the order parameter. Kulik gives the name "bogolons" to those oscillations. He arrives to the equation for the field in the superconductor

$$\nabla^2\Phi - \frac{1}{\Lambda^2}\Phi = 0 \qquad \text{(II.20)}$$

where the characteristic length Λ is frequency dependent and for zero frequency is given by

$$\Lambda(\omega=0) = (\frac{n}{m N_s \nu_i \tilde{\nu}_s})^{1/2} \qquad \text{(II.21)}$$

where n is the total density of electrons, N_s is the effective density of states for pair electrons and is approximately equal to $\pi\Delta N(0)/2kT$ near T_c, N(0) is the density of states at the Fermi surface, $1/\nu_i$ is the elastic (electron-impurity) scattering time, $1/\tilde{\nu}_s$ is the relaxation

time of the excess charge of quasiparticles and is determined by the electron-phonon relaxation time $\tau_E = 1/\nu_{ph}$ and the electron-bogolon relaxation time $1/\nu_s$; $\tilde{\nu}_s = \nu_s + \nu_{ph}$.

Kulik found that $\Lambda(\omega=0)$ increases as T approaches T_c according to $\Lambda(\omega=0) \propto (1-T/T_c)^{-1/4}$ up to a temperature T_1 at which ν_s becomes the dominant term. $\Lambda(\omega=0)$ is constant between T_1 and T_c. According to Kulik, not only the dynamic oscillations of the order parameter but also any static inhomogeneities of the order parameter in the sample will contribute to the conversion of the charge by a process similar to an Andreev reflection.

For a one dimensional filament, under the conditions such that a PSC is present, Kulik[32] found that the time-averaged electric field E(x) that determines the phase jumps decays exponentially from the center of the PSC with a characteristic length $\Lambda(\omega=0)$ given by equation (II.21). The total potential drop across the phase-slip center is related to the phase jump repetition period τ_o by the Josephson relation

$$V = \int \overline{E(x)}dx = \frac{h}{2e}\frac{2\pi}{\tau_o} \qquad \text{(II.22)}$$

Kulik[32] defines the excess current, like in the KSS model[10], as

$$J_{exc} = \frac{1}{\tau_o}\int_0^{\tau_o} J(\Theta(t))dt \qquad \text{(II.23)}$$

where Θ is the phase difference across the filament. However, in order to determined the numerical value of J_{exc}, Kulik[33] takes the average of the relation (II.8), like in the SBT model, except that, contrary to

SBT, he takes the average between q=0 (J_s=0) and q=1/$\xi\sqrt{3}$ (J_s=J_c) and he obtains J_{exc}=5J_c/8. This result appears to be inappropriate since the average of J_s should be taken over the period of the oscillation, as indicated by equation (II.23) , i.e. between two phase-slip events when J_s=0.

For a periodic array of n PSCs in a filament of length L, the I-V curve calculated by Kulik[33] coincides with the result obtained previously by Tinkham[34] for the generalization of the SBT model for n PSCs, namely

$$J(V) = J_{exc} + \frac{V_n}{2n\Lambda\rho} \coth\left(\frac{L}{2n\Lambda}\right) \qquad \text{(II.24)}$$

Figure II.4 shows the theoretical I-V curves obtained by Tinkham[34].

To complete this review, I will examine some of the ideas in the Ivlev-Kopnin model of a PSC.

According to Ivlev and Kopnin[35], a PSC can be regarded as a topological singularity of the vortex type in the two dimensional $\{x,ct\}$ space where they form a periodic structure. The electric field satisfies the relation

$$c\int_S Edxdt = \frac{n\Pi c\hbar}{e} \qquad \text{(II.25)}$$

where S is the area of a unit cell in the $\{x,ct\}$ space. Equation (II.25) is equivalent to the Josephson relation. If x_o is the length associated to the PSC, and τ_o the time period of the phase- slip process, then the average voltage across one PSC is V= $\langle E \rangle$ x_o where $\langle E \rangle$ is the space and time average of the electric field

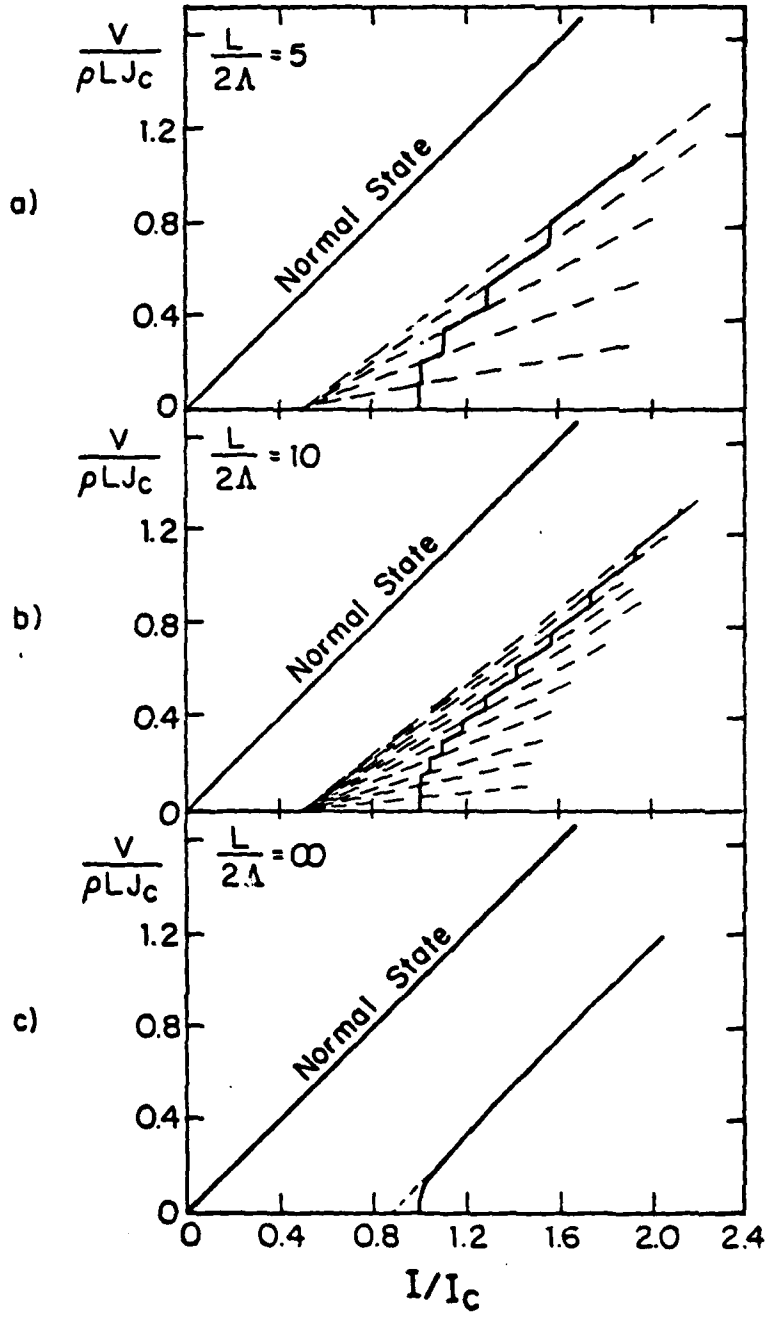

Figure II.4. Theoretical I-V curves calculated by Tinkham (reference 34) for filaments of various lengths L and for $I_{exc}=0.5I_c$.

$$\langle E \rangle = \frac{1}{x_o \tau_o} \int_S E \, dx \, dt = \frac{n \pi \hbar}{e x_o \tau_o} \qquad \text{(II.26)}$$

$$V = \frac{n \pi \hbar}{\tau_o e} = \frac{n \hbar \omega}{2e} \qquad \text{(II.27)}$$

As in the SBT model, Ivlev et al.[36] considered the structure of a PSC in two length scales, one region smaller than $(\ell_E \xi)^{1/2}$ where the order parameter and the supercurrent oscillate in time and another region of the size of the penetration length of the electric field ℓ_E which determines the relaxation of $\mu_n - \mu_s$. They solved numerically the TDGL equations for an homogeneous infinite filament like in the Kramer- Baratoff model, but in the limit $\xi \ll \ell_E$.

Ivlev et al.[37,38] found periodic oscillations of the supercurrent confined to a region $0 < x < (\ell_E \xi)^{1/2}$, but they found that the region where the order parameter oscillates is much smaller than $\xi(T)$.

In the limit $\ell_E \gg \xi$, the effect of the alternating supercurrent on the properties of the PSC can be disregarded like in the static approximation of Fink[19,20] and Galaiko[23-26] and the chemical potential of the pairs to each side of the PSC can be taken as constant. This static approximation is valid for $x \gg (\ell_E \xi)^{1/2}$ and there, the TDGL equations become a system of time independent equations. The I-V curves obtained from those static equations start with an infinite slope (for an infinite sample) at $j=j_c$, just as in Tinkham's model[34].

For $j_c \ll j \ll (\ell_E / \xi)^2 j_c$, the I-V curve has a constant slope equal to the normal resistance and shows an excess current independent of the voltage at T close to T_c, $j_{exc}=0.68\ j_c$, but it depends on the voltage at

lower temperatures.

In a region within a distance $\xi(T)\Gamma^{1/2}$ from the center, the time average of the modulus of the order parameter is much smaller than the equilibrium value, just as in Kramer's model. Γ is the pair breaking term and is taken to be $\Gamma \ll 1$ when there is a gap in the energy spectrum, which is the case in the Ivlev-Kopnin calculations. In the region $\xi\Gamma^{1/2} \ll x \ll (\xi \ell_E)^{1/2}$ the oscillations of the order parameter and of the nonequilibrium potential are small, but the oscillations of the supercurrent are still considerable. At $x \gg (\ell_E \xi)^{1/2}$ all quantities become time-independent. Figure II.5 shows the approximate analytic solution of the dynamic equations corresponding to the phase slippage process obtained by Ivlev and Kopnin[38]. Those solutions are valid in the temperature range where the phase-slip frequency $\omega \ll 1/\tau_E$ and the pair breaking term $\Gamma \ll 1$.

$$\left(\frac{\tau_E k_B T_c}{\hbar}\right)^{-2} \ll 1-T/T_c \ll \left(\frac{\tau_E k_B T_c}{\hbar}\right)^{-6/5}$$

In tin, this range corresponds to $0.0002 \ll 1-T/T_c \ll 0.005$. In the limit $\Gamma \ll 1$, the penetration length of the electric field is, according to Ivlev et al., equal to $0.42\,\xi/\Gamma^{1/2}$.

Ivlev and Kopnin[39] have also attacked the problem of calculating the I-V curve of a ODSF under the effects of microwave irradiation. In their approximation, they assume that the region $x < \xi\,\Gamma^{1/2}$ does not contribute to the calculation of the I-V curves . They found current steps at voltages such that

$$\Omega = m\omega \qquad \text{(II.28)}$$

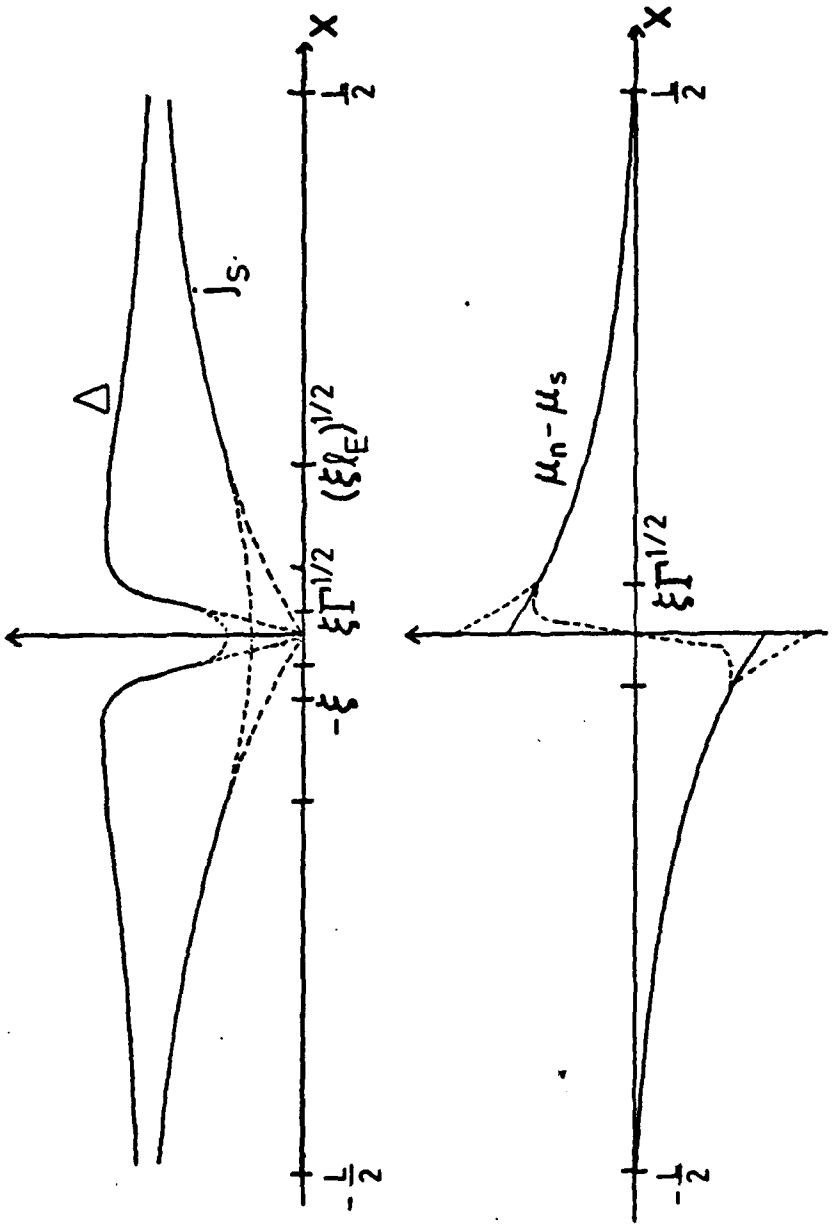

Figure II.5. Approximate analytic solution of the dynamics equations corresponding to phase slippage process obtained by Ivlev and Kopnin (reference 38).

where Ω is the frequency of the microwave field, m is an integer and ω is the Josephson frequency of the phase-slip process. In order to calculate the magnitude of the current steps it is necessary to know the exact form of the time dependent supercurrent. Ivlev and Kopnin[39] have simplified the problem by assuming that the space and time dependence of the order parameter can be approximated by

$$\Delta(x,t) \propto \begin{cases} \tanh\,(|x|/\xi\sqrt{2}) & \text{if } |x| > x_2(t) \\ \tanh\,(x_2(t)/\xi\sqrt{2}) & \text{if } |x| < x_2(t) \end{cases} \qquad \text{(II.29)}$$

where $x_2(t)$ oscillates from zero to $X_{max} \approx \xi\,\Gamma^{1/2} \ll \xi$ so that $\tanh x_2(t)/\xi\sqrt{2} \approx x_2(t)/\xi\sqrt{2}$. They found that the size of the steps is given by

$$\frac{\delta j_m}{j} = 2\left(1 - \frac{\sigma_n E}{j}\right)\frac{\sigma_d}{\sigma_n}\,A_m \qquad \text{(II.30)}$$

σ_n is the normal conductivity of the sample, E is the d.c. electric field across the PSC, σ_d is the differential conductivity dj/dE.

$$A_m = \left(\frac{\pi^5}{28\,\zeta(3)\,u}\right)^{1/2} \frac{e^2 D\;E\,E_\sim}{(T_c - T)^{1/2}(\omega m)^{5/2}}\,\frac{|a_m|}{\Gamma} \qquad \text{(II.31)}$$

$E_\sim$ is the amplitude of the a.c. electric field in the superconductor, D is the diffusion constant and a_m is a factor that depends on the form of $X_2(t)$

$$a_m \propto \frac{\omega}{2\pi}\int_0^{2\pi/\omega} (x_2(t')/\xi\sqrt{2})(1 - \cos(\omega m t'))dt' \qquad \text{(II.32)}$$

These results are a very rough approximation but they constitute the first attempt to explain quantitatively the magnitude of the Josephson steps in PSCs taking into account the spatial distribution of the a.c. supercurrent

As we have seen in this review, the problem of the structure of a phase-slip center has been approached in different ways. Nevertheless, all the models coincide in the fact that the structure and dynamics of a PSC has to be considered on at least two length scales: a short region where all the rapid oscillatory phenomena occur, and a longer region determined by the relaxation of the nonequilibrium potential. In the rest of this report, I will refer to those regions as the "core" and the "asymptotic wings" of the PSC. Recently, Baratoff[12,22] introduced a third region that he calls the "matching region" between the core and the wings and where the decay of the nonequilibrium potential is non-exponential. However, since no observations relating directly to this region have been made, it will be referred to only infrequently in the rest of this report. In fact, since the simple SBT model works so well, and anticipates most of the general features of the subsequent more microscopic theories, it will be the primary descriptive model that is used.

Next,to complete this review of earlier work, I will describe briefly the most prominent experiments carried out on PSCs since they were first observed 15 years ago until the present.

II.5 PREVIOUS EXPERIMENTS ON PHASE-SLIP CENTERS

The step-like structure connected to the appearance of PSCs was observed for the first time in the R versus T curves of tin whiskers[1]. Later, they were observed in the I-V curves of tin whiskers[2] (1972), microbridges of tin[3] (1974), aluminum[4] (1976), indium[5] (1976) and niobium[6] (1979) and also in the I-V curves of indium whiskers[7] (1980).

One of the most important properties of those I-V curves is that it is possible, in principle, to determine the diffusion length of the quasiparticle charge (or characteristic decay length of the nonequilibrium potential) Λ_{Q^*} by measuring the incremental differential resistance. According to the SBT model, for the nth step, we have

$$\left(\frac{dV}{dI}\right)_{n+1} - \left(\frac{dV}{dI}\right)_{n} = \rho \frac{2\Lambda_{Q^*}}{wd} \qquad \text{(II.33)}$$

where wd is the cross-sectional area of the filament and ρ is the normal resistivity of the sample.

Many experiments on PSCs have been focused primarly in determining Λ_{Q^*} by means of the equation(II.33). However, the values obtained by using this method differ from the true values because the heat generated in the PSCs adds some curvature to the I-V curves and the measured values of dV/dI are overestimated. This was the case of the experimental results on tin microbridges obtained by SBT[3] who were unable to detect the divergence at T_c of Λ_{Q^*} and consequently, they concluded that the inelastic scattering time τ_E rather than the branch mixing time τ_{Q^*} determined the appropriate diffusion length of the quasiparticles. It had been shown theoretically[13,14,15] that the

relaxation time of the quasiparticle charge imbalance mode of disequilibrium τ_{Q^*}, which determines Λ_{Q^*}, diverges at T_c as $\tau_{Q^*} \propto (1-T/T_c)^{-1/2}$, so that Λ_{Q^*} should diverge as $\Lambda_{Q^*} \propto (1-T/T_c)^{-1/4}$.

This contradiction between experimental results and theoretical prediction puzzled many researchers for some time. The first observation of the divergence at T_c of Λ_{Q^*} was reported by Jillie[5] who measured the differential resistance of the I-V curves of indium microbridges. This result raised the question of whether this effect was dependent on the superconductor used.

Kadin et al.[40] subsequently showed how heating effects can obscure the divergence of the differential resistance as T approaches T_c, and after correcting their data for heating effects they were able to observe the temperature and magnetic field dependence of the differential resistance of tin microbridges in the presence of a magnetic field. Their results agree well with the transverse mode relaxation time in the presence of a pair-breaking mechanism as derived by Schmid and Schön[15].

It is also possible to measure directly the potential of the pairs μ_s and the potential of the quasiparticles μ_n by attaching sets of tunnel junction probes on a microbridge. The first of this type of measurements were carried out by Dolan and Jackel[11]. They attached a set of silver probes and a set of lead probes to a long tin microbridge. They measured the voltage at different probes and found that the nonequilibrium potential $\mu_n - \mu_s$ decayed exponentially away from the center of the PSC, supporting the description of the PSC according to

the SBT model. Dolan and Jackel also observed the expected temperature divergence of this directly measured decay length. Their data corresponds to a relaxation time $\tau_{Q^*}=(0.9\pm0.2)\times10^{-10}\text{sec}(1-T/T_c)^{-1/2}$.

Using a similar geometry, Skocpol and Jackel[41] observed the reduction of the energy gap at the core of the PSC. Their samples were tin microbridges with lead tunnel junction probes. By measuring the I-V curves of the tin/tin oxide/lead junctions, they were able to obtain the value of the energy gap along the microbridge. They found that the first PSC appears where the gap is minimum and, once the PSC appears, the gap is depressed by more than 90 %. This result confirmed the models of Kramer et al.[27-29] Ivlev et al.[35-38] and Octavio et al.[30]. Figure II.6 shows the experimental results of Skocpol and Jackel[41].

Stuivinga et al.[42] prepared long aluminum strips with normal copper probes, and they measured the decay with distance from the center of the PSC of the normal potential. They found that the relaxation time diverges at T_c as $(1-T/T_c)^{-1/2}$. This is the expected temperature dependence if inelastic (electron-phonon) scattering time is the predominant mechanism in relaxing the charge imbalance. However, Stuivinga et al.[43] had predicted that in materials like Al and Zn, where the inelastic scattering time τ_E is relatively long, the relaxation of the charge imbalance is dominated by the pair breaking effect of the supercurrent and therefore, the measured relaxation time should diverge faster than $(1-T/T_c)^{-1/2}$ as T approaches T_c. They explained this discrepancy between their theoretical model and their experimental results in terms of the dependence with position (because of $J_s(x)$) of

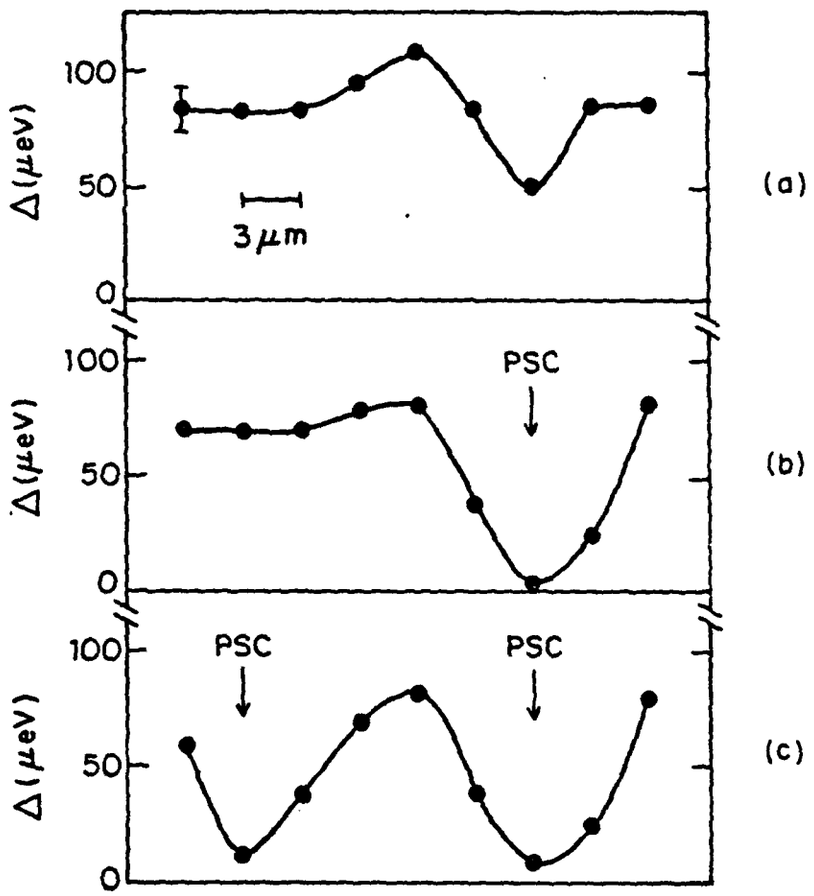

Figure II.6.Experimental measurements of the energy gap along a tin microbridge obtained by Skocpol and Jackel (reference 41).

the relaxation time associated with that mechanism.

The oscillations of the order parameter, or more precisely, the oscillations of the supercurrent in a PSC have been detected in different ways. Skocpol et al. (SBT)[3] observed the current steps in the I-V curves of long (120 μm) tin microbridges irradiated with microwaves (f = 10 GHz) at voltages corresponding to n times (n=1,1/2,1/3) the Josephson voltage in the first and second PSC. Tidecks and Minnigerode[44] observed Josephson steps in the I-V curves of tin whiskers (500 μm long) irradiated with microwaves of various frequencies (from f=0.2 GHz to f=1 GHz). They proposed an expression for the magnitude of the steps using an approximation for the spatially averaged time dependent supercurrent

$$I_s(t) = \frac{1}{2} I_c(1 + \cos\varphi(t)) \qquad \text{(II.34)}$$

$$\varphi(t) = \varphi(0) + \frac{2e}{\hbar}\int_0^t V(t')dt' \qquad \text{(II.35)}$$

Their result for the time average of the supercurrent is

$$\langle I_s(t)\rangle = \frac{1}{2} I_c(1 - \frac{2e}{2\hbar\omega} V_a\cos(\varphi(0) - \varphi(a)) \qquad \text{(II.36)}$$

where V_a and φ_a are the amplitude and phase of the microwave voltage in the sample.

According to equation (II.36), the magnitude of the steps, normalized to the critical current, is proportional to the microwave voltage. However, no comparison between this model and the experimental results is discussed in reference 44.

Josephson steps have also been observed in the I-V curves of "long" Nb nanobridges (from L=0.12 μm to L=0.9 μm) by Laibowitz et al.[6] and also in the I-V curves of In whiskers by Tiedecks et al.[7].

In a different type of measurement , Skocpol and Jackel[41] have detected the oscillations of the pair potential μ_s in a PSC by observing small current steps induced in the I-V curves of superconducting tunnel probes located in the vicinity of a PSC in a tin microbridge.

Other experimental evidences that prove the oscillatory nature of PSCs have been the observation of voltage locking between two PSCs and the detection of standing charge imbalance waves. The latter effect was observed by Kadin et al.[45] in In microbridges of various lengths and it occurs when the wavelength of the charge imbalance wave λ and the length of the microbridge L are such that $2L=(n+1/2)\lambda$ where n=0,1,...

Voltage locking occurs when the waves emitted by one PSC modulate the voltage driving the other PSC. This coherent behavior has been detected by Lindelof et al.[46,47] who measured the radiation emitted by pairs of short microbridges made of tin or indium with various separations between the microbridges, and also by Jillie et al.[48,49] who measured directly the I-V curves of pairs of short indium microbridges.

According to SBT, PSCs occur where the supercurrent I_s reaches the critical value $I_c(x)$ at some point in the filament. When a PSC is already present, the supercurrent is depressed in its neighborhood, $I_s(x)= I-I_n(x)$ (see figure II.1). In consenquence, successive PSCs are more likely to occur far from the ones already present. This apparent

enhancement of the critical current in the vicinity of a PSC was observed by Meyer et al.[50] in the I-V curves of tin whiskers with potential probes and also by Lindelof and Hansen[47] in pairs of tin and indium short microbridges.

This interaction via d.c. quasiparticle current was studied in more detail by Jillie et al.[9] in pairs of short indium microbridges. They measured the change of the apparent critical current of one bridge (detector) as a function of the current and voltage in the other bridge (source) in the cases of both opposing and series current bias. When the current flows in the same direction in both microbridges, an increase in the apparent critical current of the detector should be observed according to SBT. When the current flows in opposite directions, the supercurrent in the detector is increased and the apparent critical current of the detector decreases. This change in the apparent critical current is equal, in magnitude, to the quasiparticle current generated in the source that flows in the detector. On the other hand, the Joule heat generated in the source decreases the critical current of the detector independently of the relative direction of the currents.

Jillie et al.[9] separated those two effects by decomposing the change of the critical current of the detector in parts which are symmetric and antisymmetric respect to the relative direction of the currents. They found that these effects vanished for separations greater than 4 μm. This happens because in their geometry, the two-dimensional spreading of the nonequilibrium quasiparticle current

weakens the effect. They did not observe an increase in the apparent critical current of the detector because of an overwhelming heating effect. From their data, they estimated a temperature rise in the detector of 1.3 mK per each nW of power dissipated in the source. In the work to be reported here, these difficulties were overcome by use of a more favorable sample geometry.

CHAPTER III

EXPERIMENTAL TECHNIQUES

III.1 FABRICATION OF SAMPLES

Three different types of samples were prepared during the course of this work. I will refer to them as samples of type M, samples of type S, and samples of type T.

Samples of type M, used to study the effects of an external microwave radiation on a PSC, are tin microbridges of various lengths, from 1μm to 40μm, and about 1μm wide. Figure III.1 shows four samples of type M. Samples of type S, used to study the interaction between two PSCs, consist of a tin microbridge 40μm long and about 1μm wide with four side probes, all part of the same film. The distance between the probes was chosen to be of the order of the quasiparticle diffusion length so that only one PSC nucleates in any of the five segments of the bridge when current is fed through the adjoining probes. The probes were made wider than the bridge to allow application of currents well above the critical current of the bridge without loss of superconductivity in the probes. Figure III.2 shows two samples of type S. Samples of type T, used to measured the nonequilibrium potential in a PSC, also consist of a tin microbridge 40μm long and about 1μm wide, but rather than side probes, they have four tunnel junction probes. In some of the samples of type T, the middle segment of the microbridge was made narrower than the rest of the microbridge in order to facilitate the nucleation of a PSC in that location. This turned out to be a successful technique, as will be discussed later. Figure III.3 shows two samples of type T.

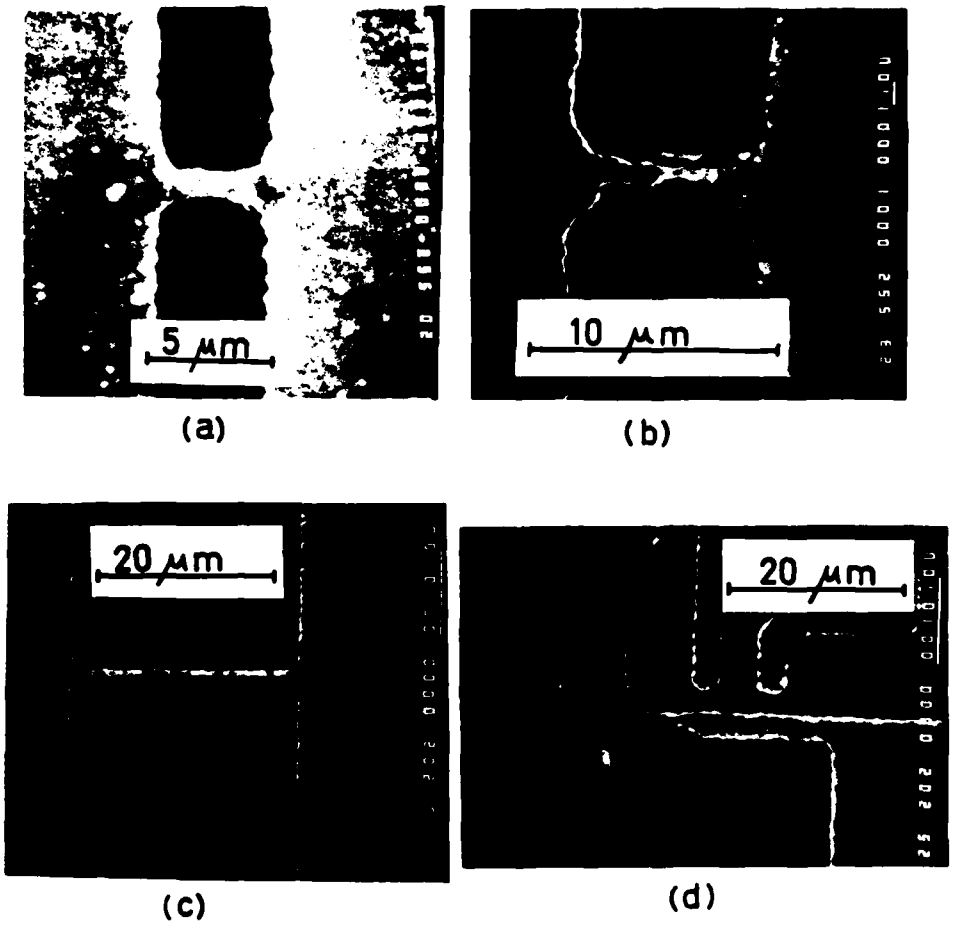

Figure III.1.SEM pictures of samples (a) M-29, (b) M-15, (c) M-30 and (d) M-25. Sample M-25 was made with the same mask used to make samples of type T, but doing a single tin evaporation. The microbridge is the horizontal strip.

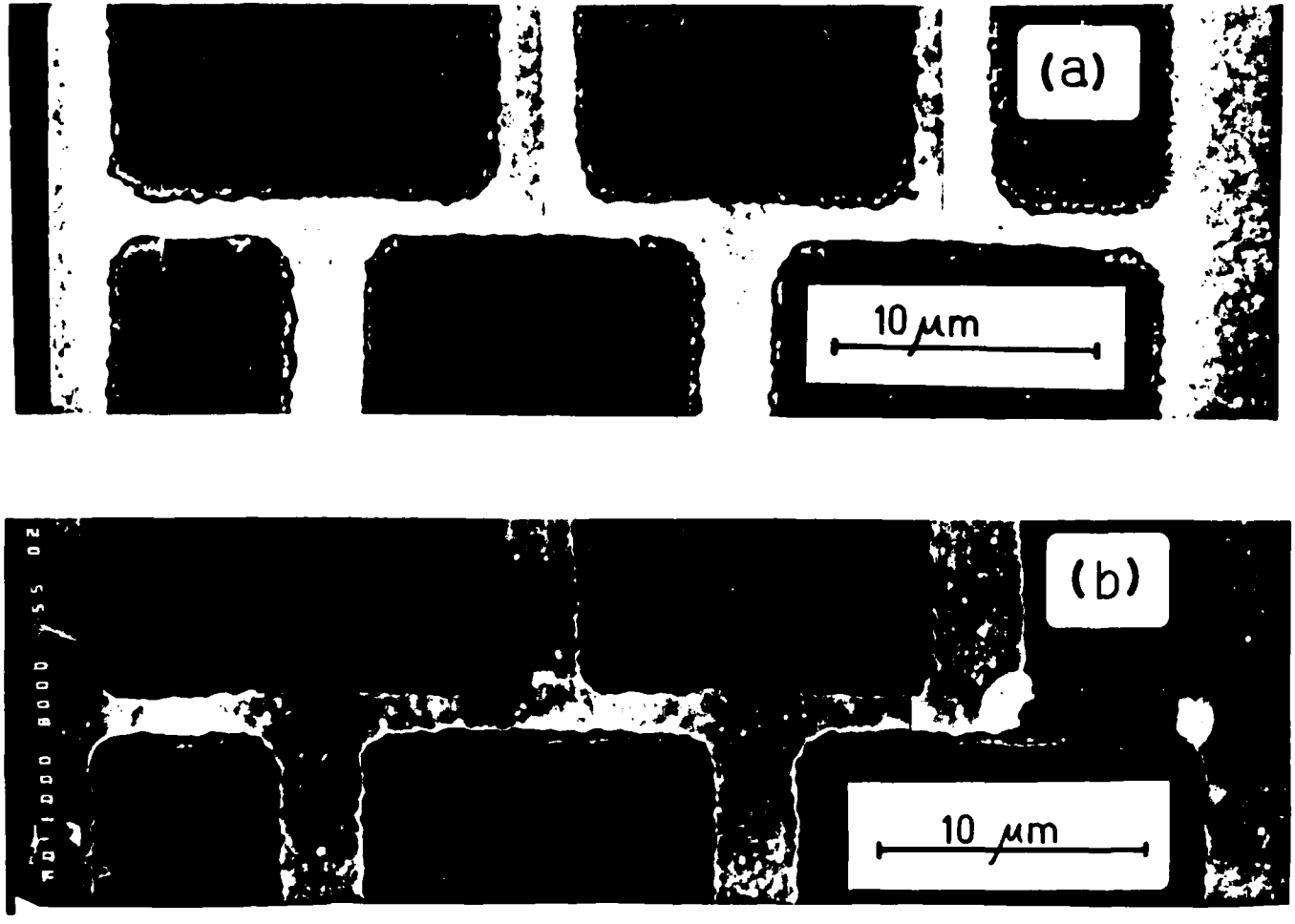

Figure III.2.SEM pictures of samples (a) S-1 and (b) S-2. In S-2 it is possible to see the contour of the heat front propagating from the burnt-out segment.

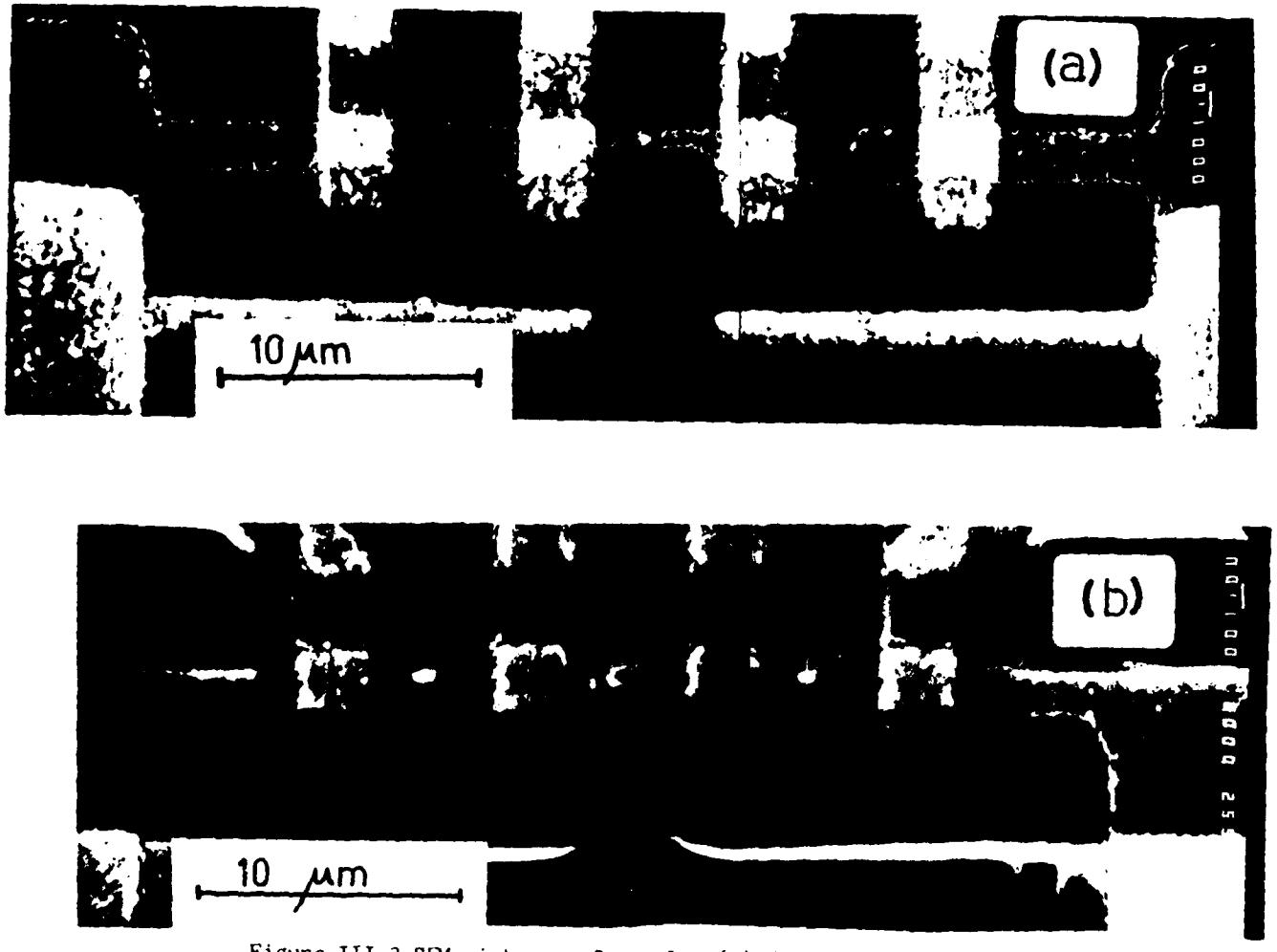

Figure III.3.SEM pictures of samples (a) TN-1 and (b) TN-2. The middle segment of TN-2 burnt out.

All our samples were fabricated using photolithographic techniques which I will describe in the following sections, beginning with the substrate cleaning procedures.

III.1.1 SUBSTRATE CLEANING PROCEDURE

Anyone involved in microfabrication and thin film technology knows that there is no universal recipe for cleaning substrates. It depends on the substrate material, the purpose of the cleaning and the time that one is willing to spend cleaning. We have combined several existing methods to make a simpler one that we found to be effective for cleaning our glass substrates.

Our substrates were made from microscope slides 1 mm thick which had been cut into pieces of dimensions 1"x1/4", 1"x1/2" or 1"x1"; this means that our substrates are subjected to considerable handling before they are cleaned. We start by wiping the substrate with a piece of lint-free wiping cloth wet with ethanol in order to remove the grossest dirt. We used ethanol because it did not dissolve the disposable gloves.

The next step is to boil the substrate in trichloroethylene (TCE) for five minutes. TCE dissolves most of the organic contaminants. This step is followed by sequential ultrasonic agitation in TCE, acetone and methanol for approximately five minutes in each solvent. Finally, the substrates are dried with filtered pure nitrogen and then they are stored in tightly sealed containers.

As will be discussed in section III.1.3, during the fabrication of

our masks we need to prepare chrome-coated 1"x1" glass slides. We found that in order to improve the quality of the Cr films, in particular to avoid pinholes, it was necessary to include an additional step in the cleaning process. Before the substrates were boiled in TCE, they had to be boiled in a solution of about 1 part of Micro in 10 parts of water for about 30 minutes and then rinsed thoroughly in distilled water and dried with pure nitrogen; the other steps were then followed. (Micro is a liquid laboratory cleaner manufactured by International Products Corp.).

III.1.2 PREPARATION OF THE PHOTORESIST STENCIL

In order to prepare our samples we used a lift-off technique developed by Dunkleberger[51] and Dolan[52]. Their method consists of fabricating two layers of photoresist separated by a thin film of aluminum. The pattern is defined in the top layer of photoresist, which is offset from the substrate by the bottom layer of photoresist. We used Shipley AZ1350J photoresist to prepare the stencils.

The clean substrate is placed in a photoresist spinner, covered with a few drops of photoresist and spun at 5500 RPM for 25 seconds to obtain a 1.5μm thick layer of photoresist. The substrates covered with photoresist are then baked at 95°C ± 5°C for 25 minutes and exposed with ultraviolet light for about 3 minutes to make the photoresist completely soluble in the developer. We usually wait more than 10 minutes between the bake and the exposure in order to allow the photoresist to recover the moisture lost during the bake.

A 800 Å to 1000 Å film of aluminum is deposited on top of the exposed photoresist and then a second layer of 1.5 μm of photoresist is spun on top of the Al film. This second layer has to be baked at a temperature a few degrees lower than the temperature at which the first layer is baked (which is higher than the 90 °C temperature recommended by Shipley), otherwise, lumps on the surface of the aluminum film appear due to the release of gases from the bottom layer of photoresist during the second bake. The sandwich (exposed photoresist)/aluminum/(unexposed photoresist) is now ready to be used.

Contact printing was used to copy the pattern from the mask onto the top layer of photoresist. The masks consist of a chrome film patterned on a 2"x2" piece of comformable glass 0.25 mm thick. The substrate coated with photoresist is placed in a hole in a plexiglass block. The chrome mask is held by suction in intimate contact with the substrate. The exposure time was 90 seconds for samples placed 2 feet away from the ultraviolet (UV) light lamp. The portions of photoresist exposed to the UV light are then removed by soaking the sample in the developer (1 part Shipley Microposit 351 in 5 parts of distilled water). The photoresist is developed for approximately 60 seconds.

The aluminum film is etched in a solution of 84% H_3PO_4, 5% H_2O, 5% CH_3COOH and 5% HNO_3 by volume. The bottom layer of photoresist is partially removed by immersing the sample in the developer for only a few seconds (usually between 10 and 15 seconds) in order to create an undercut under the top layer. Finally, the sample is immersed in the aluminum etch in order to get rid of the aluminum film under the

overhanging edge of photoresist, by doing so the undercut can be inspected by looking from the top using an optical microscope. Figure III.4 shows photoresist stencils ready to be used to prepare (a) a sample of type M and (b) a sample of type T.

Figure III.5(b) shows a close-up of the stencil shown in figure III.4(b). The undulations in the surface of the photoresist in figure III.5(a) are produced by standing waves formed when there is a separation between the mask and the surface of the photoresist during the contact printing. Very often, residues of photoresist on the chrome mask prevent a good contact, for that reason it is necessary to inspect the mask carefully and to clean it in case that it is not perfectly clean before doing the contact printing. Good contact between the mask and the photoresist was found to be more critical than the exposure time and the developing time for obtaining vertical walls in the pattern of photoresist.

The mask used to make the samples of type M and the samples of type S was made by a commercial firm (Advance Reproductions Corporation. North Andover, Massachusetts). A photograph of the entire mask is shown in figure III.6(a). The dark areas are the areas covered with chrome, the white areas correspond to the areas that become metallized during the deposition of the samples. The mask consists of six sections. The widest of them is the mask used to make the samples of type S and a blow-up of its middle part is shown in figure III.6(d). Each one of the other five sections contain four microbridges of various lengths. Figures III.6(b) and III.6(c) show a blow-up of two of those masks.

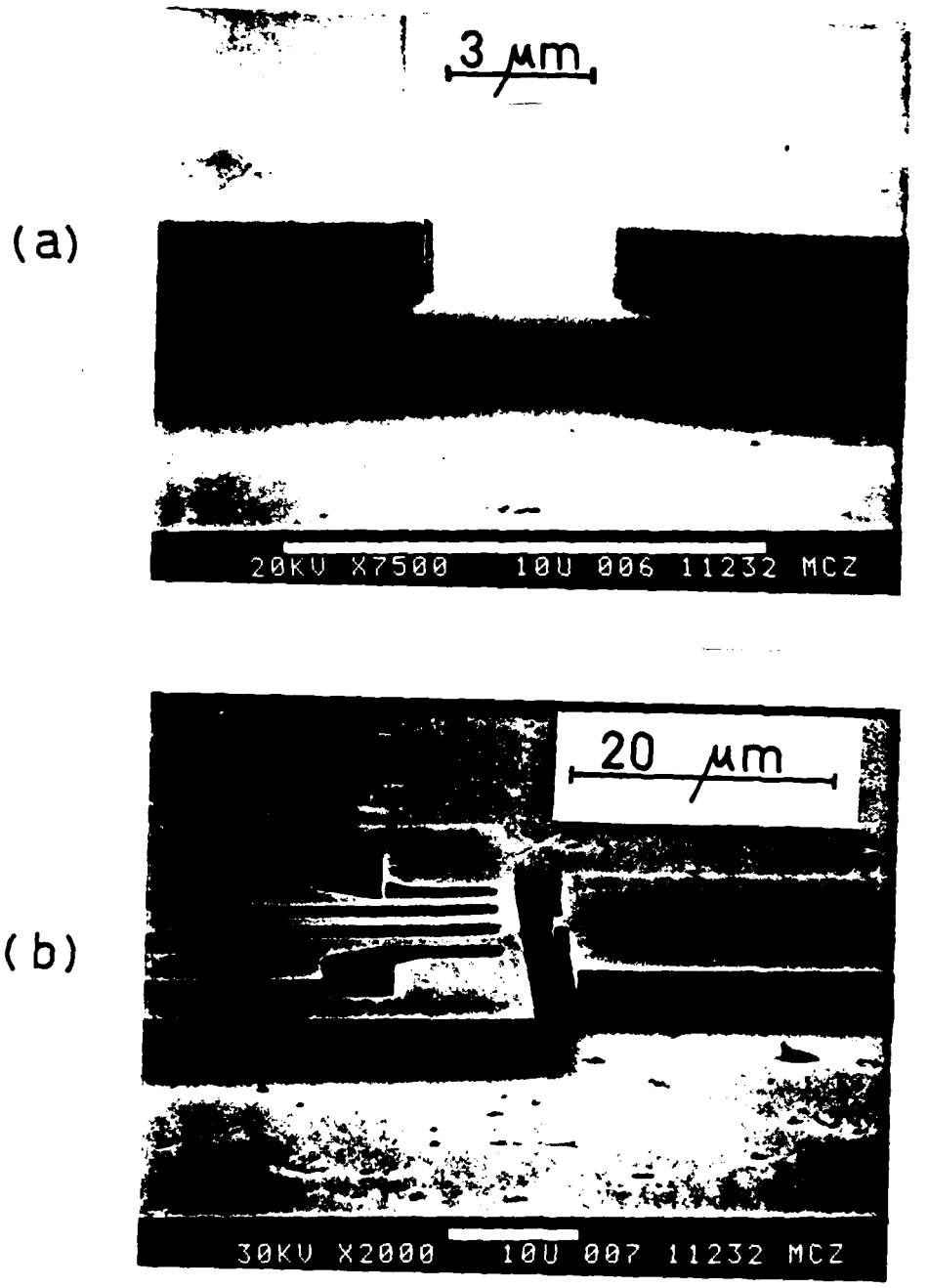

Figure III.4.SEM pictures of photoresist stencils ready to be used to prepare (a) a sample of type M and (b) a sample of type T.

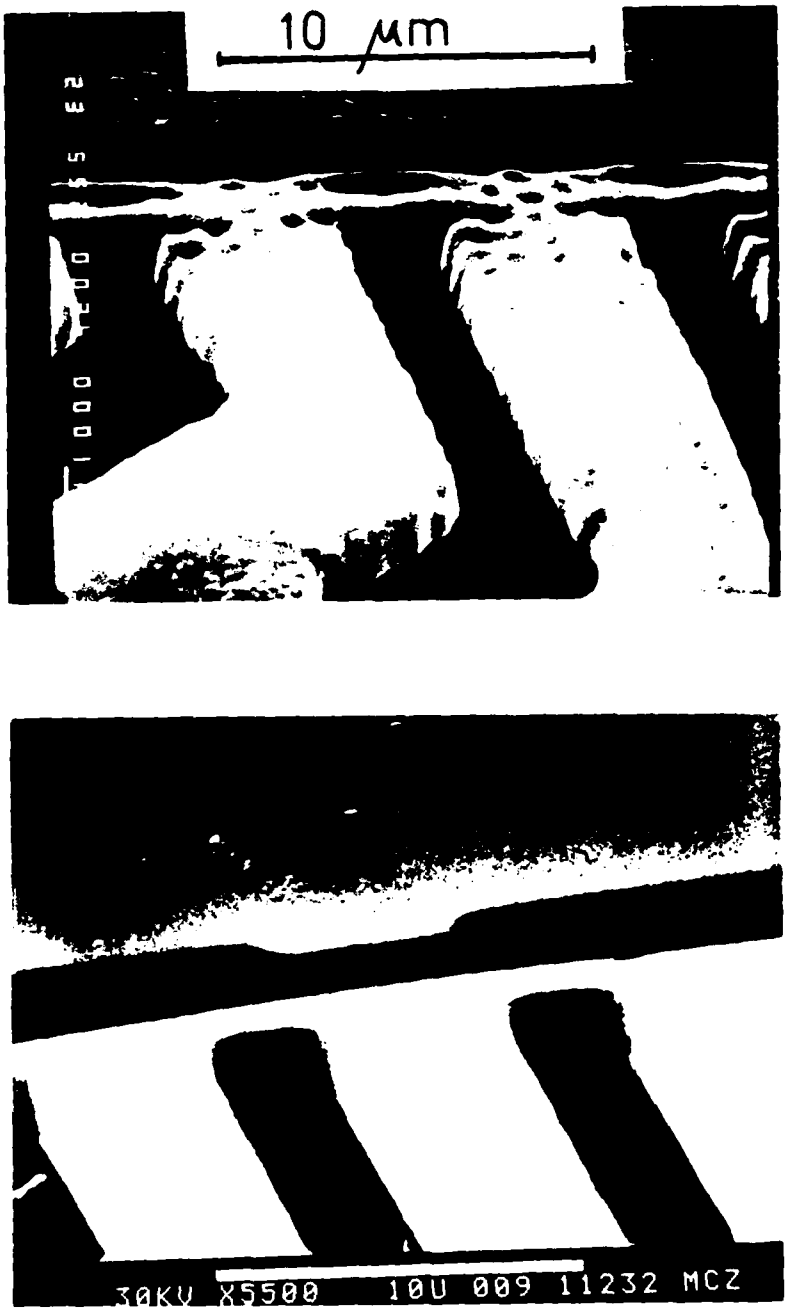

Figure III.5. Close-up of two stencils used to prepare samples of type T. We can see the difference between a bad (a) and a good (b) contact printing. See text for details. Both pictures were taken at the same magnification.

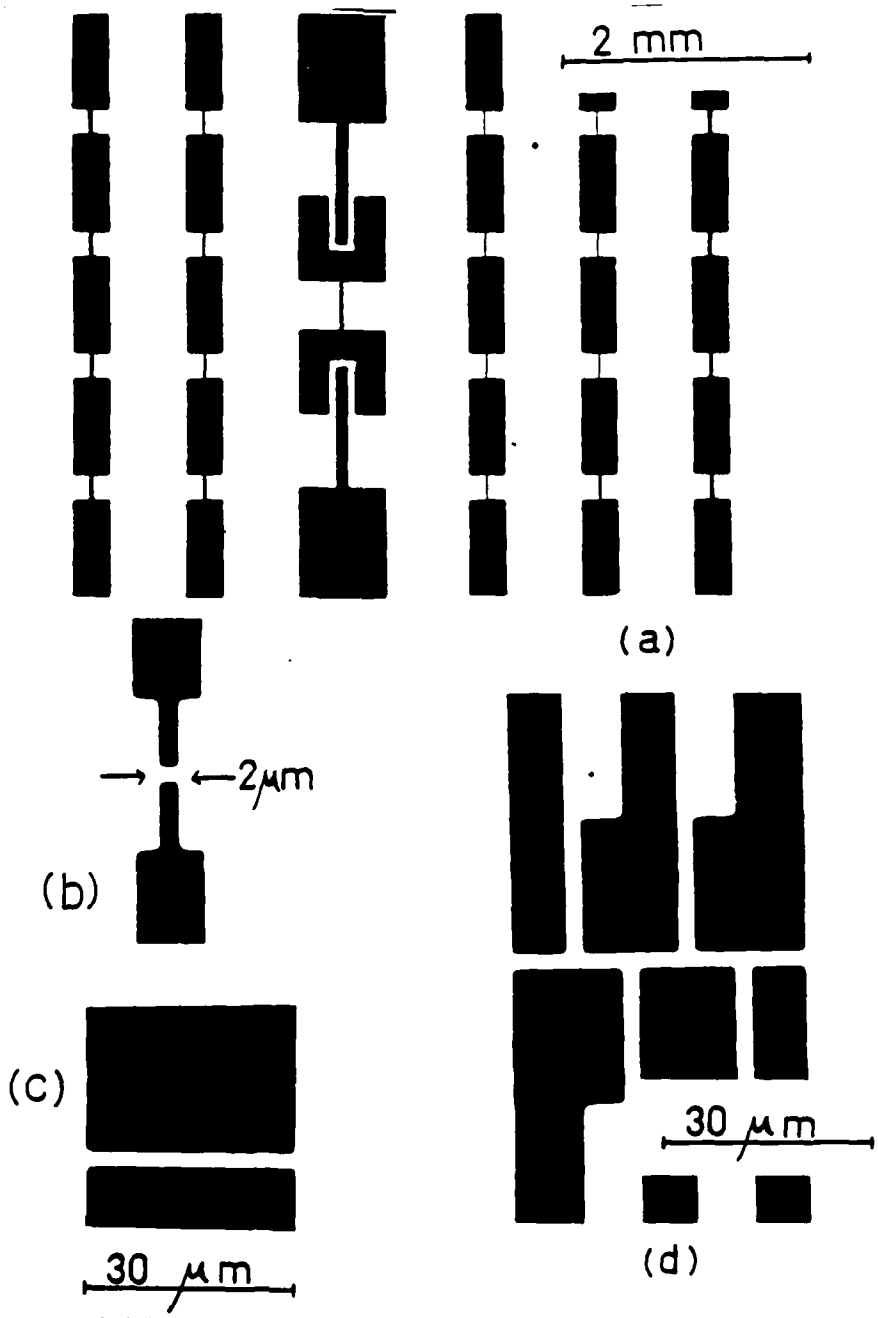

Figure III.6.(a) Micrograph of the entire mask used to make samples of type M and samples of type S and close-up of the masks used to make samples of type S (d) and samples of type M (b),(c).

From the original or master mask, we made separate copies of each one of those six sections in individual 2"x2" plates of conformable glass precoated with chrome.

The narrowest linewidth in the original masks is 2μm which becomes wider during the processes of making the copy in the conformable glass and preparing the photoresist stencil. We can see in figure III.4(a) that the line has become 3μm wide. This widening of the line is compensated by doing an oblique evaporation for the deposition of the samples. During the evaporation the substrate is held at an angle relative to the horizontal plane. By doing this, the width w of the bridge fabricated is considerably narrower than the mask opening. From figure III.7 we can see that $w=a-h\tan\theta$. This technique also allows us to produce samples of type S in which the bridge is made narrower than the probes. More details of the evaporation techniques are given in section III.1.4; but first, I would like to explain briefly how we made the mask used to produce the samples of type T.

III.1.3 FABRICATION OF MASKS

As it was mentioned in the previous section, the mask used to make samples of type S and samples of type M was made by a commercial firm. At that time we did not have the expertise nor the facilities to produce our own masks. We had tried making masks of aluminum film and using a diamond knife, but we found that it was a time-consuming process with little success and the masks produced did not last long due to the softness of the aluminum film and their poor adhesion to the glass substrates. As the need for producing samples of diverse geometries for

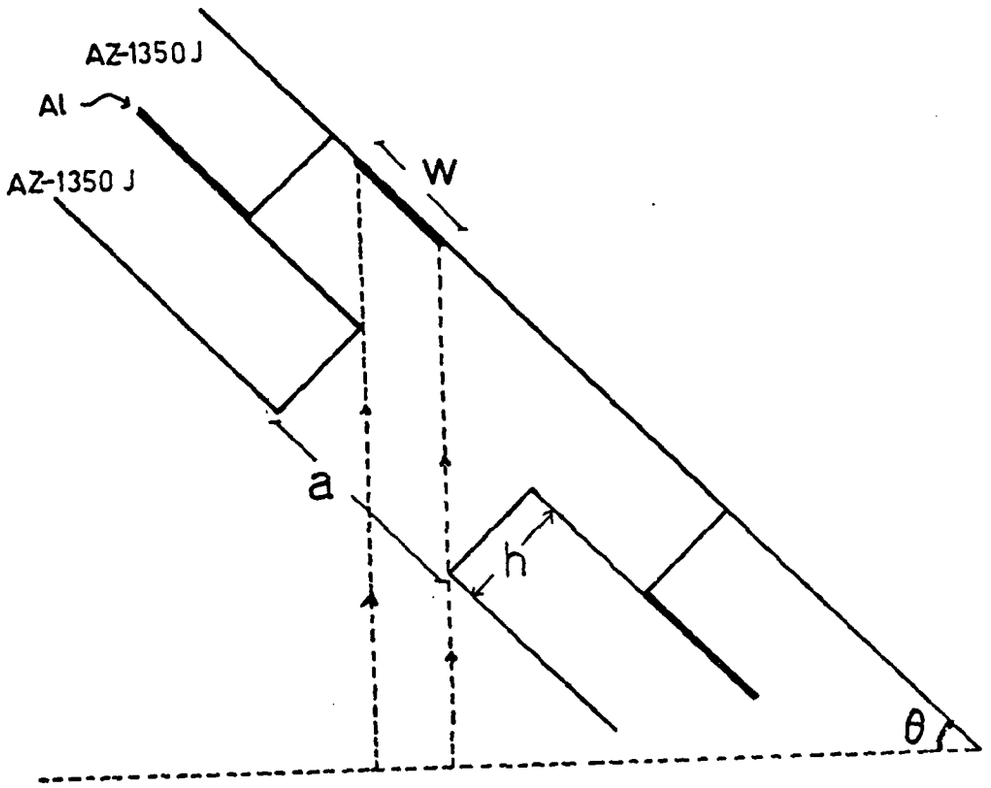

Figure III.7.Diagram of the oblique evaporation technique. $w=a-h\tan\theta$.

different members of our group became more apparent, and we found that we could not afford to order new commercial masks, W. C. Danchi[53] set up a system to produce our own masks. With a light board, a few sheets of rubylith, a few sheets of clear acetate, black tape of various widths and some glass plates precoated with chrome and photoresist, he was able to produce masks with lines as narrow as 5μm by making sucessive reduction of a pattern.

The first step is to make a pattern in rubylith or with black tape. (Rubylith is a material consisting of a thin red film laminated with a heavier clear backing so that the red film can be scribed and peeled away, leaving the desired pattern). This pattern is reduced 25 times by taking a picture with a 35 mm camera. The 35 mm negative is used to make a copy by contact printing on a 1"x1" glass slide coated with chrome. (Those are the 1"x1" glass slides that require the additional cleaning step mentioned in section III.1). The next step consists of doing a 10x reduction of the chrome copy using an optical microscope. This second step was possible thanks to D. J. Frank[54] who designed a projection attachment to use with our Zeiss microscope. By using different objectives, it is possible to do 10x, 20x, 50x and 100x reductions.

In order to make the samples of type T, it is necessary to have a mask with lines 2μm wide or narrower, which means that we had to use the objective with the highest resolution. On the other hand, the area illuminated gets smaller as the power of the objective is increased. For that reason we had to make our masks in three separate reductions.

The part of the mask that defines the pads is made by reducing the rubylith pattern 25 times using the 35 mm camera. Then, a 25x10x reduction is made to produce the intermediate region that connects the pads to the smallest region, and finally a 25x50x reduction is made to produce the narrowest lines. We obtained lines as narrow as 1.5μm using this technique. Figure III.8(a) shows a picture of one of those masks. Figures III.8(b) and III.8(c) show a blow-up of the central part of the mask for two different masks, both used to make samples of type T, but one (b) with a microbridge of uniform width and the other (c) with a microbridge with a narrow segment in the middle.

III.1.4 EVAPORATION OF THE SAMPLES

Most of our tin samples were evaporated onto glass substrates maintained at liquid nitrogen temperature, and a few samples were deposited at room temperature. We did not find any difference in the quality of those films as long as they were deposited at a very high rate, 200 Å/sec or higher.

The vacuum system consists of a mechanical pump with a molecular sieve trap and a cryopump, with an ultimate pressure of about 10^{-7} Torr. Some of our earliest samples of type M were made in the "old" evaporator with a diffusion pump instead of a cryopump, the ultimate pressure being also about 10^{-7} Torr.

Samples of type M and samples of type S were made in a single evaporation of a tin film 1000 Å thick with the substrate forming an angle θ with the horizontal plane as indicated in figure III.7.

In order to prepare samples of type T, we evaporated a 1000 Å thick

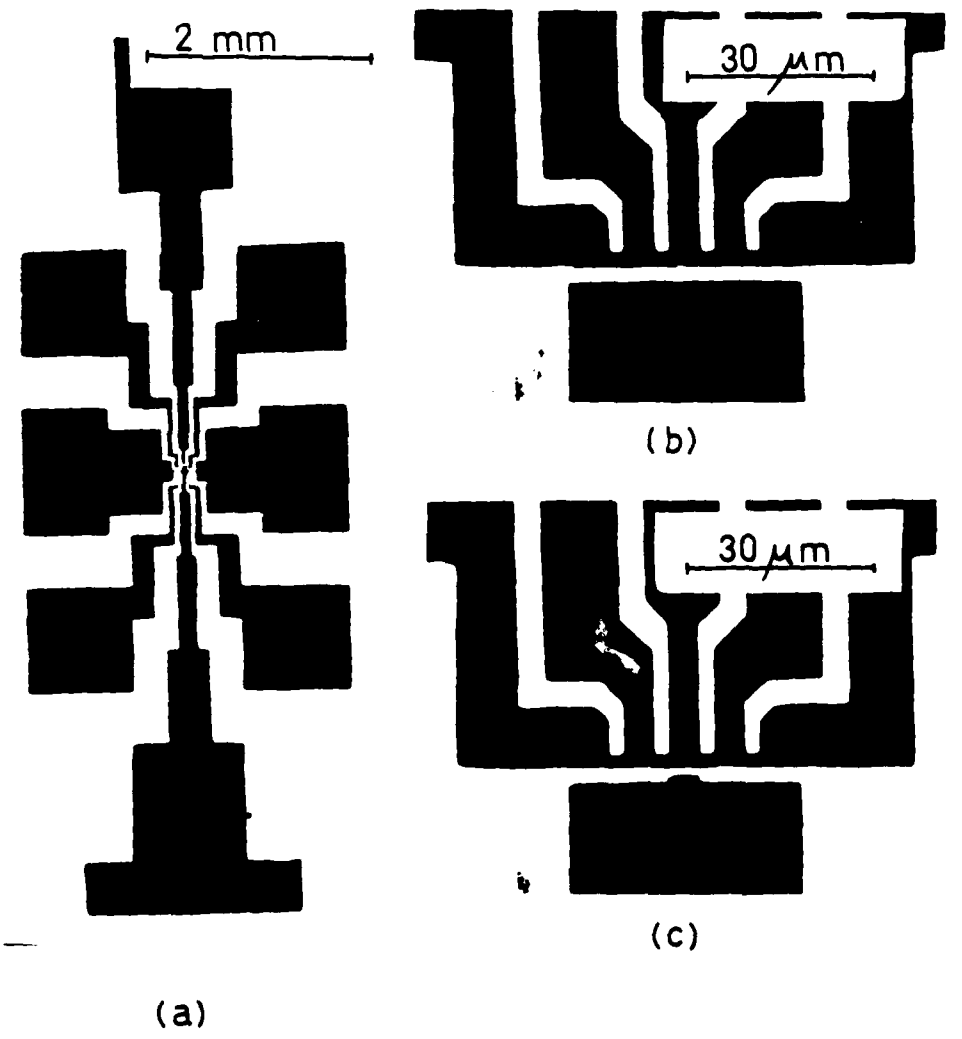

Figure III.8.(a) Micrograph of one mask used to make samples of type T.
(b)(c) Close-ups of the central part of the masks.

tin film, oxidized it in a glow discharge of pure oxygen, and after rotating the substrate to the correct angle, a layer of normal metal was deposited. The glow discharge was maintained for a period of between 30 seconds and 100 seconds, depending on the desired barrier resistance. The initial pressure of the oxygen was $3x10^{-2}$ Torr. We used silver or indium as the normal electrodes. (The indium is normal in the range of temperature in which the measurements were made). The samples are removed from the evaporator and acetone is sprayed on them to dissolve the unexposed photoresist and lift off the unwanted metal.

Next, I would like to describe other methods of fabrication that we tried during the progress of this work.

III.1.5 OTHER METHODS OF FABRICATION

The diamond knife technique was the first technique that we used to fabricate microbridges. In order to make cuts on a thin film, the substrate is slid beneath a diamond knife that can be moved vertically, so that it is possible, in principle, to control the pressure with which the knife is placed against the film. The substrate can be moved horizontally in two perpendicular directions by means of differential screws attached to the translation stage, so that parallel cuts can be made, like those shown in figure III.9(b), (c) and (d), creating a long constriction connecting two large areas of the film. To produce short microbridges, like the one shown in figure III.9(a), movement of the substrate along only one direction is needed.

As we can see in figure III.9, the width and the depth of the cut is different for different samples, this happens because it is very

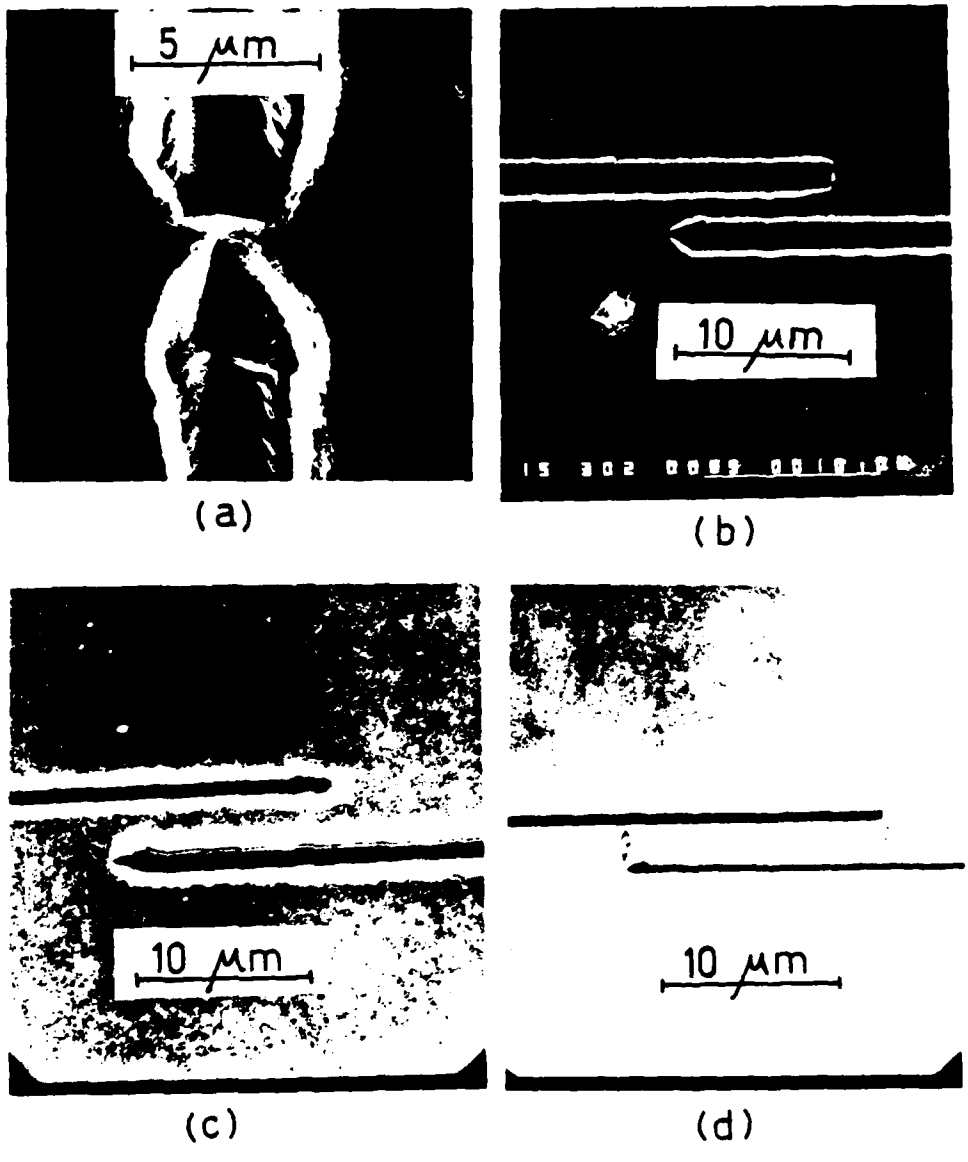

Figure III.9.Microbridges fabricated using the diamond knife technique.
(a) Sample MD-2.

difficult to see when the knife is touching the film and therefore, it is hard to decide how much the knife can be moved downward. Sometimes the position of the knife relative to the film changed during the dragging, and as a consequence, the film was not cut completely leaving metallic shorts in parallel with the microbridge. Other inconveniences with the diamond knife technique are: firstly, the fact that the microbridges produced by this method are thicker at the edges because of the metal pushed by the knife during the cuts, and secondly, the variety of geometries that are possible to fabricate is very limited. More details about the diamond knife technique of microfabrication can be found in references 55 and 56.

Another technique that was used but abandoned later consists of the lift-off of a single layer of photoresist treated with chlorobenzene. This technique was developed by Hatzakis et al.[57] and it consists of soaking the baked photoresist in chlorobenzene either before or after the exposure. (I found that this method works best when the soak is done after the exposure). This process strengthens the surface of the photoresist making it harder to dissolve in the developer and consequently, an undercut profile is obtained. Figure III.10 shows SEM pictures of two profiles of AZ1350J that have been soaked in chlorobenzene for (a) 5 minutes and (b) 10 minutes after the exposure. The thickness of the hardened layer of photoresist agrees well with the results reported in reference 57. This technique works very well to produce clean lift-offs; however, the photoresist stencils can not be used for oblique evaporations

(a)

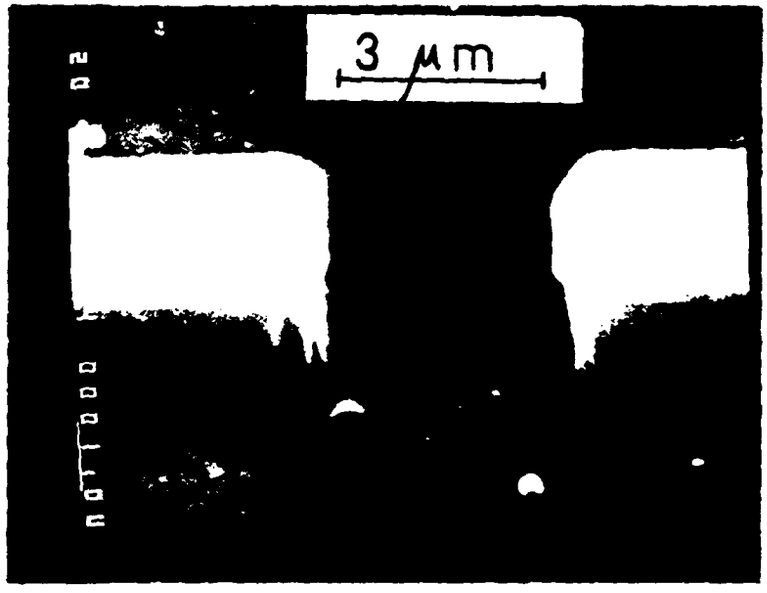

(b)

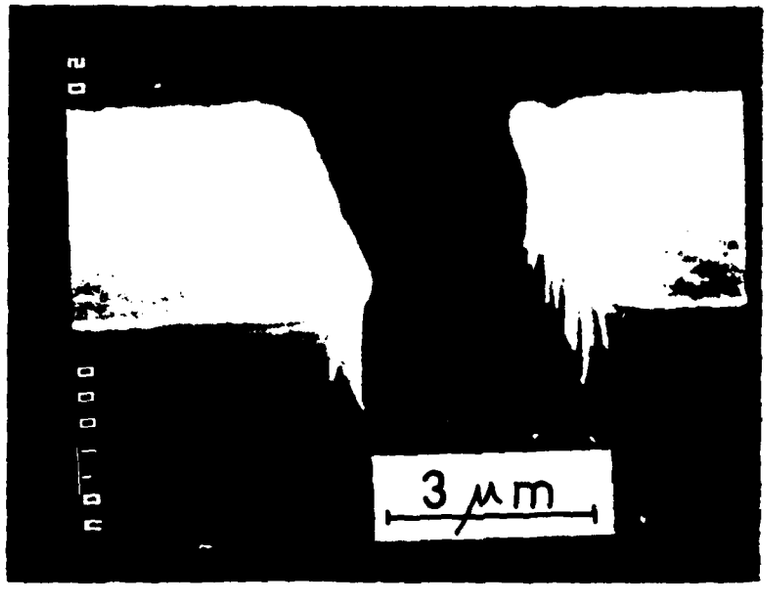

Figure III.10.SEM picture of stencils of AZ1350J photoresist treated with chlorobenzene.

III.2 MEASUREMENT TECHNIQUES

In order to attach leads to the samples, indium patches were applied to the substrates before the evaporation. After the samples were made, wires were connected to the indium patches using a battery-powered soldering iron. In samples of type S and sample of type T, one current lead and one voltage lead are attached to each end of the microbridge and to each one of the four probes.

Measurements on samples of type M were taken using a two-terminal or a four-terminal configuration, depending on what kind of set-up was used to apply microwaves to the samples. In some experiments, the samples were placed in an X-band waveguide at a distance equal to $\lambda_g/4$ from the closed end. In those experiments the samples were two-probed because the slit through which the sample is inserted in the waveguide is almost as narrow as the thickness of the glass substrates. In other experiments, the microwave radiation was applied to the sample using a semi-rigid coaxial cable of 0.141" outer diameter terminated in an inductive loop. This loop was placed parallel to the sample at a distance about 8 mm from it. In those experiments the samples were four-probed. We used BNC connectors to adapt the waveguide to the coaxial cable and we found experimentally that the microwave radiation is attenuated by 20 dB when the BNC-coaxial-loop configuration is used instead of the waveguide.

For all the samples, the voltage leads are continuous copper wires connecting the samples directly to a Keithley Nanovoltmeter. The current leads are connected to a ten-pin connector and from there to

battery-powered current sources. Up to this point the banks have been shorted together by wide segments of the film which are now scraped with a Circon microknife. The samples are tested for continuity at room temperature by applying a small current, usually less than $5\mu A$, and measuring the voltage with the Nanovoltmeter.

The samples are immersed directly into the liquid helium bath whose temperature was controlled using a pressure regulator. During the measurements, the temperature was kept constant within one millidegree for up to five hours, as confirmed by a germanium thermometer. Figure III.11 shows a schematic diagram of the circuit used to measure the I-V curves of the samples.

Once the fabrication of the samples was completed, the most serious problem encountered was that of burnout, meaning the destruction of the microbridge by accidental electric pulses caused by turning electronic equipment on and off, or by simply touching the leads connected to the sample. Sometimes, samples burned out without apparent reason. Figure III.12 shows different levels of destruction, from areas about 1 $(\mu m)^2$, to enormous catastrophes where the area destroyed is as big as 10^4 $(\mu m)^2$. The results presented in this report were obtained with the samples that survived for the longest period of time, and for which we were able to obtain the greatest amount of data.

Table III.1 lists some of the physical properties of samples of type T and samples of type S. Table III.2 lists physical properties of samples of type M. The dimensions were measured using scanning electron

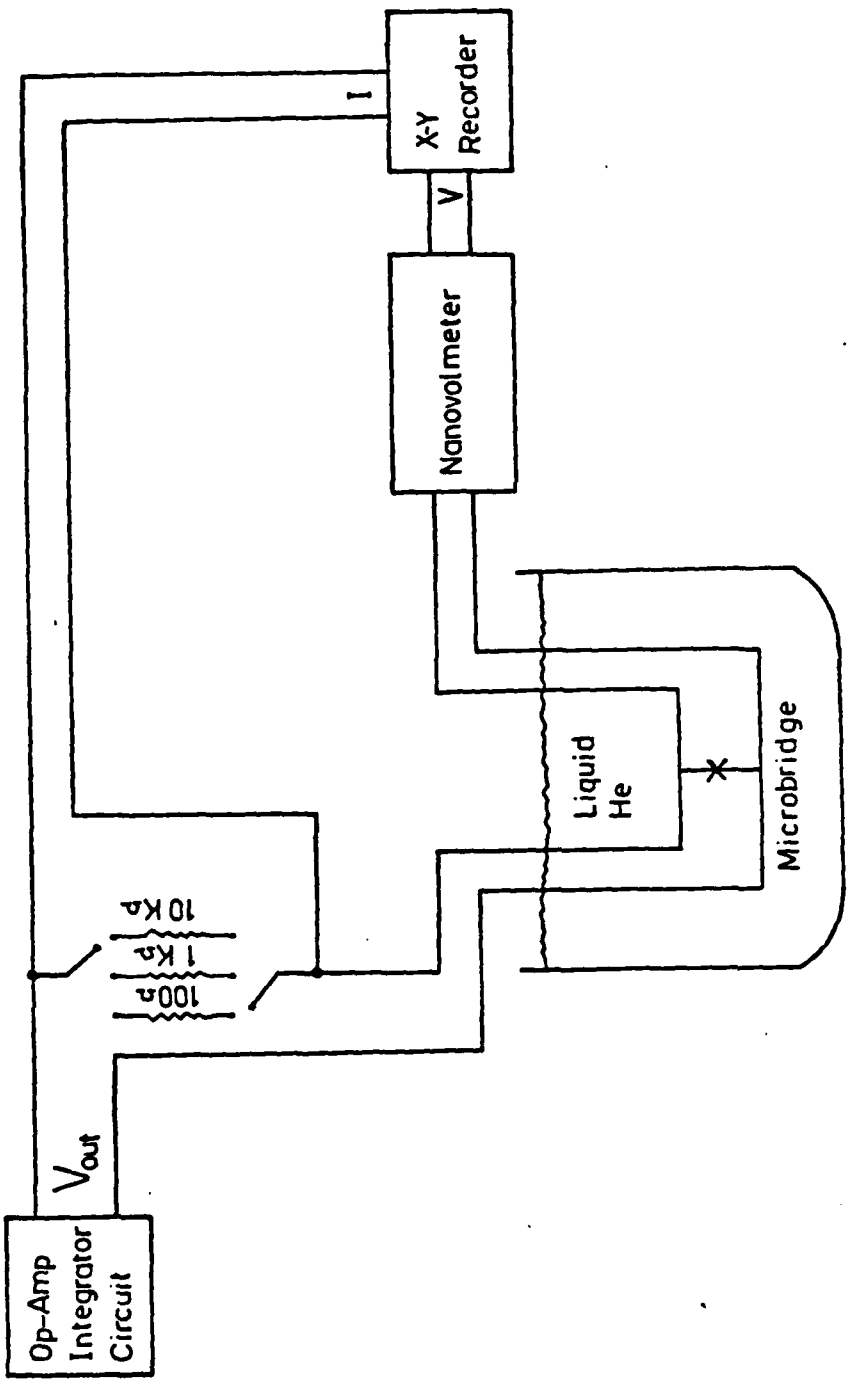

Figure III.11.Schematic diagram of the experimental set-up used to measure I-V curves.

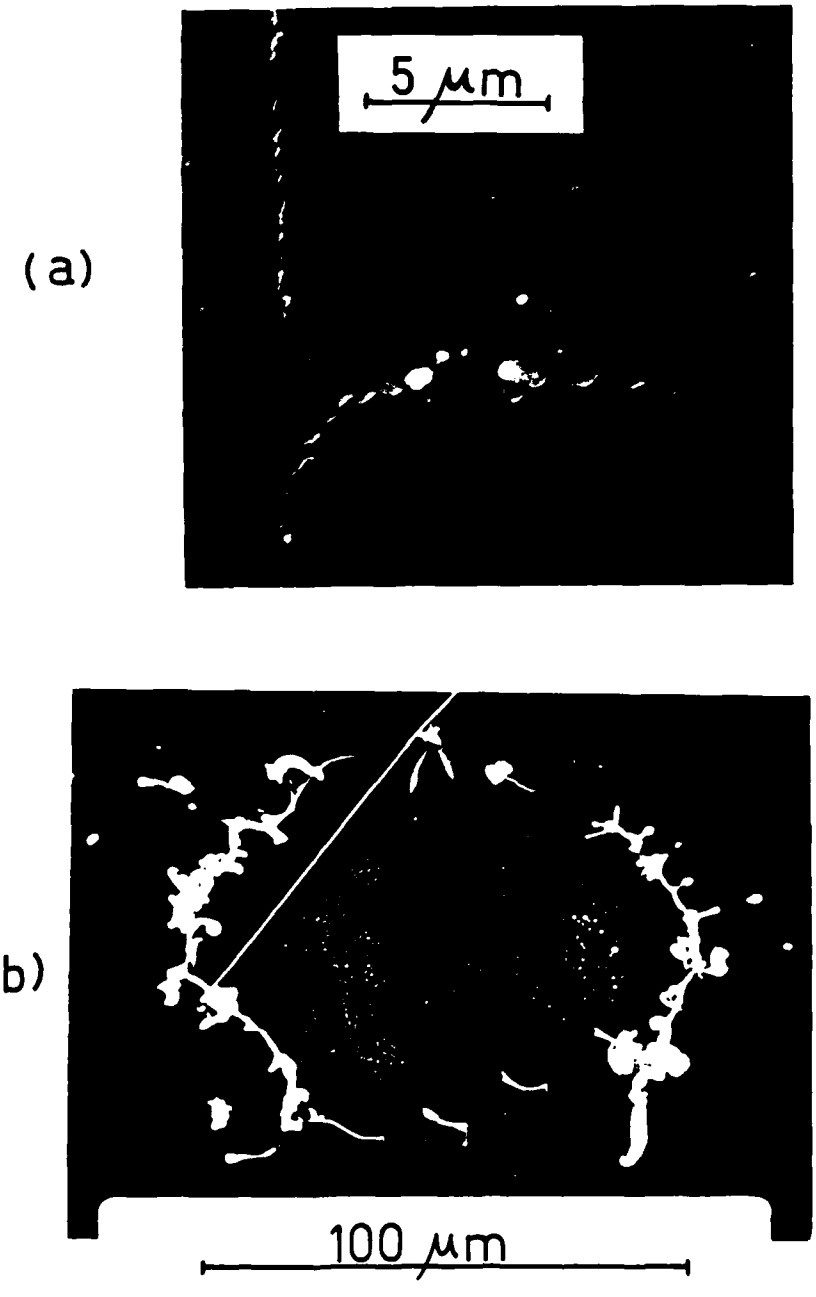

Figure III.12.SEM picture of burnt-out microbridges. The fiber in (b) is a whisker crystal that grew out of the film which had been stored for more than a year before this picture was taken.

micrographs, and the mean free path was obtained from the resistivity ratio, using the resistivity of tin at room temperature[58] $\rho = 11.5 \mu\Omega\,cm$ and the value of the product[59] $\rho\ell = (1.05 \pm 0.08) \times 10^{-5} \mu\Omega cm^2$. The GL coherence length $\xi(T)$ is calculated using the relations

$$\xi(T) = \xi(0)(1-T/T_c)^{-1/2} \qquad \text{(III.1)}$$

$$\xi(0) = 0.74\,\xi_o(1+0.75\,\xi_o/\ell)^{-1/2} \qquad \text{(III.2)}$$

where ℓ is the mean free path and ξ_o is the BCS coherence length. In tin[60,61], $\xi_o = 2300$ Å.

Equations III.1 and III.2 are derived from [62]

$$\xi(T) = \frac{\pi\xi_o}{2\sqrt{3}} \frac{H_c(0)}{H_c(T)} \frac{\lambda_L(0)}{\lambda_{eff}(T)} \qquad \text{(III.3)}$$

λ_{eff} is the modified London penetration depth to take into account the effect of the impurities and close to T_c is given by

$$\lambda_{eff}(T) = \lambda_L(T)(1+0.75\,\xi_o/\ell)^{1/2} \qquad \text{(III.4)}$$

TABLE III.1.SOME PHYSICAL PROPERTIES OF SAMPLES OF TYPE S AND SAMPLES OF TYPE T.

SAMPLE	NORMAL METAL PROBE	WIDTH [μm]	THICKNESS [Å]	MEAN-FREE PATH [Å] AT T=4.2K	RESISTIVITY RATIO	BRIDGE RESISTANCE AT T=4.2K [Ω]	RESISTANCE OF TUNNEL JUNCTIONS C,L,D,M [Ω]
S-1 (type S)	-----	1.3	1010	2400	26	1.0	-------
TN-1 (type T)	In	2.1 0.7*	1020	1200	13	2.8	29 ,27,26,29
TN-2 (type T)	Ag	2.4 1.2*	1090	1800	20	0.70	47,49,50,53
TU-1 (type T)	Ag	2.4	1080	800	9	1.3	12,2.4,4.1,6.6

*width of the middle segment

TABLE III.2. SOME PHYSICAL PROPERTIES OF SAMPLES OF TYPE M SHOWING JOSEPHSON STEPS

SAMPLE	LENGTH [μm]	WIDTH [μm]	THICKNESS [μm]	RESISTIVITY RATIO	MEAN-FREE PATH [μm] AT 4.2 K	COHERENCE LENGTH ξ(0) [μm]	$\frac{dJ_c}{dT}\left[\left(\frac{\mu A}{\mu m^2}\right)^{2/3}\frac{1}{mK}\right]$	JOSEPHSON STEPS
M-D2**	4.0	≅1.0	0.102	9	0.082	0.095	-------	n=1/2,1,2
M-9++	7.4	3.2	0.135	16	0.146	0.115	1.3	n=1
M-12+	5.5	≅1.0	0.100	32	0.291	0.135	-------	n=1/2,2/3, 3/4,1,4/3, 3/2,2,3,4
M-15+	7.8	1.0	0.110	23	0.209	0.126	1.5	n=1,2
M-19+	5.5	1.2	0.106	17	0.155	0.117	1.4	n=1
M-21+	10.4	2.1	0.107	23	0.209	0.126	2.2	n=1
M-23+	36	2.0 1.0#	0.110	31	0.282	0.134	2.1	n=1
M-29+	4.6	1.2	0.118	19	0.173	0.121	1.8	n=1/3,1,2,3

\# width of narrow segment
** samples made in "old" evaporator
\+ samples made by oblique evaporation
++ samples made using a photoresist stencil treated with chlorobenzene
MD-2 was made using a diamond knife
MD-2 and M-12 have variable width and J_c is not proportional to $(1-T/T_c)^{3/2}$

CHAPTER IV

RESULTS AND DISCUSSION

IV.1. SAMPLES OF TYPE S: INTERACTING PHASE-SLIP CENTERS

We examined the I-V characteristics of each of the five segments of the bridge. The current was sequentially applied between consecutive probes and the voltage measured between the same pair of probes (for example, C to L). Figure IV.1 shows a set of I-V curves taken in this way for each of the five segments of sample S-1. The first voltage step in each of the I-V curves corresponds to the appearance of a phase-slip center in the microbridge and the other voltage steps correspond to PSCs in the probes. We took the same set of I-V curves while measuring the voltage between the ends of the bridge (leads A and B) in order to check that the first voltage jumps occur in the bridge. We notice that the critical current of the probes is more than twice the critical current of the microbridge, as expected since the probes are about twice as wide as the microbridge.

For each segment we have measured the critical current at different temperatures and we have found that it follows the relation $I_c \propto (1-T/T_c)^{3/2}$ predicted by the Ginzburg-Landau theory. The extrapolation to $I_c=0$ in the graph of $I_c^{2/3}$ versus T is the mean-field critical temperature T_c. The results (with precision of $\pm$1mK) for successive segments AC, CL, LD, DM, and MB of the sample S-1 are T_c= 3.757, 3.745, 3.744, 3.746 and 3.746 K, respectively. In the same order, the slopes of $J_c^{2/3}$ versus T for each segment are 1.9, 1.9, 2.2, 2.3, and 2.1 $(\mu A/(\mu m)^2)^{2/3}(mK)^{-1}$.

We have studied the interaction of a PSC in one segment of the

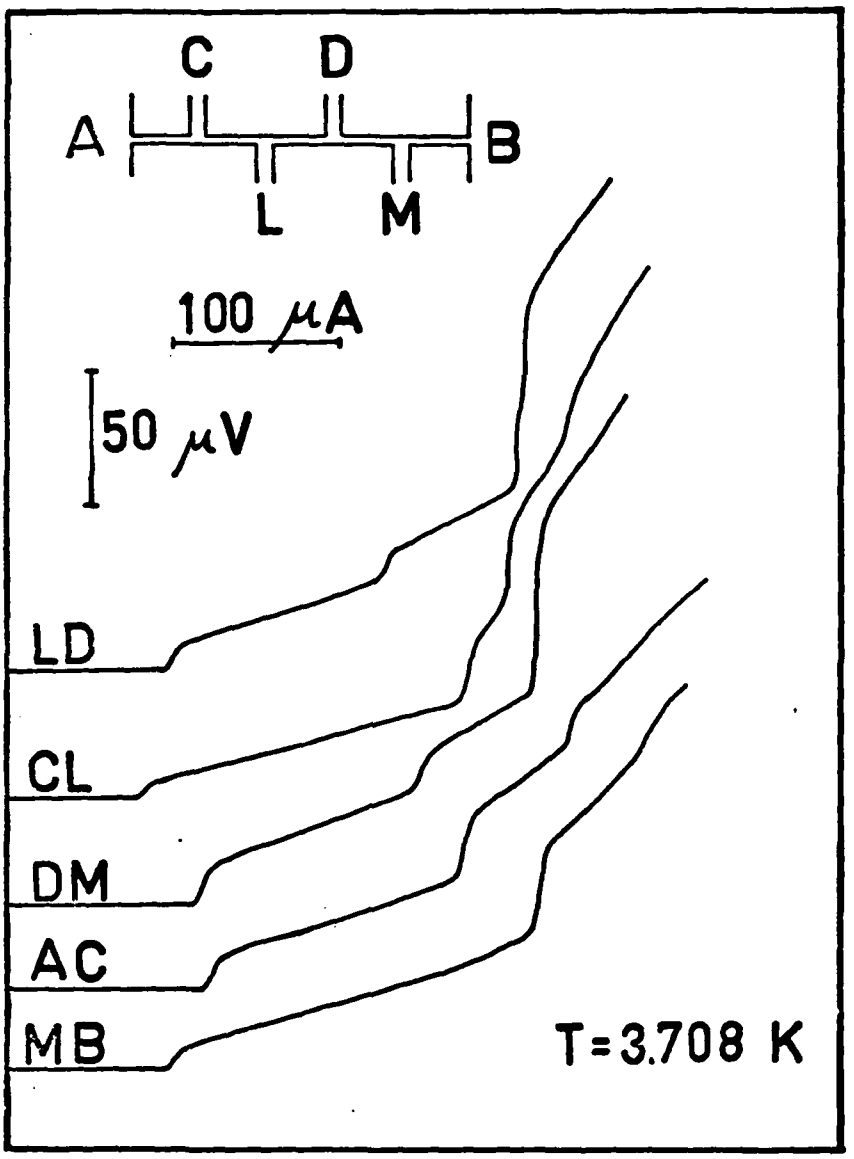

Figure IV.1.I-V characteristics of each one of the five segments of sample S-1. Variations in I_c along the bridge are due to imperfections such as nonuniform width. The inset shows the sample geometry.

microbridge with PSCs in the other segments of the same microbridge. Consider, for example, the effects that a PSC in segment LD has on the appearance of a PSC in segment CL. We measured the I-V characteristic of segment CL with no current flowing in segment LD (figure IV.2, curve I(LD)=0). We also measured the same I-V for fixed values of I(LD)≠0. No effect is seen as long as I(LD) is less than the critical current of the segment LD. For larger values of I(LD) we see a change in the (apparent) critical current of CL. The critical current of CL is increased or decreased depending on whether the current in the two segments is flowing in the same direction or in opposite directions, respectively.

We notice that for the same value of I(LD), the magnitude of the change of I_c(CL) is not the same in both biasing directions. This is because the heat generated in LD tends to decrease the critical current of CL (by increasing its temperature), independent of the relative direction of the current. (The large voltage step in the I-V curves for the case of current flowing in opposite directions result from the breakdown of superconductivity in probe L, where I(LD) and I(CL) add constructively).

In the same way that Jillie[9] did with his interacting short microbridges, we decomposed the change of the critical current of each segment ΔI_c, into a symmetric (even) part, ΔI_c^s, and an antisymmetric (odd) part ΔI_c^a. Here the symmetry refers to the effect of the relative directions of the current in the source and detector segments.

We define $I_n(0)$ as the value of the normal current at the center of

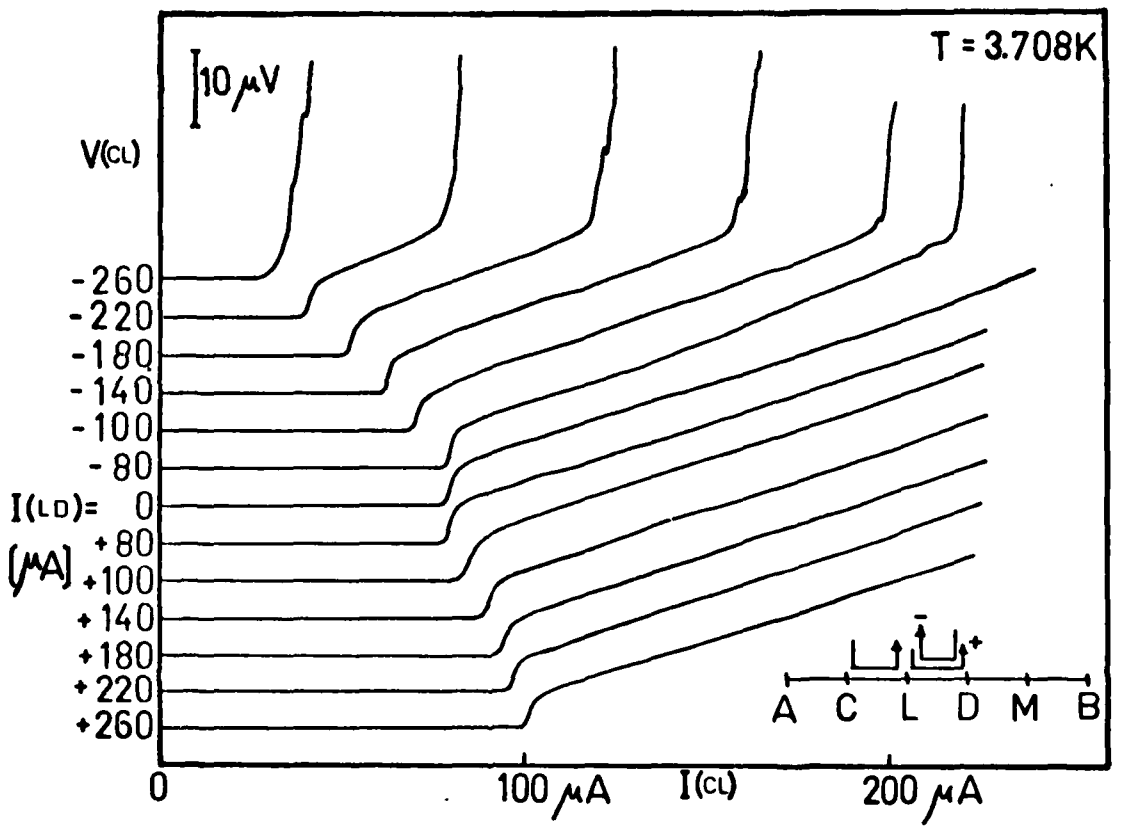

Figure IV.2. I-V characteristics of the segment CL of the sample S-1 taken for different fixed values of the current through the segment LD. (+) or (-) correspond to the cases when the current in the two segments flow in the same or in opposite directions, respectively.

the phase-slip center (source). This normal current is a fraction of the total current and can be measured directly from the I-V curves. Following the SBT model[3], we take $I_n(0)$ to be equal to the voltage across the PSC divided by the differential resistance of the PSC in the linear region. In segment LD we have found that $I_n(0)=I(LD)-0.60I_c(LD)$, which is very close to the SBT prediction $I_n(0)=I-0.65I_c$. Similar results were found in other segments.

In figure IV.3 we have plotted $\Delta I_c^s(CL)$ and $\Delta I_c^a(CL)$ as a function of $I_n(0)$ in segment LD. Since the presence of a PSC in CL reacts back on the PSC in LD, for each point in figure IV.3 we have determined this $I_n(0)$ from the voltage measured across LD just at the threshold for a voltage to develop in the I-V curve of CL at the (shifted) $I_c(CL)$.

First, I will discuss the antisymmetric, "heating-independent" part, caused by the quasiparticles generated in the phase-slip center in LD that diffuse into CL. This causes the magnitude of the supercurrent to change in order to maintain the total current through CL equal to the external applied current. Consequently, for a fixed value of total current through CL (before the appearance of a phase-slip center in CL), the supercurrent will be smaller (or larger) than the current applied, producing an increase (or decrease) of the apparent critical current of CL. This change is equal in magnitude to the value (measured at CL) of the quasiparticle diffusive current generated in LD. Therefore, the value of the slope of $\Delta I_c^a(CL)$ versus $I_n(0)$ gives the fraction f(x) of the quasiparticle current generated in LD that reaches the segment CL.

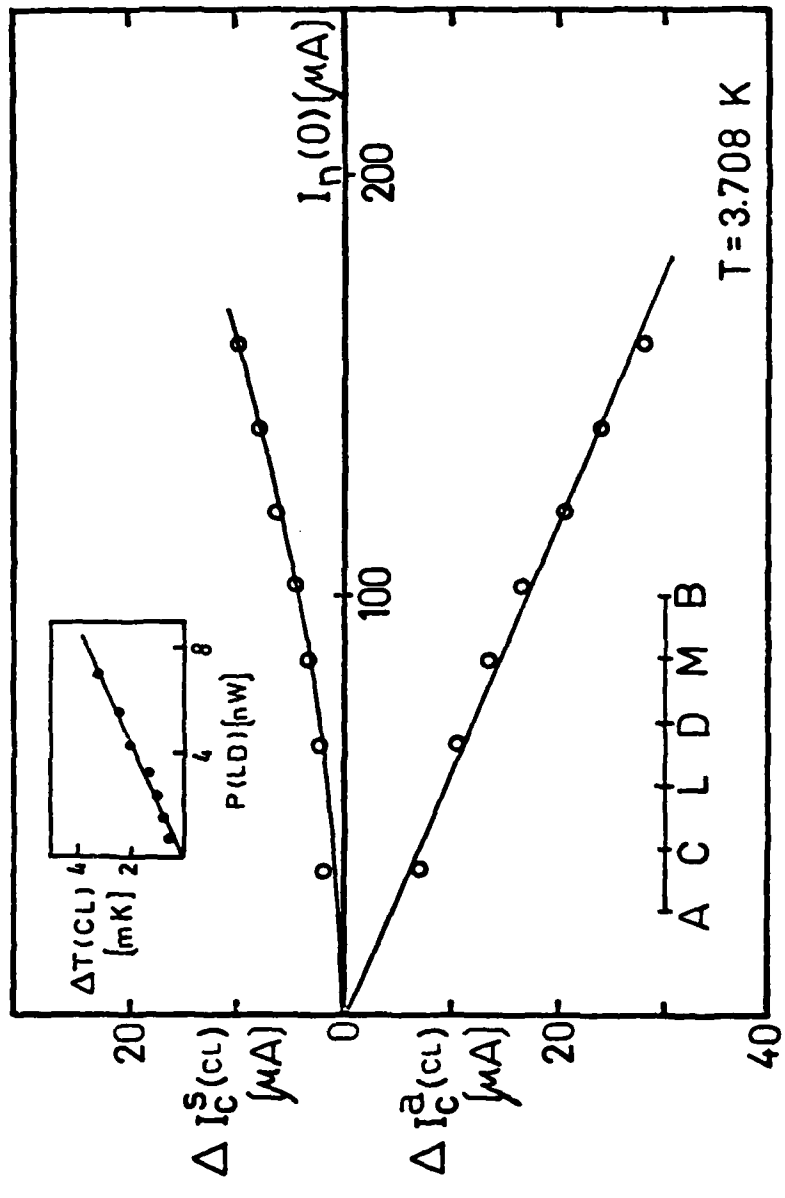

Figure IV.3. Symmetric ΔI_c^s and antisymmetric ΔI_c^a parts of the change of the critical current of CL of the sample S-1 as a function of the quasiparticle current in the center of the phase-slip center in LD. The inset shows the linear temperature rise at CL as a function of the power dissipated in LD.

In a uniform filament, this fraction should be equal to $\exp(-x/\Lambda_{Q^*})$, where x is the distance between the phase-slip center source and the detector. Our geometry is more complicated since we have to take into account the effects of the probes, which provide another channel into which the quasiparticles can diffuse, causing a more rapid decrease in f(x) from one observation point to the next. The effect of the phase-slip center in DM on the critical current of CL is shown in figure IV.4. The I-V curves of CL were taken for different fixed values of I(DM).

Figure IV.5 shows the results for f(x) at T=3.708K. By definition, f(x=0)=1 at the sources, and it decays with distance. The dotted straight lines are guides to the eye. However, their parallelism is consistent with the assumptions that Λ_{Q^*} is about the same everywhere along the bridge and that the same fraction of quasiparticle current is lost by diffusion into each of the four probes C, L, D, and M, so that f(x) falls in geometric progression from point to point. The horizontal error bars indicate the uncertainty in our knowledge of the exact location of the core of the phase-slip center in each segment.

In order to obtain a value for the diffusion length Λ_{Q^*} from the data shown in figure IV.5, it is necessary to know what fraction of quasiparticle current is lost to the probes. This can be determined theoretically by solving the steady-state diffusion equation for the charge imbalance

$$\nabla^2 Q^* = \frac{Q^*}{\Lambda^2_{Q^*}} \qquad \text{(IV.1)}$$

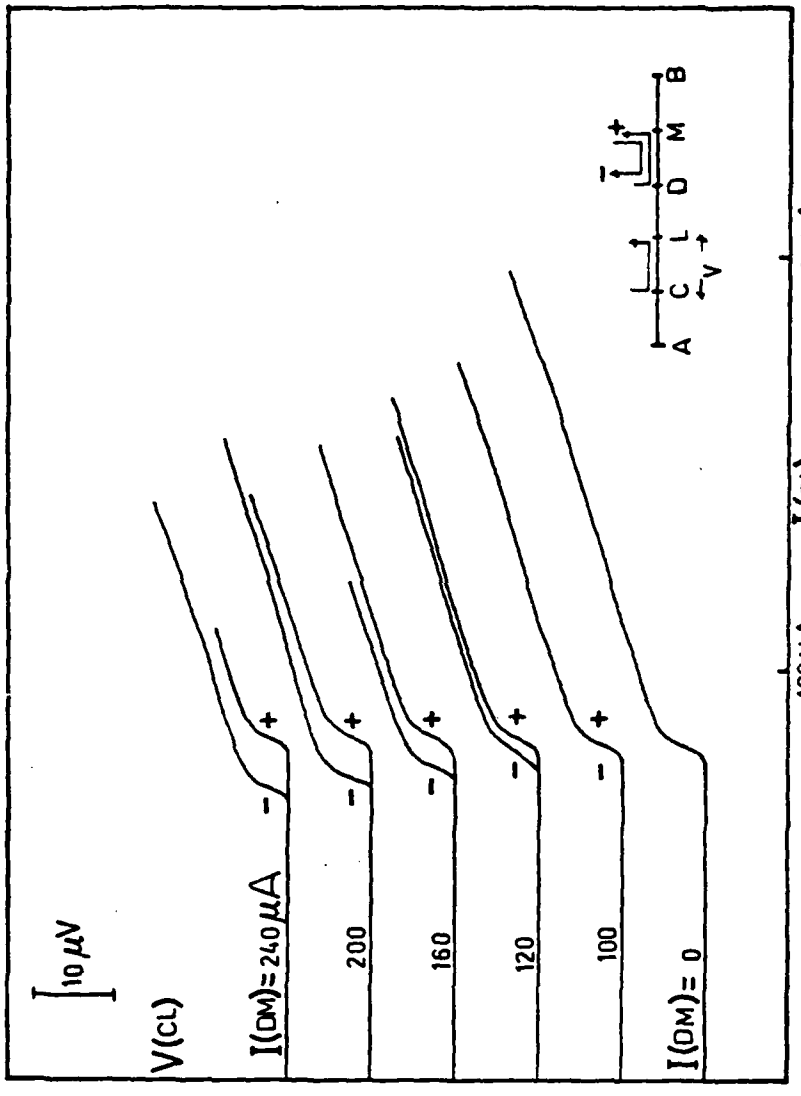

Figure IV.4.I-V characteristic of the segment CL of sample S-1 taken for different fixed values of the current through DM. (+) or (-) correspond to the cases when the current in the two segments flow in the same or in opposite directions, respectively.

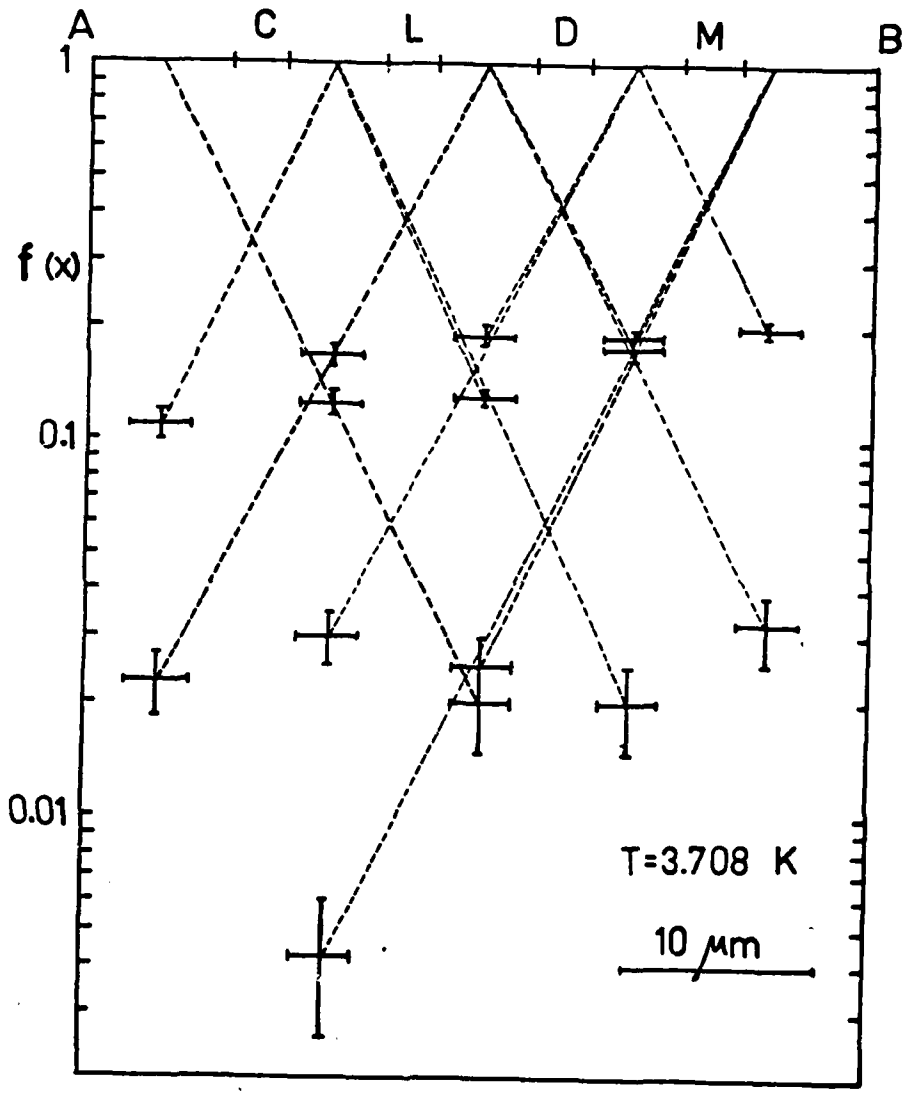

Figure IV.5. Decay with distance from the source of the surviving fraction of quasiparticle current generated in phase-slip centers in the sample S-1. See text for details.

This diffusion equation for Q* is the dc limit of the more general charge imbalance equation derived earlier[10].

We have solved this diffusion equation numerically for the particular geometry of sample S-1 and have calculated the diffusion current along the bridge, normalized to its value at the center of the phase-slip center. We solved this problem in the case when the phase-slip center is in the segment LD of the bridge and also when the phase-slip center is in the segment MB. We compared the results for different values of Λ_{Q^*} with the data and found that the best fit is for $\Lambda_{Q^*}=(6.0\pm 1.0)\mu m$. These data were taken at T=3.708K, corresponding to $1-T/T_c=0.01$. Using the literature values[63], $v_F=0.65\times10^8$ cm/sec and[59] $\rho\ell=1.05\times10^{-5}\mu\Omega\cdot cm^2$, we infer that for sample S-1 the mean free path $\ell=24\times10^{-6}$ cm and that the measured value of Λ_{Q^*} at $T/T_c=0.99$ corresponds through equation (II.9) to

$$\tau_{Q^*}=\frac{3\Lambda^2}{v_F\ell}Q^* = (7\pm 2)\times10^{-10}\text{sec}$$

Near T_c, τ_{Q^*} is expected[13,14,15] to vary as $(1-T/T_c)^{-1/2}$, this implies that our measured value corresponds to

$$\tau_{Q^*} = (0.7\pm 0.2)\times(1-T/T_c)^{-1/2}\times10^{-10}\text{ sec}$$

or

$$\tau_{Q^*} = (1.2\pm 0.4)\,\Delta(0)/\Delta(T)\times10^{-10}\text{ sec}$$

Although our method is entirely different, this result is in excellent agreement with the value obtained by Clarke and Paterson[63] by tunnel injection technique.

We turn now to the symmetric change of the critical current of the detector PSC, to confirm that it can be accounted for by the heat generated in the source PSC. We can estimate the temperature rise (ΔT) in the detector for a given power generated at the source by measuring ΔI_c^s and then using the graph I_c (of the detector) versus T to determine the temperature rise in the segment CL, $\Delta T(CL)$, caused by the phase-slip center in the segment LD. The inset in figure IV.3 shows the dependence of $\Delta T(CL)$ on the power dissipated in LD, P(LD). The data points fall on a straight line, the slope of which corresponds to a temperature rise in CL of 0.46mK per each nW of power dissipated in LD. The curve ΔI_c^s versus $I_n(0)$ in figure IV.3 , calculated using this ratio, gives an excellent fit. We now check whether this fitted value for $\Delta T/P$ is reasonable.

According to the SBT model[3], the temperature rise at the center of the PSC, for power dissipation IV, is

$$\frac{\Delta T}{IV} = \frac{1}{(2\eta + \Lambda_{Q^*})\alpha w} \qquad \text{(IV.2)}$$

where $\eta = (Kd/\alpha)^{1/2}$ is the thermal healing length, K is the thermal conductivity of the metal, α is the heat transfer coefficient (to the helium bath and to the substrate) per unit area, and w and d are the width and the thickness of the microbridge. The expression (IV.2) was derived for a one-dimensional filament and can not be compared directly with our experimental result since the sample S-1 has a more complicated geometry.

In order to estimate the magnitude of η and α, we have to solve the equation governing ΔT in the sample S-1 and then compare with our experimental result. Outside the source, this equation has the same form (see reference 64) as the diffusion equation for Q*, the only change being replacement of Λ_{Q^*} by η. Therefore, we can use our numerical solution of the diffusion equation to estimate the temperature rise at different points in the microbridge for different values of with the boundary condition that $dT/dx = (2Kdw)^{-1}P(LD)$ at the center of the PSC. The thermal conductivity can be calculated from ρ by use of the Wiedemann-Franz law $K = \pi^2 k_B^2 T/3e^2\rho$. For the sample S-1, K=0.22 watt/K cm at T_c.

We found that our temperature rise data correspond to a thermal healing length $\eta = (12 \pm 1)\,\mu m$ and a heat transfer coefficient $\alpha = (1.5 \pm 0.2)$ watt/K cm^2. This value is consistent with the experimental values obtained by Skocpol[64,55]. He found that for tin films on glass or sapphire substrates and in vacuum or in direct contact with the normal helium bath, the values of α fall in the range 1.0 to 3.5 watt/K cm^2.

The small temperature rise in the microbridge slightly affects the magnitude of the antisymmetric interaction, since Λ_{Q^*} is a temperature-dependent parameter. We observed this effect in the data points of $\Delta I_c^a(CL)$ in figure IV.3. Those points do not fall exactly on a straight line, but instead, they follow a curve with slightly increasing slope as the current through LD increases. This variation is small and it is reflected in the error bars in figure IV.5, and it is

also included in the quoted uncertainty in the value for Λ_{Q^*}. The straight line in figure IV.3 is an average of all points including the origin.

Another effect that should be taken into account is the depression of the gap due to the presence of a phase-slip center, as observed experimentally by Skocpol and Jackel[41]. However, this effect relaxes exponentially within a coherence length, which for sample S-1 is equal to 1.3μm at T=3.708 K. If we assumed that the gap went to zero at the core of the phase-slip center in LD, the value of the gap at the middle of CL would be $\Delta(x=7.8\mu m)=\Delta_\infty(1-e^{-7.8/1.3})=0.998\Delta_\infty$ and the decrease in the critical current of CL due to this effect alone would be less than 1%. This is, of course, very small compared with the measured $\Delta I_c^s(CL)$. Therefore we can conclude that the heat generated in the phase-slip center source is mainly responsible for the symmetric change ΔI_c^s in the detector.

IV.2.SAMPLES OF TYPE T:

IV.2.1.MEASUREMENTS OF THE NONEQUILIBRIUM POTENTIAL

In our experiments with samples of type T, the current is applied along the microbridge and the voltage is measured between each normal probe and one end of the microbridge. When the current exceeds the critical current of the weakest point, a phase-slip center is formed. In samples with a narrow segment, like the one shown in figure III.3, the first PSC nucleates in that segment. In the set of I-V curves shown in figure IV.6 we can see that the biggest voltage drop occurs between probes L and D.

On either side of the core of the PSC, where it makes a "step" change, the potential of the pairs is constant (see figure II.1). Therefore, the voltage measured is the potential difference between the pairs and the quasiparticles $(\mu_n-\mu_s)/e$. This difference is related to the current density J_n in the following way: $\vec{J}_n \propto \vec{\nabla}(\mu_n-\mu_s)$.

Equations (II.11), (II.12) and (II.13) show that in a uniformly wide filament, J_n and $(\mu_n-\mu_s)$ decay exponentially with the same characteristic length Λ_{Q^*}. In order to observe this exponential decay, our data must be corrected for the fact that the middle segment of the microbridge is narrower than the rest. Suppose, for example, that the width of the middle segment is equal to 1/N times the width of the rest of the bridge; then for a given current, the voltage drop in that segment would be N times larger than the voltage drop in the same segment if the bridge were uniformly wide. We made that correction in analyzing the data from samples TN-1 and TN-2. Figure IV.7 shows the results for sample TN-2 before and after such correction was made. We

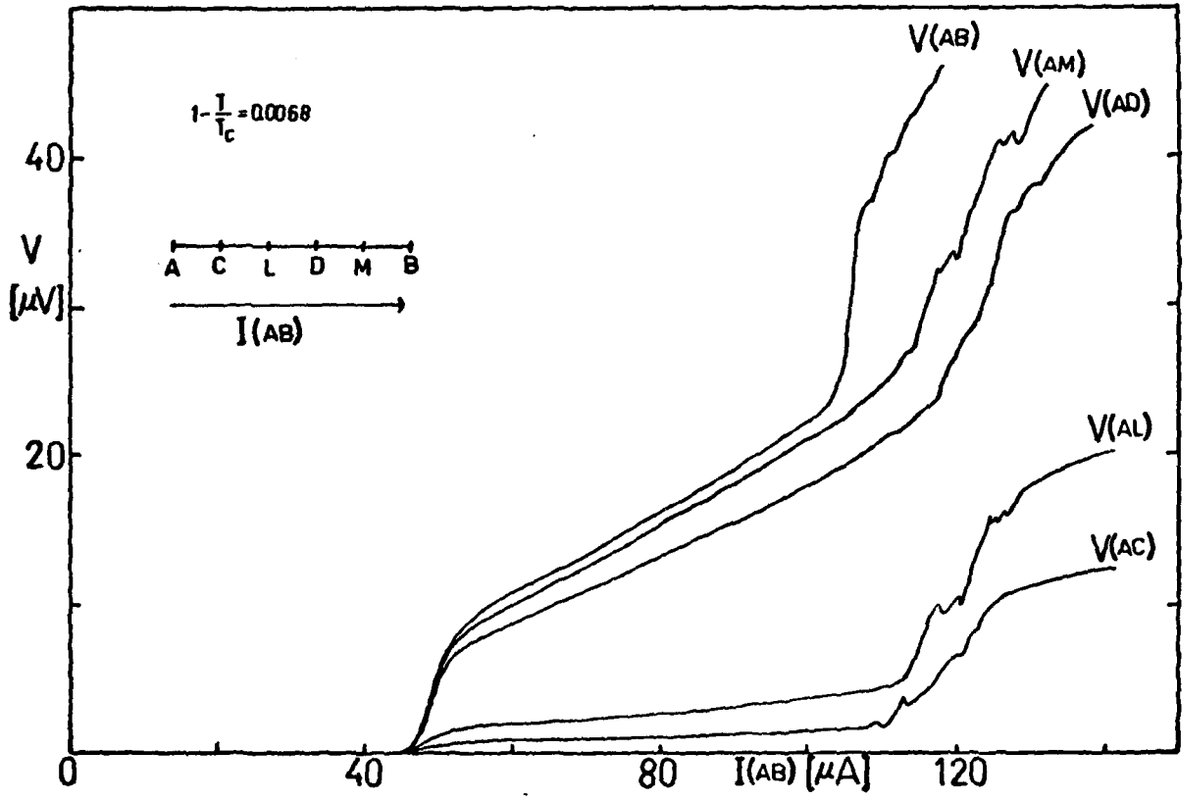

Figure IV.6.Set of I-V curves of sample TN-2. The current is applied between the ends of the microbridge (A and B) and the voltage is measured between A and each one of the normal probes C, L, D, and M and also between A and B.

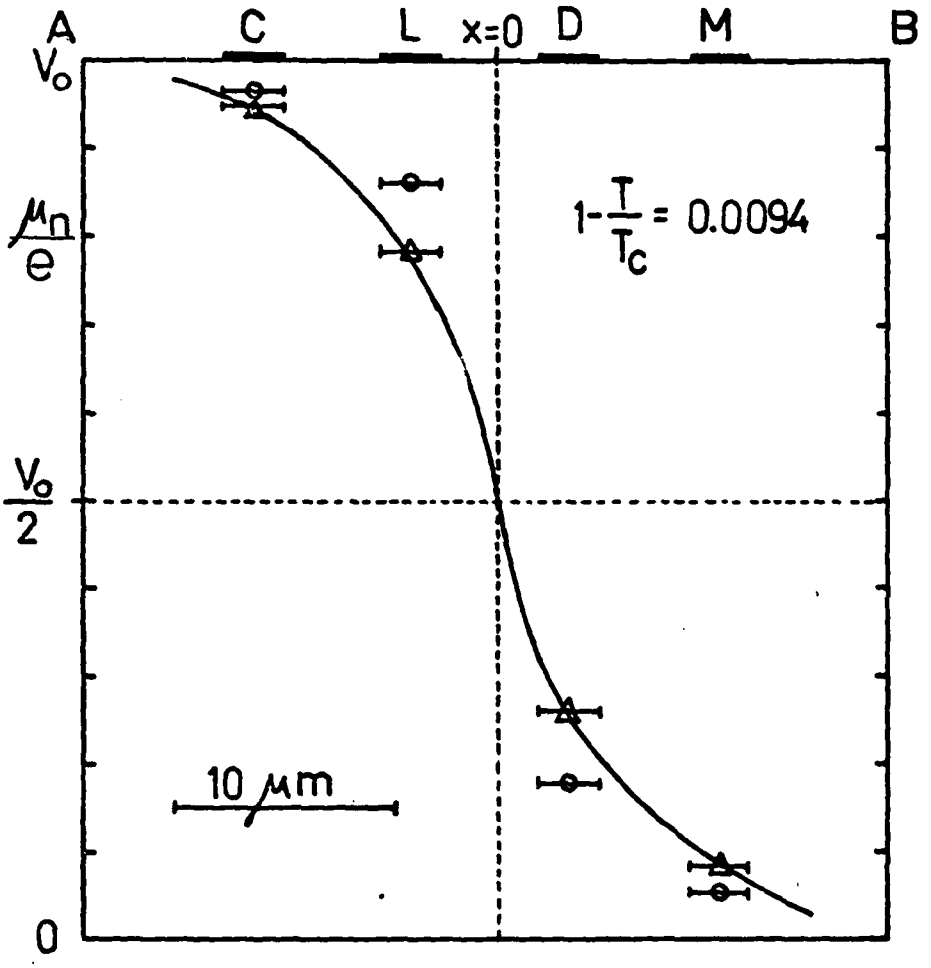

Figure IV.7. μ_n/e versus tunnel probe position for sample TN-2. The circles represent the raw data. The triangles represent the data after the geometrical correction was made. Reference potential is μ_s to the right of the PSC location.

chose x=0 at the point where the voltage drop is half the total voltage drop between the ends of the microbridge. The horizontal error bars indicate the size of the normal probes. By making $x_1=0$ in equations (II.11) and (II.12), we can write

$$\frac{(\mu_n-\mu_s)}{e} = \frac{V_o}{2} e^{-x/\Lambda_{Q^*}} \qquad (x>0) \qquad (IV.3)$$

and

$$\frac{(\mu_n-\mu_s)}{e} = -\frac{V_o}{2} e^{x/\Lambda_{Q^*}} \qquad (x<0) \qquad (IV.4)$$

where V_o is the total voltage drop between the ends of the bridge. To test these predictions, in figures IV.8 and IV.9 we plot log v(x), where $v(x)=2|\mu_n-\mu_s|/eV_o$, as a function of x, for samples TN-2 and TN-1, respectively. The straight lines show that the decay is in fact exponential. The slope of those lines is a direct measure of the diffusion length of the quasiparticle charge Λ_{Q^*}.

In sample TU-1, without constriction, the first phase-slip center appeared in segment MB. Figure IV.10 shows a plot of log v(x) as a function of x for $x<0$. No geometrical correction was necessary since TU-1 has uniform width.

We have studied the temperature dependence of Λ_{Q^*} for samples of type T and found that Λ_{Q^*} diverges at the critical temperature. We have fitted Λ_{Q^*} to the expected form $\Lambda_{Q^*}(T)=\Lambda_{Q^*}(0)(1-T/T_c)^{-1/4}$ and the corresponding τ_{Q^*} to the expression $\tau_{Q^*}(T)=\tau_{Q^*}(0)(1-T/T_c)^{-1/2}$. In table IV.1 a list is shown of our results for $\Lambda_{Q^*}(0)$ and $\tau_{Q^*}(0)$ for our samples. In order to facilitate comparison with Clarke's results,

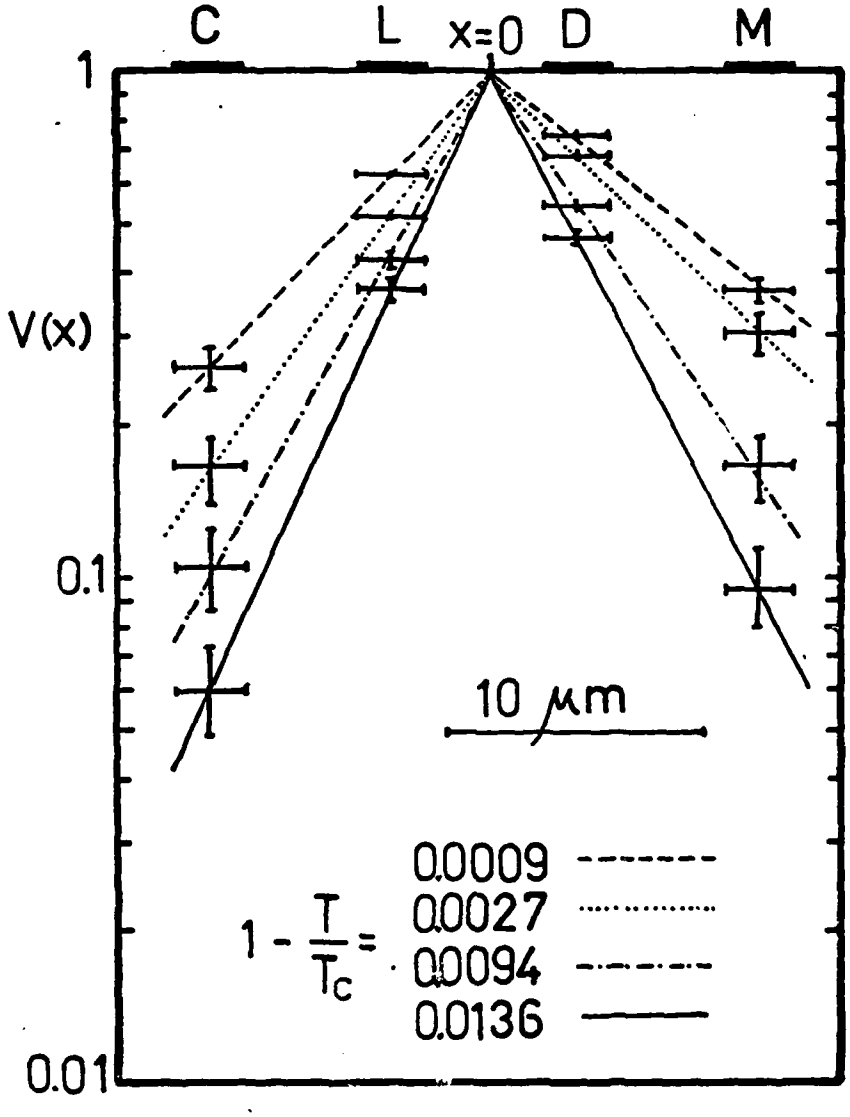

Figure IV.8. Semilog plot of the normalized quasiparticle potential versus tunnel probe position in sample TN-2. v(x) is defined in the text.

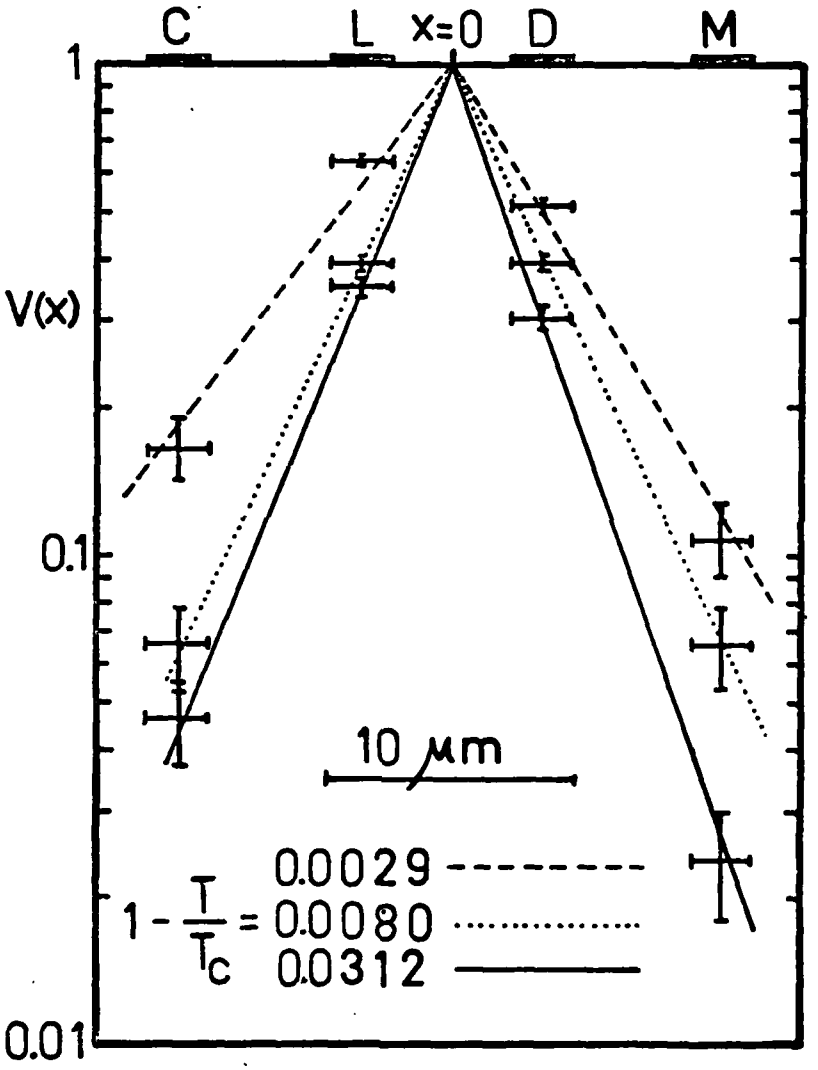

Figure IV.9. Semilog plot of the normalized quasiparticle potential versus probe position in sample TN-1. v(x) is defined in the text.

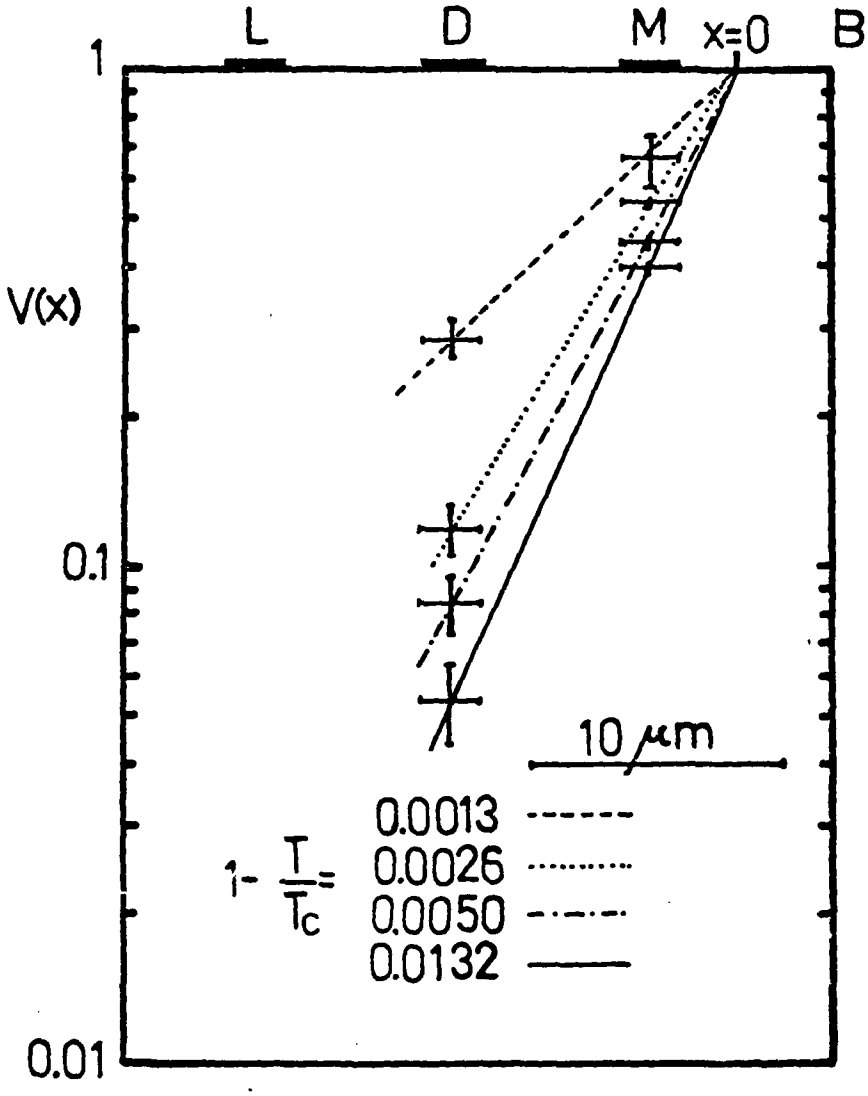

Figure IV.10.Semilog plot of the normalized quasiparticle potential versus probe position in sample TU-1. v(x) is defined in the text.

we have also quoted our results in the form $\tau_{Q*}\Delta(T)/\Delta(0)$, using the relation[65] $\Delta(T)/\Delta(0) \simeq 1.74(1-T/T_c)^{1/2}$, near T_c.

The values of $\tau_{Q*}(T)\Delta(T)/\Delta(0)=1.74\,\tau_{Q*}(0)$ listed in table IV.1 agree extremely well with the value obtained for the sample S-1, $\tau_{Q*}\Delta(T)/\Delta(0)=(1.2\pm0.4)\times10^{-10}$ sec and with the value $\tau_{Q*}\Delta(T)/\Delta(0)=(1.0\pm0.2)\times10^{-10}$ sec obtained by Clarke[63] for tin samples very close to T_c in experiments where a nonequilibrium quasiparticle population had been created by current injected through a tunnel barrier.

Very close to T_c, τ_{Q*} can be written as[13,14,15]:

$$\tau_{Q*} = \frac{4k_BT_c}{\pi\Delta(T)}\tau_E = 0.73\ \frac{\Delta(0)}{\Delta(T)}\tau_E \qquad \text{(IV.5)}$$

where τ_E is the inelastic phonon scattering time at T_c. Using our experimental results from all our samples, our value for τ_E in tin is $(1.6\pm0.4)\times10^{-10}$ sec, in excellent agreement with Clarke's[63] result, $\tau_E=(1.4\pm0.2)\times10^{-10}$ sec.

We have found that a slightly better fit of our data is obtained for values of n slightly larger than 1/4, where n is the exponent in the expression $\Lambda_{Q*}(T)=\Lambda'_{Q*}(0)(1-T/T_c)^{-n}$. The results for n and $\Lambda'_{Q*}(0)$ for the three samples are listed in table IV.2. In figure IV.11 we show the values of $\Lambda_{Q*}(T)$ obtained from our measurements in sample TN-2. We also show two fits: $\Lambda_{Q*}(T)=1.3\,\mu m(1-T/T_c)^{-0.28}$ plotted as a full line and $\Lambda_{Q*}(T)=1.5\,\mu m(1-T/T_c)^{-0.25}$ plotted as a dashed line. Evidently, the difference between the two fits is very small. For samples TN-1 and

AD-A130 914 PHASE-SLIP CENTERS AND THEIR INTERACTIONS(U) HARVARD UNIV CAMBRIDGE MA DIV OF APPLIED SCIENCES J M APONTE JUN 83 TR-21 N00014-77-C-0085 2/2

UNCLASSIFIED F/G 20/3 NL

END
DATE FILMED
8 83
DTIC

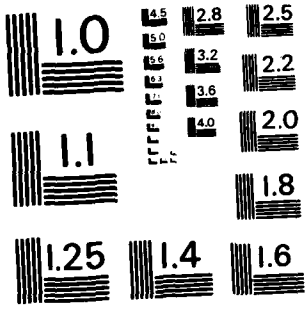

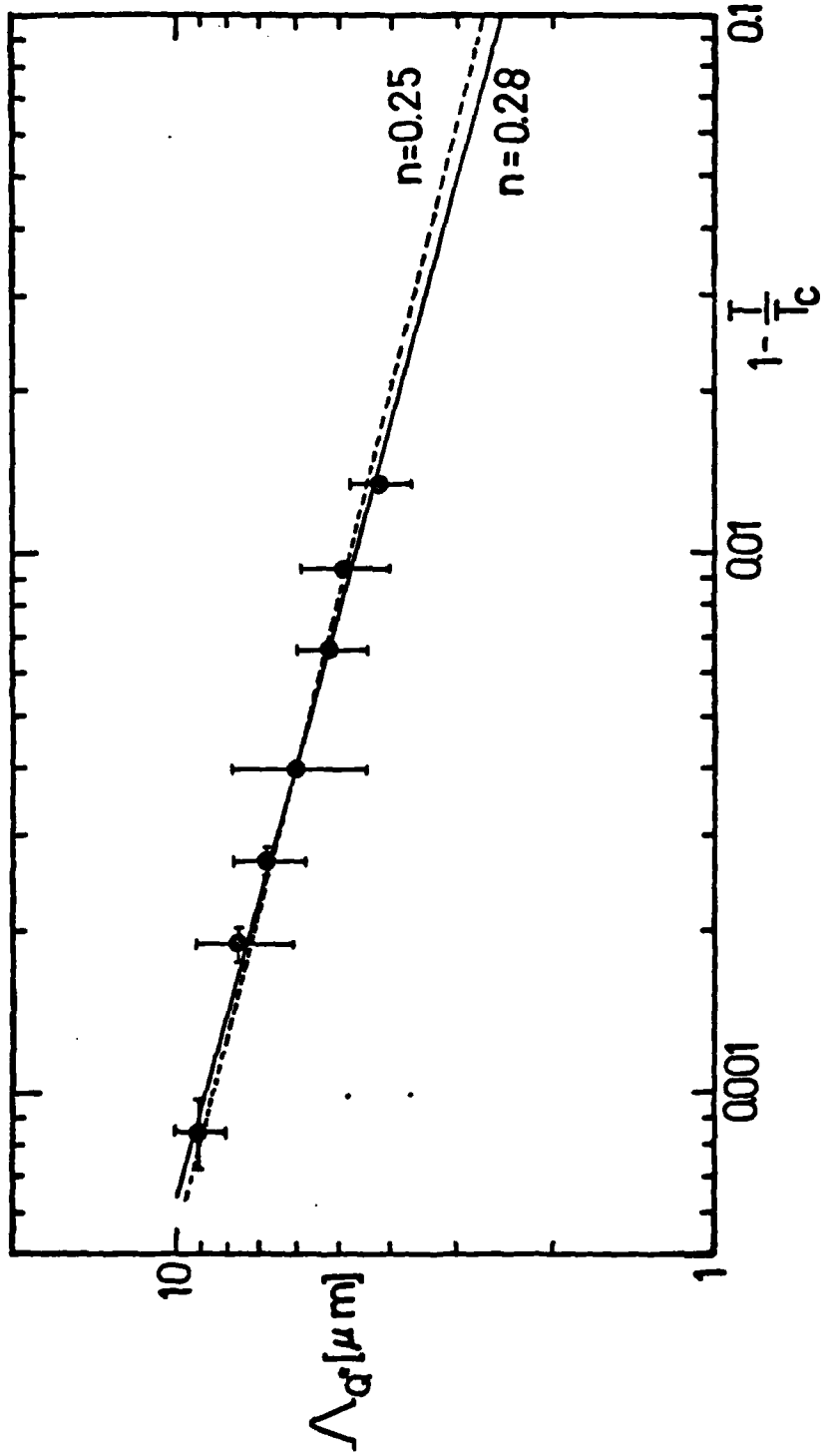

Figure IV.11. Temperature dependence of the quasiparticle diffusion length in sample TN-2. The best fit (full line) for n=0.28 is compared to the expected $(1-T/T_c)^{-1/4}$ divergence (dashed line).

TABLE IV.1. EXPERIMENTAL VALUES OF QUASIPARTICLE CHARGE DIFFUSION LENGTH Λ_{Q^*} AND RELAXATION TIME τ_{Q^*}.

SAMPLE	$\Lambda_{Q^*}(0)[\mu m]$	$\tau_{Q^*}(0)[10^{-10}sec]$	$\tau_{Q^*}(T)\Delta(T)/\Delta(0)[10^{-10}sec]$
TN-1	1.3 ± 0.3	0.7 ± 0.3	1.2 ± 0.5
TN-2	1.5 ± 0.1	0.6 ± 0.1	1.0 ± 0.2
TU-1	1.2 ± 0.2	0.8 ± 0.3	1.4 ± 0.6

TABLE IV.2. BEST VALUES OF n AND $\Lambda'_{Q^*}(0)$ FOR FIT OF OUR DATA TO $\Lambda_{Q^*}(T)=\Lambda'_{Q^*}(0)(1-T/T_c)^{-n}$.

SAMPLE	n	$\Lambda'_{Q^*}(0)[\mu m]$
TN-1	0.27 ± 0.04	1.2 ± 0.3
TN-2	0.28 ± 0.01	1.3 ± 0.1
TU-1	0.26 ± 0.04	1.1 ± 0.2

TU-1, the difference between the best fit and the $(1-T/T_c)^{-1/4}$ divergence is even smaller than for the sample TN-2 and the uncertainties in the values for the exponent n and for $\Lambda'_{Q^*}(0)$ are also bigger in the samples TN-1 and TU-1. Therefore, we are unable to conclude, from these results, that n is actually larger than 1/4. However, if the difference of n from 1/4 is real, it might be a consequence of the finite size and dynamic structure of the core of the phase-slip center as discussed in section II.4 and also of the elastic processes of relaxation[43] of charge imbalance, neither of which is considered in the derivation of equation IV.5. According to Stuivinga et al.[43], in the presence of a supercurrent at the critical value, the relaxation time for the charge imbalance can be written as

$$\tau_{Q^*} = \frac{4k_B T_c}{\pi \Delta(T)} \tau_E (1 + 1/\beta(T))^{-1/2} \qquad \text{(IV.6)}$$

where $\beta(T)$ is defined as

$$\beta(T) = \frac{3\pi}{8} \frac{\hbar}{\tau_E} \frac{1}{k_B T_c} \frac{1}{(1-T/T_c)} \qquad \text{(IV.7)}$$

Taking this effect into account, the diffusion length of the quasiparticle charge will diverge at T_c according to

$$\Lambda_{Q^*} \propto (1-T/T_c)^{-1/4} (1+1/\beta(T))^{-1/4} \qquad \text{(IV.8)}$$

From our experimental results for T_c and τ_E, we found β to be

equal to $1.5\times10^{-2}(1-T/T_c)^{-1}$. In figure IV.12 we have plotted $[(1-T/T_c)(1+1/\beta(T))]^{-1/4}$ and $(1-T/T_c)^{-1/4}$ as a function of $1-T/T_c$. We can see that the stronger temperature dependence of the theoretical Λ_{Q^*} when the effects of the supercurrent are included, showing how this effect can be partially responsible for the deviation from 1/4 of our experimental values of the exponent n.

If we use equations (IV.6) and (IV.7) to fit our data, we will find that the best value for τ_E is slightly larger than the value obtained using equation (IV.5); however, this difference would be less than 10% and in consequence, we take $\tau_E=(1.6\pm0.4)\times10^{-10}$ sec, obtained from equation (IV.5), to be the correct value of the inelastic scattering time of our tin samples. It is also important to point out that in the derivation of equation (IV.6) it is assumed that the supercurrent is position-independent which is not true in a phase-slip center.

IV.2.2.INJECTION EXPERIMENTS

We have injected normal current into the microbridge through the normal probes in samples of type T. We measured the effect of that injected current on the appearance of the first PSC in the microbridge. Figure IV.13 shows a set of I-V curves taken in sample TN-1 for different fixed values of the current injected through D. For $I(DB)=10\mu A$ the voltage across the junction D is $260\mu V$; therefore, the energy of the injected quasiparticles is larger than the energy gap in the microbridge at that temperature. This injected current has the same effect on the critical current of the PSC in LD as the effect of the

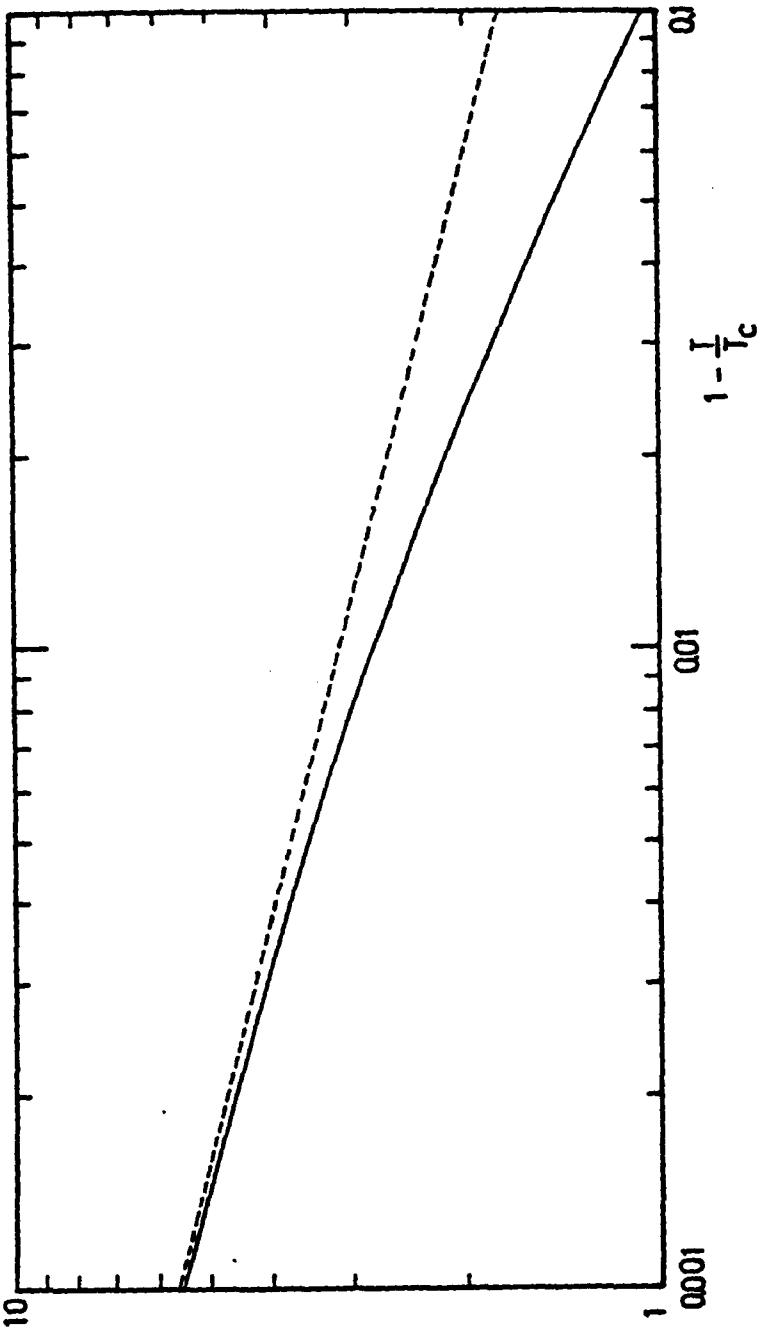

Figure IV.12.Effect of the supercurrent on the relaxation of the quasiparticle charge. The dashed line is $(1-T/T_c)^{-1/4}$. The full line is $[(1-T/T_c)(1+1/\beta(T))]^{-1/4}$. See text for details.

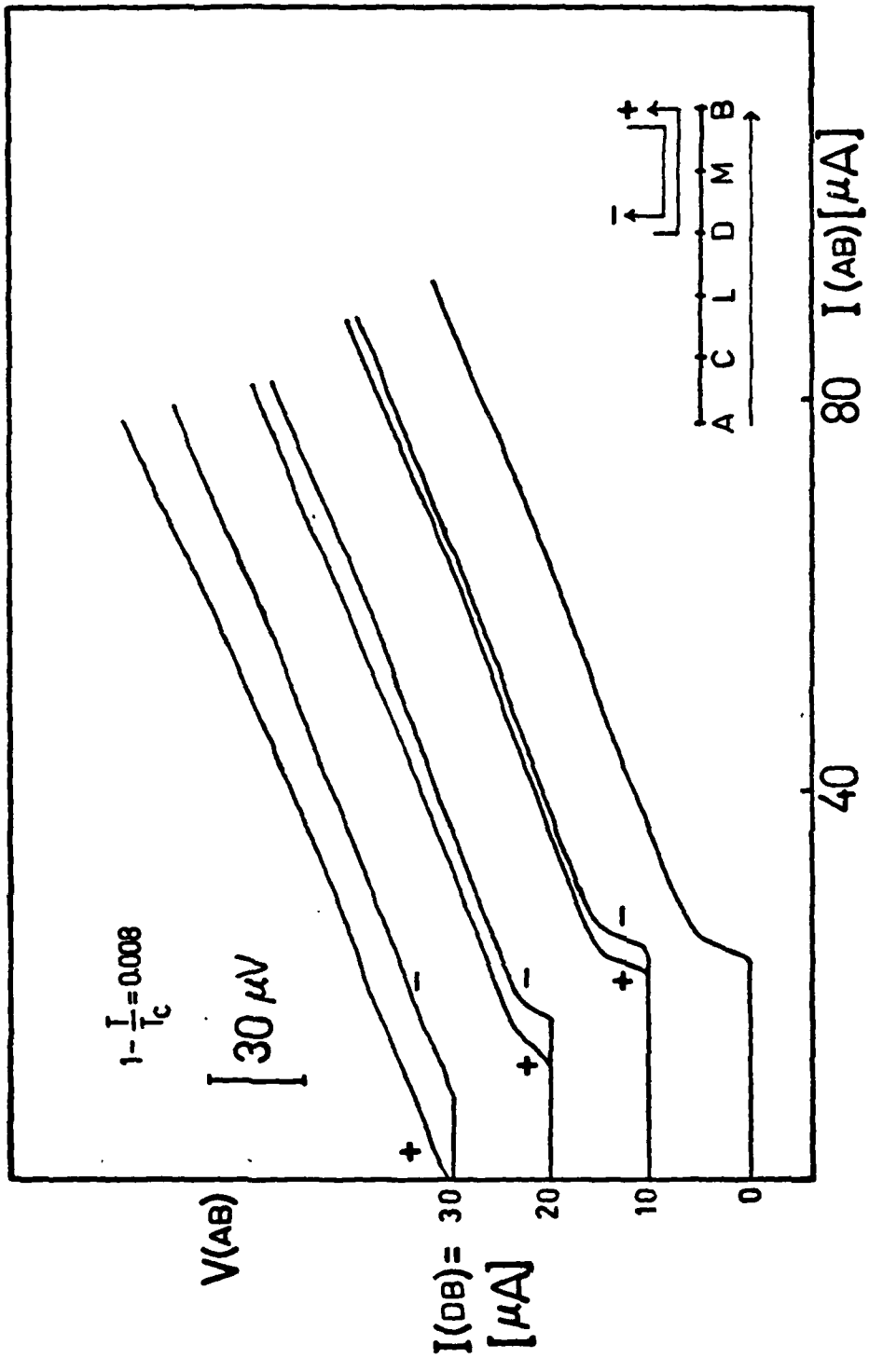

Figure IV.13.Set of I-V curves taken in sample TN-1 for different fixed values of the current injected through D.

quasiparticle current generated in one PSC has on the appearance of other PSCs as discussed in section IV.1.

We measured the change in the critical current of the segment LD when the normal current is injected through D and also when the normal current is injected through M. We extracted the part that depends on the relative direction of the currents, ΔI_c^a. Assuming that the nonequilibrium current decays exponentially between M and D, Λ_{Q^*} is obtained from:

$$\frac{\Delta I_c^a(\text{LD}) \text{ (current injected through M)}}{\Delta I_c^a(\text{LD}) \text{ (current injected through D)}} = \exp(-x_{DM}/\Lambda_{Q^*}) \qquad \text{(IV.9)}$$

We found that $\Lambda_{Q^*}=(3.7\pm 1.2)\mu$m at $1-T/T_c=0.008$ which agrees very well with the value $\Lambda_{Q^*}=(4.3\pm 1.0)\mu$m that we obtained from measurements of the nonequilibrium potential created by a PSC in sample TN-1.

In order to write equation IV.9 we have assumed that the ratio of quasiparticle charge injected to the total injected current is the same for all the junctions. This assumption is valid since this ratio approaches unity at T_c, independent of the resistance of the junction[66].

We have also measured the nonequilibrium potential induced by the injected current. The current is applied between one probe and one end of the microbridge and the voltage measured between each one of the other probes and the other end of the microbridge. We observed the decay of this potential with the distance from the injection site and assuming that this decay is exponential, the magnitude of Λ_{Q^*} is

obtained. Within the limited precision of this measurements, the results in samples TN-1 and TU-1 agree with the values of Λ_{Q^*} obtained from measurements of the nonequilibrium potential in a PSC. These results are:

SAMPLE	$1-T/T_c$	Λ_{Q^*}(from injection exp.)	Λ_{Q^*}(from PSC data)
TN-1	0.0011	$(10 \pm 4)\mu m$	$(7.1 \pm 1.6)\mu m$
TN-1	0.0081	$(5 \pm 2)\mu m$	$(4.3 \pm 1.0)\mu m$
TU-1	0.0071	$(5 \pm 2)\mu m$	$(4.0 \pm 0.7)\mu m$

IV.3.SAMPLES OF TYPE M: EFFECTS OF MICROWAVES ON PHASE-SLIP CENTERS

We measured the I-V curves of microbridges of various lengths (samples of type M) at various temperatures and for different applied microwave power. Our purpose was to study experimentally the effect of the length of the microbridge on the power dependence of the magnitude of the Josephson steps and to compare with the Bessel-function type of dependence for short microbridges.

Josephson steps had been previously observed in long microbridges of tin[3] and niobium[6] and in whiskers of tin[44] and indium[7]. However, no quantitative analysis was made in those previous works. From the theoretical point of view, we are still lacking of a model that predicts the magnitude of the current steps in the I-V curves of superconducting filaments irradiated with microwaves. The main complication has to do with the fact that the oscillations of the supercurrent in a phase-slip center are not restricted to a point, but instead, they propagate as damped waves[10] along the filament.

The expression (II.36), proposed by Tidecks et al.[44], is a simplification of the problem since it only considers the time dependence of the supercurrent. Their model does not explain the appearance of harmonic and subharmonic current steps.

A more realistic model has been worked out by Ivlev and Kopnin[38,39]. In their approximation, discussed in section II.4, the supercurrent is independent of x for $x<x_2(t)$, where $x_2(t)$ oscillates between 0 and $X_{max}\approx\xi\Gamma^{1/2}<<\xi$ and the supercurrent has the form of a saw-tooth function in time. For $(\xi\ell_E)^{1/2}>x>x_2(t)$, the oscillations of

the supercurrent decay with x until they are negligible for $x>(\xi \ell_E)^{1/2}$. Γ is the pair breaking parameter and it is taken to be $\Gamma<<1$ in the Ivlev and Kopnin model, ℓ_E is the penetration length of the electric field.

The magnitude of the m_{th} subharmonic current step is given by equation (II.30) which can be rewritten in the form

$$\frac{\delta I_m}{I_{exc}} = 2 \frac{\sigma_d}{\sigma_n} A_m \propto E_\sim \qquad \text{(IV.10)}$$

where A_m is given by equation (II.31) , σ_n is the normal conductivity of the sample, σ_d is the differential conductivity dI/dV, and $E_\sim$ is the microwave field in the superconductor.

According to equations (IV.10) and (II.36), the magnitude of the Josephson steps increases indefinitely with the microwave power applied. Experimentally, heating effects, not included in those models, reduce the critical current of the microbridge and therefore, reduce the width of the current steps.

In the experiments that I am reporting here, other effects were present that made any quantitative analysis of the power dependence of the size of the current steps very difficult. First of all, the samples of type M exhibit an enhancement of the critical current induced by the microwave radiation. This effect, the Wyatt-Dayem effect[67,68], had been previously observed in both short ($L<\xi(T)$) and long ($L>>\xi(T)$) microbridges.

Figures IV.14 and IV.15 show sets of I-V curves of samples M-29 taken at different powers of the applied microwave radiation. In figure

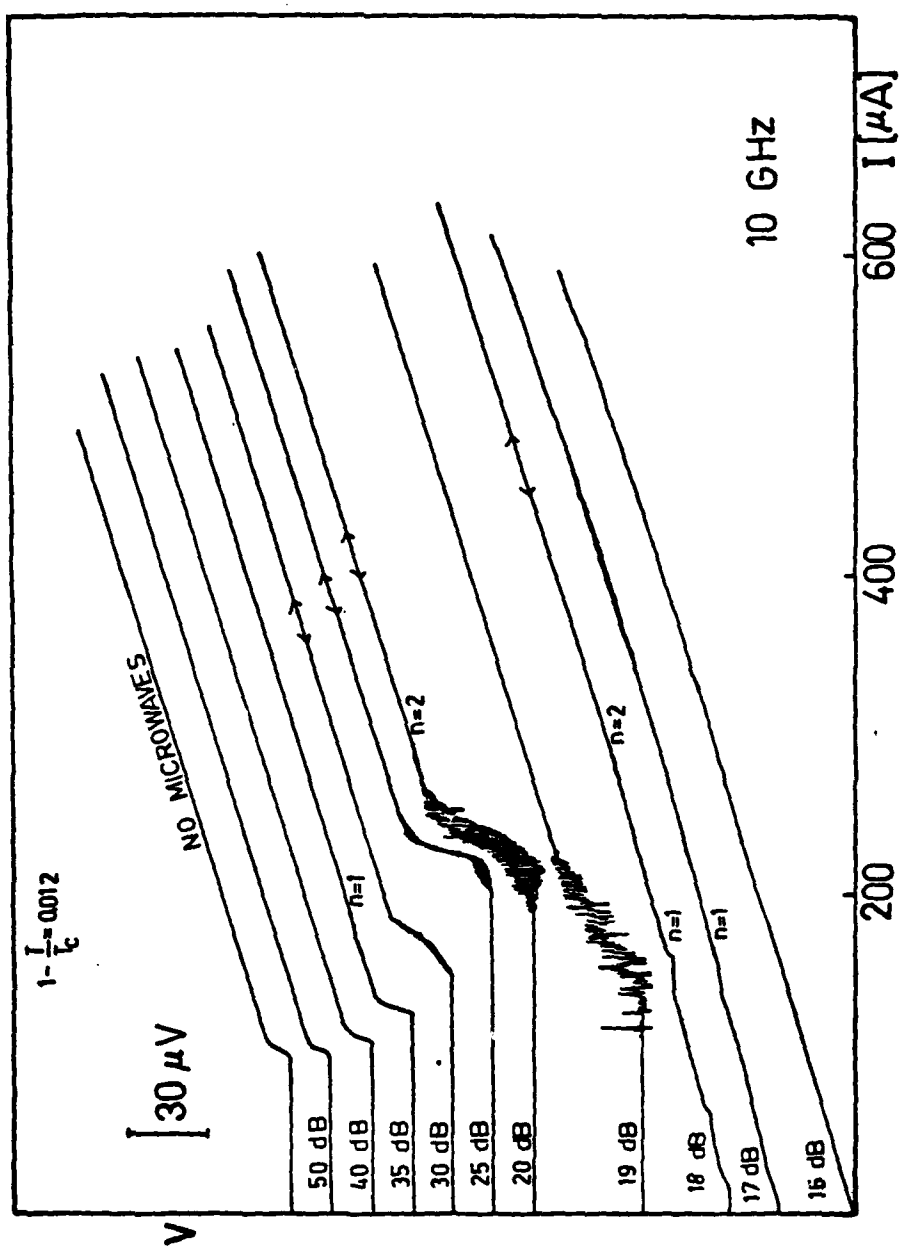

Figure IV.14.I-V curves of sample M-29 at various levels of microwave power. See text for discussion.

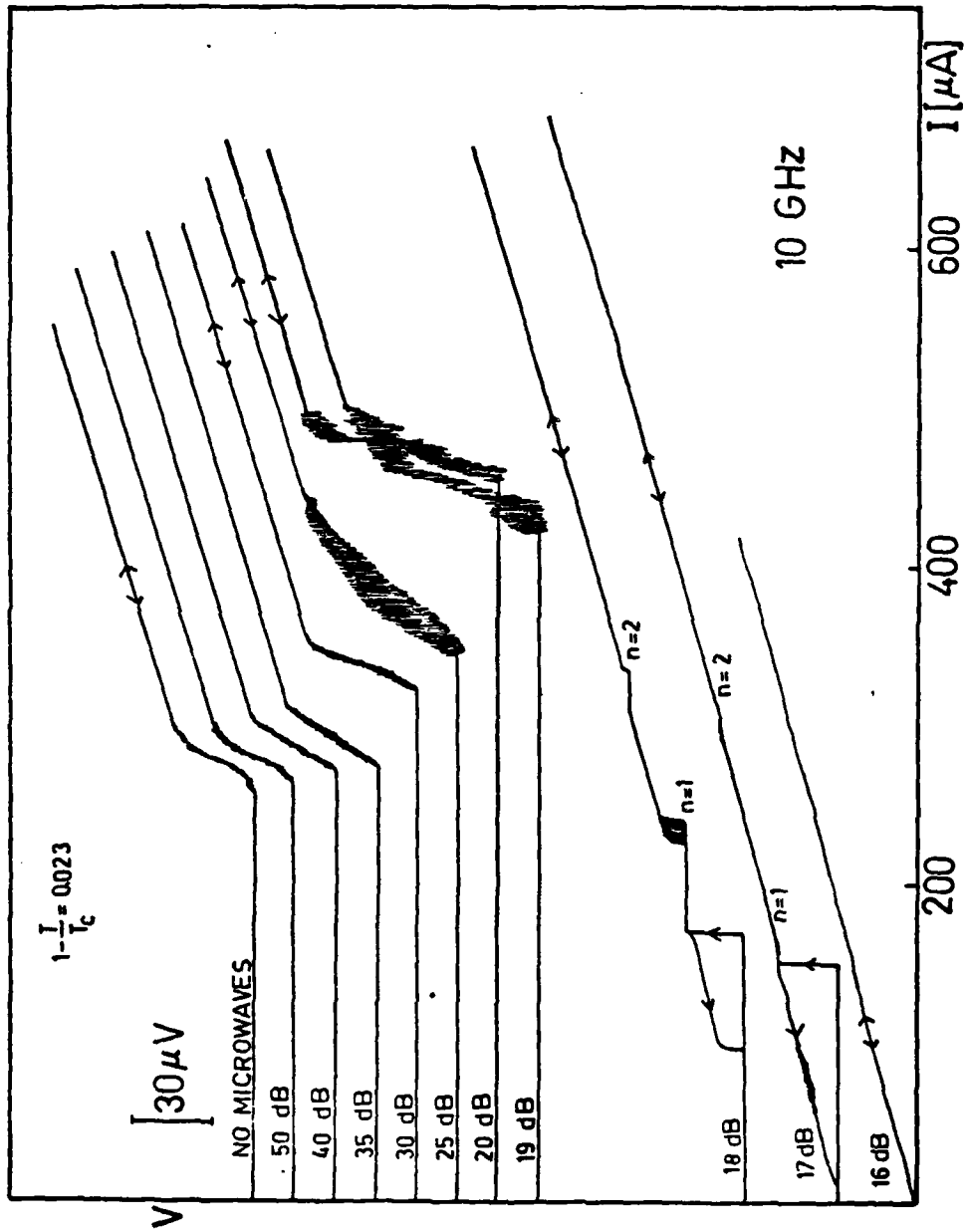

Figure IV.15.I-V curves of sample M-29 at various levels of microwave power. See text for discussion.

IV.14 we can see the first Josephson step (V_1=21μV) at 35dB. As the power is increased, the critical current increases and the voltage jump becomes larger than V_1 and in consequence, the first Josephson step is not seen. Then, as the microwave power is increased even further, the critical current is depressed and the current steps reappear. The noisy onset of the voltage in the I-V curves at 19dB and 20dB can perhaps be explained in terms of the variations of the microwave power coupled to the sample and the combination of two opposite effects: the enhancement of the critical current (Wyatt-Dayem effect) and the depression of the critical current caused by the heat generated by the microwaves. This noisy onset was observed in the narrowest samples where heating effects are more important.In figure IV.15, the first voltage jump is larger than V_1 and the Josephson steps are only seen for levels of power such that the critical current is reduced below its value with no microwaves.

The I-V curves shown in figures IV.14 and IV.15 correspond to a sample with length of the order of Λ_{Q*} and therefore only one PSC can nucleate there. In longer microbridges, where two or more PSCs can coexist, the observation of microwave steps becomes more difficult. On one hand, all the samples exhibit the Wyatt-Dayem effect and on the other, the range of current and voltage between the onset of the first and the second PSCs is usually very small.

We have made long microbridges with a narrow segment in the middle, using the mask to make samples of type T but doing only the tin evaporation. One of those samples in shown in figure III.1(d). In those samples, the I-V curves show a long range of constant differential

resistance after the first voltage jump. We observed very small current steps at V_1 in one of those samples.

Our data are summarized in table III.2 and figure IV.16. In table III.2, the order of the observed Josephson steps are indicated. Figure IV.16 is a plot of the length versus the width of each one of the samples of type M, normalized to the temperature-dependent G-L coherence length of the sample. Each sample is represented by a line instead of a point because the microwave experiments were performed at various temperatures and therefore, at various values of $\xi(T)$. The long microbridges with a narrow segment are marked with horizontal bars.

The thickest lines indicate where the Josephson steps were observed. Unfortunately, we have not been able to identify a systematic explanation for the observability of steps in only a fraction of samples of similar dimensions.

The vertical dashed line indicates the critical width below which vortices cannot exist, according to Likharev[69], and the horizontal dashed line indicates the critical length above which the current-phase relation becomes a multivalued function. According to this classification, the upper left region corresponds to long superconducting filaments, which have been the subject of this thesis.

No conclusion was obtained from the quantitative analysis of the power dependence of the magnitude of the steps in our samples because of the difficulties discussed above.

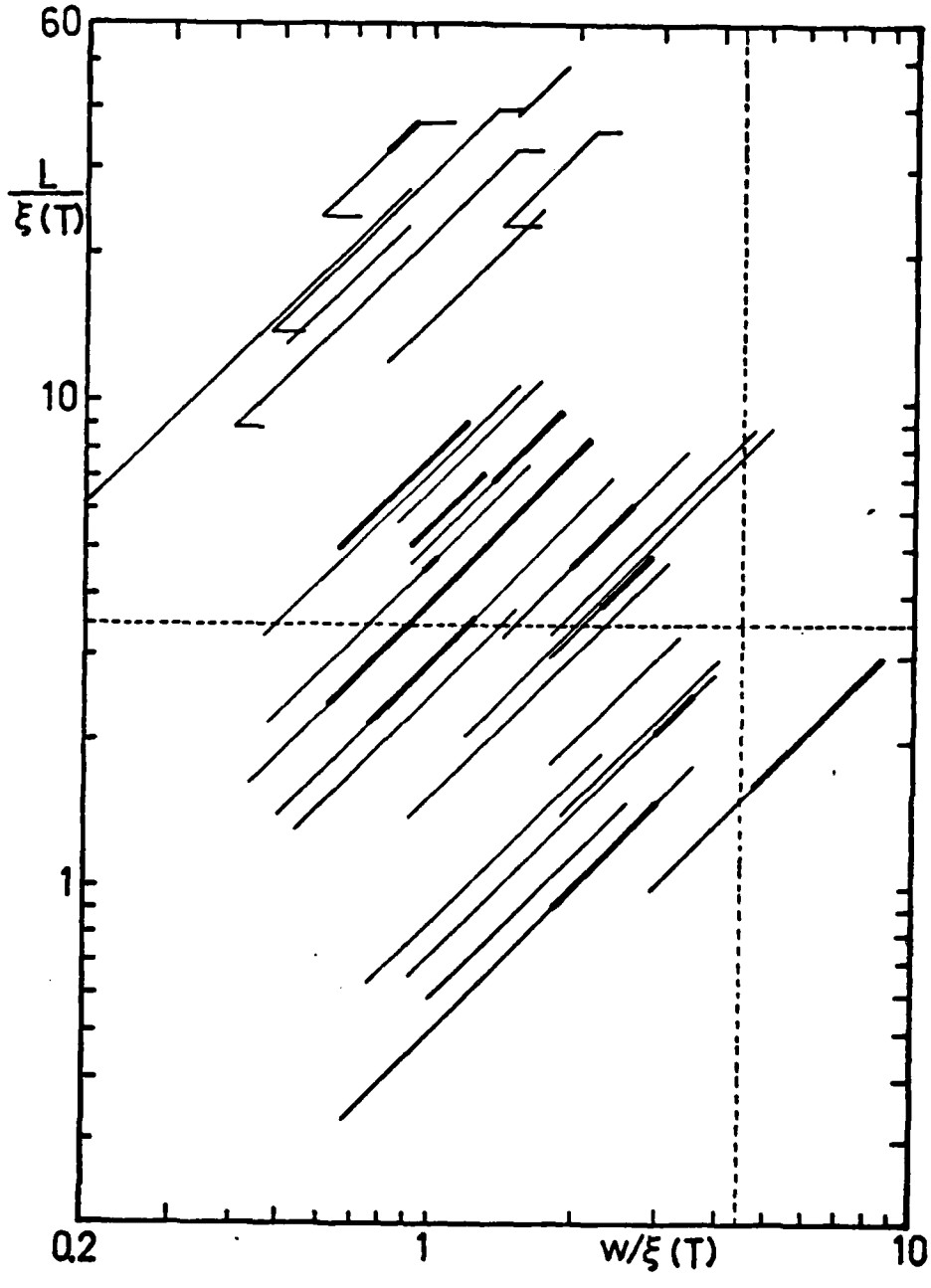

Figure IV.16. Length versus width of samples of type M normalized to their respective temperature-dependent coherence length. The thick black lines indicate where Josephson steps were observed. According to Likharev, the upper left region corresponds to one-dimensional filaments.

CHAPTER V

CONCLUDING SUMMARY

The most important accomplishment during the course of this work has been the experimental determination of the relaxation time of the quasiparticle charge in tin from measurements of the one-dimensional diffusion of a non-equilibrium population of quasiparticles created by a phase-slip center or by a normal current externally injected in a long microbridge.

In one experiment we have observed how the diffusive currents of quasiparticle charge and energy (heat) generated in a phase-slip center (PSC) in a tin microbridge affect the properties of other PSCs in the same microbridge. We have measured the decay with distance between the two PSCs (the source and the detector) of the quasiparticle current, and we have obtained a value for the diffusion length of $\Lambda_{Q^*}=(6\pm1)\mu m$ at $T=0.99T_c$. From the heating effect data we determined that the heat transfer coefficient is $\alpha=(1.5\pm0.2)$watt/Kcm^2 for our tin samples on glass substrate and in direct contact with the liquid He bath.

In another experiment we have measured the quasiparticle potential in tin microbridges with attached normal tunnel junction probes. We have observed the exponential decay of this potential with distance from the center of the PSC, and we have observed the divergence at T_c of the characteristic decay length. We found that $\Lambda_{Q^*}(T)=\Lambda_{Q^*}(0)(1-T/T_c)^{-n}$ with $n\simeq0.25$.

In the samples with attached tunnel junctions, we have also measured the nonequilibrium potential induced by a normal current injected through one of the junctions and we observed the decay of this

potential with the distance from the injection site. The effect of that injected current on the appearance of the first PSC in the microbridge was also measured and the decay with distance between the injection site and the PSC was observed. From those injection experiments we also obtained a value of Λ_{Q^*} which agrees with our previous results on the same samples.

The relaxation time τ_{Q^*} associated with the experimental value of the diffusion length Λ_{Q^*} was obtained from the relation $\tau_{Q^*}=3\Lambda_{Q^*}^2/v_F\ell$. We found that, for all our samples and in all the experiments, $\tau_{Q^*}(T)=(0.7\pm 0.2)\times 10^{-10}\text{sec}(1-T/T_c)^{-1/2}$. This result indicates that the relaxation of the quasiparticle charge is dominated by electron-phonon scattering processes.

The inelastic scattering time τ_E for electrons at the Fermi surface and at T_c was determined from the theoretical relation $\tau_{Q^*}(T)=4k_BT_c\tau_E/\pi\Delta(T)$, which can be written as $\tau_{Q^*}(T)=0.42\tau_E(1-T/T_c)^{-1/2}$. We found that $\tau_E=(1.6\pm 0.4)\times 10^{-10}$sec in tin. This value agrees very well with values found in the literature.

Finally, we fabricated tin microbridges of various lengths, from $L\approx 1\mu m$ to $L\approx 40\mu m$. We measured the I-V curves of those microbridges when irradiated with microwaves, and we observed well-defined Josephson steps in microbridges up to $10\mu m$ long and tiny steps in a sample $36\mu m$ long. These observations prove the oscillatory character of the supercurrent at the core of the PSC. On the other hand, no conclusion was obtained from the quantitative analysis of the power dependence of the magnitude of the steps , because of the presence of other effects

such as the Wyatt-Dayem effect and heating effects. The complications due to these effects also prevented us from being able to predict the observability of Josephson steps based on the measured physical properties of the samples.

In summary, we have performed various types of measurements on phase-slip centers in tin microbridges where we demonstrate the exponential decay of both the quasiparticle current and the nonequilibrium potential and the existence of oscillations of the supercurrent at the Josephson frequency. We have obtained values of the relaxation time τ_{Q^*}, the magnitude and temperature dependence of which agree well with the expected relaxation time of the branch imbalance mode of disequilibrium.

REFERENCES

1. W. W. Webb and R. J. Warburton
"Intrinsic quantum fluctuations in uniform filamentary superconductors", Phys. Rev. Lett. 20, 461 (1968).

2. J. Meyer and G. v. Minnigerode
"Instabilities in the transition curve of current-carrying one-dimensional superconductors", Phys. Lett. 38A, 529 (1972).

3. W. J. Skocpol, M. R. Beasley and M. Tinkham
"Phase-slip centers and nonequilibrium processes in superconducting tin microbridges", J. Low Temp. Phys. 16, 145 (1974).

4. T. M. Klapwijk and J. E. Mooij
"Phase-slip centers in superconducting aluminum", Phys. Lett. 57A, 97 (1976).

5. D. W. Jillie
Ph.D. Thesis, State University of New York, Stony Brook (1976).

6. R. B. Laibowitz, A. N. Broers, J. T. C. Yeh and J. M. Viggiano
"Josephson effect in Nb nanobridges", Appl. Phys. Lett. 35, 891 (1979).

7. R. Tidecks and G. Slama
"Breakdown of superconductivity in current-carrying indium whiskers", Z. Physik B37, 103 (1980).

8. J. M. Aponte and M. Tinkham
"Spatial decay of the quasiparticle current in phase-slip centers", J. Low Temp. Phys. 51, 189 (1983).

9. D. W. Jillie, J. E. Lukens and Y. H. Kao
"Observation of interactions between two superconducting phase-slip centers", Phys. Rev. Lett. 38, 915 (1977).

10. A. M. Kadin, L. N. Smith and W. J. Skocpol
"Charge imbalance waves and nonequilibrium dynamics near a superconducting phase-slip center", J. Low Temp. Phys. 38, 497 (1980).

11. G. J. Dolan and L. D. Jackel
"Voltage measurements within the nonequilibrium region near phase-slip centers", Phys. Rev. Lett. 39, 1628 (1977).

12. A. Baratoff
"Matching regions adjacent to the core of a phase-slip center", Physica 109 & 110B, 2058 (1982).

13. M. Tinkham and John Clarke
"Theory of pair-quasiparticle potential difference in nonequilibrium superconductors", Phys. Rev. Lett. 28, 1366 (1972).

14. M. Tinkham
"Tunneling generation, relaxation, and tunneling detection of hole-electron imbalance in superconductors", Phys. Rev. B6, 1747 (1972).

15. Albert Schmid and Gerd Schön
"Linearized kinetic equations and relaxation processes of superconductors near T_c", J. Low Temp. Phys. 20, 207 (1975).

16. J. S. Langer and Vinay Ambegaokar
"Intrinsic resistive transition in narrow superconducting channels", Phys. Rev. 164, 498 (1967).

17. W. A. Little
"Decay of persistent currents in small superconductors". Phys. Rev. 156, 396 (1967).

18. D. E. McCumber and B. I. Halperin
"Time scale of intrinsic resistive fluctuations in thin superconducting wires", Phys. Rev. B1, 1054 (1970).

19. H. J. Fink
"Current transitions of superconducting whiskers", Phys. Lett. 42A, 465 (1973).

20. H. J. Fink
"A new superconducting state", Phys. Stat. Sol .(b) 60, 843 (1973).

21. H. A. Notarys and J. E. Mercereau
"Dynamics of small superconductors", Physica 55, 424 (1971).

22. A. Baratoff
"Self-consistent nonequilibrium description of phase-slip states in superconducting filaments", Phys. Rev. Lett. 48, 434 (1982).

23. V. P. Galaiko
"Critical currents for resistive states in superconducting channels", Sov. Phys. JETP 39, 181 (1974).

24. V. P. Galaiko
"Microscopic theory of resistive current states in superconducting channels", Sov. Phys. JETP 41, 108 (1975).

25. V. P. Galaiko
"Features of the volt-ampere characteristics and oscillations of the electric potential in superconducting channels", Sov. Phys. JETP 44, 141 (1976).

26. V. P. Galaiko
"Kinetic equations for relaxation processes in superconductors", Sov. Phys. JETP 34,203 (1972).

27. L. Kramer and A. Baratoff
"Lossless and dissipative current-carrying states in quasi-one-dimensional superconductors", Phys. Rev. Lett. 38, 518 (1977).

28. L. Kramer and R. J. Watts-Tobin
"Theory of dissipative current-carrying states in superconducting filaments", Phys. Rev. Lett. 40, 1041 (1978).

29. R. J. Watts-Tobin, Y. Krahenbuhl and L. Kramer
"Nonequilibrium theory of dirty, current-carrying superconductors: phase-slip oscillators in narrow filaments near T_c",
J. Low Temp. Phys. 42, 459 (1981).

30. M. Octavio and W. J. Skocpol
"Charge imbalance waves and time-dependent Ginzburg-Landau theory", Physica 107B, 173 (1981).

31. I. O. Kulik
"Frequency dependence of the penetration depth of an electric field in a superconductor", Sov. J. Low Temp. Phys. 5, 656 (1979).

32. I. O. Kulik, A. N. Omel'yanchuk and V. A. Khlus
"Phase-slip dynamics and excess current in long superconducting bridges", Sov. J. Low Temp. Phys. 6, 480 (1980).

33. I. O. Kulik
"Resistive phase-slip states in superconducting channels", Solid State Comm. 35, 383 (1980).

34. M. Tinkham
"The interaction of phase-slip centers in superconducting filaments", J. Low Temp. Phys. 35, 147 (1979).

35. B. I. Ivlev and N. B. Kopnin
"Resistive state of superconductors", JETP Lett. 28, 592 (1978).

36. B. I. Ivlev, N. B. Kopnin and L. A. Maslova
"Resistive state of superconductors", Sov. Phys. Solid State 22, 149 (1980).

37. B. I. Ivlev, N. B. Kopnin and L. A. Maslova
"Dynamics of the resistive state of a superconductor", Sov. Phys. JETP 51, 986 (1980).

38. B. I. Ivlev and N. B. Kopnin
"The structure of phase-slip centers and the resistive state of narrow superconducting channels", J. Low Temp. Phys. 44, 453 (1981).

39. B. I. Ivlev and N. B. Kopnin
"The a.c. Josephson effect in a resistive state of narrow superconducting channels", Solid State Comm. 41, 107 (1982).

40. A. M. Kadin, W. J. Skocpol and M. Tinkham
"Magnetic field dependence of relaxation times in nonequilibrium superconductors", J. Low Temp. Phys. 33, 481 (1978).

41. W. J. Skocpol and L. D. Jackel
"Internal structure of phase-slip centers in superconducting microstrips", Physica 108B, 1021 (1981).

42. M. Stuivinga, J. E. Mooij and T. M. Klapwijk
"Non-equilibrium potential of phase-slip centers in superconducting Al strips", Physica 108B, 1023 (1981).

43. M. Stuivinga, J. E. Mooij and T. M. Klapwijk
"Current-induced relaxation of charge imbalance in superconducting phase-slip centers", J. Low Temp. Phys. 46, 555 (1982).

44. R. Tidecks and G. von Minnigerode
"The influence of high-frequency radiation on the V-I characteristic of superconducting tin whiskers", Phys. Stat. Sol. (a) 52, 421 (1979).

45. A. M. Kadin, C. Varmazis and J. E. Lukens
"Evidence for charge imbalance waves in phase-slip centers", Physica 107B, 159 (1981).

46. P. E. Lindelof, J. Bindslev Hansen, J. Mygind, N. F. Pedersen and O. H. Sorensen.
"Coherent Josephson radiation from an array of two Dayem bridges", Phys. Lett. 60A, 451 (1977).

47. P. E. Lindelof and J. Bindslev Hansen
"Coherent behavior of two Dayem bridges", J. Low Temp. Phys. 29, 369 (1977).

48. D. W. Jillie, J. E. Lukens and Y. H. Kao
"Voltage locking in two coupled microbridge Josephson junctions", IEEE. Trans. Mag. MAG-13, 578 (1977).

49. D. W. Jillie, M. A. H. Nerenberg and James A. Blackburn
"Voltage locking and other interactions in coupled superconducting weak links. II.Experiment", Phys. Rev B21, 125 (1980).

50. J. D. Meyer and R. Tidecks
"Mutual influence of voltage steps in the I-V characteristics of current-carrying superconducting tin whiskers", Solid State Comm. 24, 643 (1977).

51. L. N. Dunkleberger
"Stencil technique for the preparation of thin-film Josephson devices", J. Vac. Sci. Technol. 15, 88 (1978).

52. G. J. Dolan
"Offset mask for lift-off photoprocessing", Appl. Phys. Lett. 31, 337 (1977).

53. W. C. Danchi
Private communication.

54. D. J. Frank
Ph.D. Thesis, Harvard University (1982). Technical Report No 20, Division of Applied Sciences. Harvard University (1983).

55. W. J. Skocpol
Ph.D. Thesis, Harvard University (1974). Technical Report No 8, Division of Engineering and Applied Physics, Harvard University (1974).

56. M. Octavio
Ph.D. Thesis, Harvard University (1977). Technical Report No 13, Division of Applied Sciences, Harvard University (1978).

57. M. Hatzakis, B. J. Canavello and J. M. Shaw
"Single-step optical lift-off process", IBM J. Res. Develop. 24, 452 (1980).

58. Robert C. Weast, ed.
CRC Handbook of Chemistry and Physics, 60th ed. (CRC Press, 1981) p. E.85.

59. R. G. Chambers
"The anomalous skin effect". Proc. R. Soc A215, 481 (1952).

60. J. P. Burger, G. Deutscher, E. Guyon and A. Martinet
"Behavior of the first- and second-kind superconducting films near their critical fields". Phys. Rev. 137, A853 (1965).

61. Jens Feder and David S. McLachlan
"Superheating and supercooling in single spheres of tin, indium and gold-plated indium", Phys. Rev. 177, 763 (1969).

62. M. Tinkham
"Introduction to Superconductivity". Chapter 4.
McGraw-Hill, 1975.

63. John Clarke and James L. Paterson
"Measurements of the relaxation of quasiparticle branch imbalance in superconductors", J. Low Temp. Phys. 15, 491 (1974).

64. W. J. Skocpol, M. R. Beasley and M. Tinkham
"Self-heating hotspots in superconducting thin-film microbridges",
J. Appl. Phys. 45, 4054 (1974).

65. M. Tinkham
"Introduction to Superconductivity". Chapter 2.
McGraw-Hill, 1975.

66. G. E. Blonder, M. Tinkham and T. M. Klapwijk
"Transition from metallic to tunneling regimes in superconducting microconstrictions: excess current, charge imbalance, and supercurrent conversion", Phys. Rev. B25, 4515 (1982).

67. A. F. G. Wyatt, V. M. Dimitrev, W. S. Moore and F. W. Sheard
"Microwave-enhanced critical supercurrents in constricted tin films",
Phys. Rev. Lett. 16, 1166 (1966).

68. A. H. Dayem and J. J. Wiegand
"Behavior of thin-film superconducting bridges in a microwave field",
Phys. Rev. 155, 419 (1967).

69. K. K. Likharev
"Superconducting weak links", Rev. Mod. Phys. 51, 101 (1979).

ACKNOWLEDGMENTS

I would like to express my gratitude to all those who are or have been members of the Superconductivity Group at Harvard during the last five years.

I would like to thank my advisor, Professor Michael Tinkham for guidance provided throughout the course of this work and Professor William Skocpol for getting me started on the fabrication and measurements of superconducting microbridges.

I am very grateful to my classmates David Abraham and William Danchi. Dave helped me a great deal during my adaptation to the American way of life and more recently, he has shown me how to use the computer as an editing machine to type this thesis. From Bill, I learned almost everything I know about photolithography.

I would like to thank Alice White for sharing her laboratory tools with me and for producing the computer tape necessary to have our first set of masks made and Carmen Losanno of Advance Reproductions Corporation for making the masks at a reasonable price.

I am indebted to Marco Iansiti for solving numerically the diffusion equation for the geometry of samples of type S, making it possible to determine the diffusion length of the quasiparticle charge from our experimental results on interacting phase-slip centers. I also would like to thank our machinist, Louis DeFeo for constructing with outstanding precision essential parts of the laboratory equipment.

Finally, I must acknowledge Drs. Roberto Callarotti and Miguel Octavio for encouraging me to pursue postgraduate studies toward my Ph.D. degree.

My studies were financially supported by a fellowship from CONICIT (Venezuela's National Council for Scientific and Technological Research). This research was partially supported by the National Science Foundation, the Joint Services Electronics Program and the Office of Naval Research.

JASP REPORTS DISTRIBUTION LIST

(UNCLASSIFIED)

DEPARTMENT OF DEFENSE

Director
National Security Agency
ATTN: Dr. Y. J. Rhodes, R-5
Fort George G. Meade, MD 20755

Defense Documentation Center (12 copies)
ATTN: DDC-DDA
Cameron Station
Alexandria, VA 22314

Dr. George Gamota
Assistant for Research
Deputy Under Secretary of Defense for Research
and Engineering (Research & Advanced Technology)
Room 3D1067, The Pentagon
Washington, DC 20301

Defense Advanced Research Projects Agency
ATTN: (Dr. R. Reynolds)
1400 Wilson Boulevard
Arlington, VA 22209

DEPARTMENT OF THE ARMY

Commander
US Army Armament R&D Command
ATTN: DRDAR-RD
Dover, NJ 07801

Commander
US Army Ballistics Research Laboratory
ATTN: DRXBR-BAD
Aberdeen Proving Ground
Aberdeen, MD 21005

Commander
US Army Communication Command
ATTN: CC-OPS-PT
Fort Huachuca, AZ 85613

Commander
US Army Materials and Mechanics Research Center
ATTN: Chief, Applied Sciences Division
Watertown, MA 02172

Commander
US Army Material Development
and Readiness Command
ATTN: Technical Library, Rm. 7S 35
5001 Eisenhower Avenue
Alexandria, VA 22333

Commander
US Army Missile R&D Command
ATTN: Chief, Document Section
Redstone Arsenal, AL 35809

Commander
US Army Satellite Communications Agency
Fort Monmouth, NJ 07703

Commander
US Army Atmospheric Sciences Laboratory
ATTN: DELAS-SM-A (Tech Writing Sec.)
White Sands Missile Range, NM 88002

Commander
US Army Communications R&D Command
ATTN: DRDCO-COM-D-4 (Mr. John Walker)
Fort Monmouth, NJ 07703

Director
TRI-TAC
ATTN: TT-AD (Mrs. Zeiller)
Fort Monmouth, NJ 07703

Commander
US Army Electronics R&D Command
Night Vision & Electro-Optics Labs
ATTN: DELSV (Dr. Rudolf G. Buser)
Fort Monmouth, NJ 07703

Director
US Army Electronics R&D Command
ATTN: DELSD-D (Electronic Warfare Laboratory)
White Sands Missile Range, NM 88002

Executive Secretary, TCC/JSEP
US Army Research Office
P. O. Box 12211
Research Triangle Park, NC 27709

Commander
Harry Diamond Laboratories
ATTN: Mr. John E. Rosenberg
2800 Powder Mill Road
Adelphi, MD 20783

BCSA (DAMA-ARE-A)
Washington, DC 20310

Director
US Army Electronics Technology & Devices Lab
ATTN: DELET-E (Dr. Jack A. Kohn)
Fort Monmouth, NJ 07703

Director
US Army Electronics Technology & Devices Lab
ATTN: DELET-ER (Dr. S. Kronenberg)
Fort Monmouth, NJ 07703

Director
US Army Electronics R&D Command
Night Vision & Electro-Optics Labs
ATTN: Dr. Yay Balcerak
Fort Belvoir, VA 22060

Commander
US Army Research Office
ATTN: DRXRO-MS (Dr. Paul Boggs)
P. O. Box 12211
Research Triangle Park, NC 27709

Commander
US Army Missile R&D Command
Research Directorate
ATTN: DRSMI-YRD (Dr. Charles Bowden)
Redstone Arsenal, AL 35809

Commander
US Army Missile R&D Command
Advanced Sensors Directorate
ATTN: DRSMI-YRS (Dr. Don Verlage)
Redstone Arsenal, AL 35809

Director
US Army Electronics R&D Command
Night Vision & Electro-Optics Labs
ATTN: Dr. John Rhena
Fort Belvoir, VA 22060

Director
US Army Electronics R&D Command
Night Vision & Electro-Optics Labs
ATTN: Dr. William Daly
Fort Belvoir, VA 22060

Commander
US Army Missile R&D Command
Physical Sciences Directorate
ATTN: DRSMI-YRD (Dr. Michael D. Pahuy)
Redstone Arsenal, AL 35809

Commander
US Army Missile R&D Command
Physical Sciences Directorate
ATTN: DRSMI-YRD (Dr. William L. Gamble)
Redstone Arsenal, AL 35809

Commander
White Sands Missile Range
ATTN: SLCMS-SE-OS (Dr. Al L. Gilbert)
White Sands Missile Range, NM 88002

Commander
US Army Communications R&D Command
ATTN: DRDCO-TCS-SP (Dr. David Hardin)
Fort Monmouth, NJ 07703

Director
US Army Communications R&D Command
ATTN: DRDCO-COM-RF (Mr. P. A. Kolinyi)
Fort Monmouth, NJ 07703

Commander
US Army Communications R&D Command
ATTN: DRDCO-TCS-BW, (Dr. E. Lieblein)
Fort Monmouth, NJ 07703

Director
US Army Electronics Technology and Devices Lab
ATTN: DELET-M (Mr. V. Rajkovich)
Fort Monmouth, NJ 07703

Commander
US Army Electronics R&D Command
ATTN: DRDEL-CT (Dr. W. S. McAfee)
2800 Powder Mill Road
Adelphi, MD 20783

Director
US Army Electronics R&D Command
Night Vision and Electro-Optics Labs
ATTN: DELSV
Fort Belvoir, VA 22060

Senior standardization Representative
US Army Standardization Group, Canada
National Defense Headquarters
Ottawa, Ontario, Canada K1A 0K2

Commander
US Army Communications R&D Command
ATTN: DRDCO-COM-RM-4 (Dr. Felix Schwering)
Fort Monmouth, NJ 07703

Director
US Army Electronics R&D Command
Night Vision & Electro-Optics Labs
ATTN: Dr. Randy Longshore
Fort Belvoir, VA 22060

Director
US Army Electronics Technology and Devices Lab
ATTN: DELET-I (Dr. E. K. Reininger)
Fort Monmouth, NJ 07703

Commander
US Army Research Office
ATTN: DRXRO-EL (Dr. James Mink)
P. O. Box 12211
Research Triangle Park, NC 27709

Commander
Harry Diamond Laboratories
ATTN: DELHD-R (Mr. H. Sommer)
2800 Powder Mill Road
Adelphi, MD 20783

Director
US Army Electronics R&D Command
Night Vision & Electro-Optics Labs
ATTN: DELNV-EO (Dr. John Pollard)
Fort Belvoir, VA 22060

Commander
US Army Research Office
ATTN: DRXRO-EL (Dr. William A. Sander)
P. O. Box 12211
Research Triangle Park, NC 27709

Director
Division of Neuropsychiatry
Walter Reed Army Institute of Research
Washington, DC 20012

Commander
USA ARRADCOM
ATTN: DRDAR-SCF-CC (Dr. H. Coleman)
Dover, NJ 07801

Director
US Army Signals Warfare Lab
ATTN: DELSW-OE
Vint Hill Farms Station
Warrenton, VA 22186

Director
U.S. Army Electronics Technology and Devices Lab
ATTN: DELET-ED (Dr. E. H. Poindexter)
Fort Monmouth, NJ 07703

Director
US Army Electronics Technology & Devices Lab
ATTN: DELET-EP (Dr. F. Rothwarf)
Fort Monmouth, NJ 07703

U.S. Army Research Office (3 copies)
ATTN: Library
P. O. Box 12211
Research Triangle Park, NC 27709

Commander
U.S. Army Communications R&D Command
ATTN: DRDCO-COM-RM (Dr. I. Kullback)
Fort Monmouth, NJ 07703

Dr. Sidney Bobo
RCA GSD Engineering
Cherry Hill, NJ 08358

DEPARTMENT OF THE AIR FORCE

Mr. Robert Barrett
RADC/ES
Hanscom AFB, MA 01731

Dr. Carl E. Baum
AFWL (ELT)
Kirtland AFB, NM 87117

Dr. E. Champagne
AFAL/DH
Wright-Patterson AFB, OH 45433

Dr. R. P. Dolan
RADC/EEE
Hanscom AFB, MA 01731

Mr. W. Edwards
AFAL/DH
Wright-Patterson AFB, OH 45433

Professor R. E. Fontana
Head Dept. of Electrical Eng.
AFIT/ENG
Wright-Patterson AFB, OH 45433

Dr. Alan Garscadden
AFAPL/POD
Wright-Patterson AFB, OH 45433

USAF European Office of Aerospace Research & Development
ATTN: Captain A. E. Hendrickson
Box 14, FPO, New York 09510

Mr. Murray Kesselman (ISCB)
Rome Air Development Center
Griffiss AFB, NY 13441

COL R. V. Gnehm
Air Force Member, TCC
Air Force Office of Scientific Research
(AFSC) AFOSR/NP
Bolling Air Force Base, DC 20332

Chief, Electronic Research Branch
AFAL/EEL
Wright-Patterson AFB, OH 45433

Dr. Edward Altshuler
RADC/EEP
Hanscom AFB, MA 01731

Mr. John Mott-Smith (RADC)
HQ ESD (AFSC), Stop 30
Hanscom AFB, MA 01731

Dr. Richard Picard
RADC/EEPA
Hanscom AFB, MA 01731

Dr. J. Ryles
Chief Scientist
AFAL/CA
Wright-Patterson AFB, OH 45433

Dr. Allen Schell
RADC/ES
Hanscom AFB, MA 01731

[illegible] Weapons Laboratory
Kirtland Air Force Base, NM 87117

Rome Air Development Center
Griffiss AFB, NY 13441

Dr. Howard Schlossberg
Air Force Office of Scientific Research
AFSC: AFOSR/NP
Bolling Air Force Base, DC 20332

LTC J. McKenney
Air Force Office of Scientific Research
(AFSC) AFOSR/NM
Bolling Air Force Base, DC 20332

Major Clarence Gardner
Air Force Office of Scientific Research
AFSC: AFOSR/NE
Bolling Air Force Base, DC 20332

DEPARTMENT OF THE NAVY

Office of Naval Research
800 North Quincy Street
Arlington, VA 22217
Attn: Codes 230/231
427
432

Commanding Officer
Naval Research Laboratory
Washington, DC 20375
ATTN: Codes 1405 - Dr. S. Teitler
2627 - Mrs. D. Folen
5200 - A. Brodzinsky
5210 - J. E. Davey
5270 - B. D. McCombe
7500 - J. E. Shore
7550 - J. P. Davis
5510 - W. L. Faust
8005 - J. D. Brown

Director
Office of Naval Research Branch Office
666 Summer Street
Boston, MA 02210

Director
Office of Naval Research
New York Area Office
715 Broadway, 5th Floor
New York, NY 10003

Director
Office of Naval Research Branch Office
536 South Clark Street
Chicago, IL 60605

Director
Office of Naval Research Branch Office
1030 East Green Street
Pasadena, CA 91106

Naval Surface Weapons Center
ATTN: Technical Library
Code DX-21
Dahlgren, VA 22448

Dr. J. H. Mills, Jr.
Naval Surface Weapons Center
Code DF
Dahlgren, VA 22448

Naval Air Development Center
Warminster, PA 18974
ATTN: Codes 301 G. Eck
Technical Library

Dr. Gernot M. R. Winkler
Director, Time Service
U. S. Naval Observatory
Mass. Avenue at 34th Street, NW
Washington, DC 20390

G. Gould
Technical Director
Naval Coastal Systems Center
Panama City, FL 32407

Technical Director
Naval Underwater Systems Center
New London, CT 06320

Naval Research Laboratory
Underwater Sound Reference Detachment
Technical Library
P. O. Box 8337
Orlando, FL 32856

Naval Ocean Systems Center
San Diego, CA 92152
ATTN: Codes 015 - F. C. Fletcher
9102 - W. J. Dejka
932 - H. R. Wieder
512 - J. H. Richter

Naval Weapons Center
China Lake, CA 93555
ATTN: Codes 601 - F.C. Essig
5515 - M. H. Ritchie

Donald E. Kirk
Professor & Chairman, Electronic Engineering
Sp-304
Naval Postgraduate School
Monterey, CA 93940

Mr. J. C. French
National Bureau of Standards
Electronics Technology Division
Washington, DC 20234

Harris P. Stone
Office of Research, Development, Test & Evaluation
NOP-987
The Pentagon, Room 5D760
Washington, DC 20350

Dr. A. L. Slafkosky
Code RD-1
Headquarters, U.S. Marine Corps
Washington, DC 20380

Dr. R. J. Mueller
Naval Air Systems Command
AIR-310
Washington, DC 20361

Mr. Wayne D. Peterson
Naval Electronics Systems Command
Code 038
NC 01
2511 Jefferson Davis Hwy
Arlington, VA 20360

Naval Sea Systems Command
NC 03
2531 Jefferson Davis Hwy
Washington, DC 20362
ATTN Code 03C - J. H. Huth

David Taylor Naval Ship Research & Development Center
Bethesda, MD 20084
ATTN: Code 522.1 - Technical Library
Code 18 - G. H. Gleissner

Naval Surface Weapons Center
White Oak
Silver Spring, MD 20910
ATTN: Codes WR-00-Technical Library
R-65-S. S. Aligaier

Dr. Edward C. Why
Code 1012
Naval Underwater Systems Center
New London Laboratory
New London, CT 06320

Dr. Martin Rendelberg
Code 36
Naval Underwater Systems Center
New London Laboratory
New London, CT 06320

Dr. D. J. Sousa
Code 34
Naval Underwater Systems Center
New London Laboratory
New London, CT 06320

OTHER GOVERNMENT AGENCIES

Dr. Herbert S. Bennett
Director
Division of Materials Research
National Science Foundation
1800 G Street
Washington, DC 20550

Dr. Jay Harris
Program Director
Devices and Waves Program
National Science Foundation
1800 G Street
Washington, DC 20550

Los Alamos Scientific Laboratory
ATTN Near Library
P. O. Box 1663
Los Alamos, NM 87545

Dr. Dean Mitchell
Program Director, Solid-State Physics
Division of Materials Research
National Science Foundation
1800 G Street
Washington, DC 20550

M. Lane Thornton
Deputy Director Institute for
Computer Sciences & Technology
National Bureau of Standards
Washington, DC 20234

Head, Electrical Sciences & Analysis Section
National Science Foundation
1800 G Street, NW
Washington, DC 20550

Deputy Director for Research
Research and Technology Division
Office of Aeronautics and Space Tech.
NASA
Washington, DC 20546

Judson C. French, Director
Center for Electronics and Electrical Engineering
A361 Technology Bldg.
National Bureau of Standards
Washington, DC 20234

Dr. Ben Rubin
Chief, Sensing & Detection
Electronics Division, Code RE
NASA HQ
600 Independence Avenue, SW
Washington, DC 20546

Mr. Herbert Ernst
Manager, Data Management Program, Code RRI-5
NASA HQ
600 Independence Avenue, SW
Washington, DC 20546

Mr. John Rea
Assistant Chief, Information Processing Division
Code 560
Goddard Space Flight Center
Greenbelt, MD 20771

Mr. Charles Hudson
Aerospace Technologist
Langley Research Center
Hampton, VA 23665

Mr. John Gould
Chief, Design Techniques Branch
George C. Marshall Space Flight Center
Marshall Space Flight Center, AL 35812

NON-GOVERNMENT AGENCIES

Director
Columbia Radiation Laboratory
Columbia University
538 West 120th Street
New York, NY 10027

Director
Coordinated Science Laboratory
University of Illinois
Urbana, IL 61801

Director
Division of Applied Sciences
Harvard University
Pierce Hall
Cambridge, MA 02138

Director
Electronics Research Center
The University of Texas
P. O. Box 7728
Austin, TX 78712

Director
Electronics Research Laboratory
University of California
Berkeley, CA 94720

Director
Electronics Sciences Laboratory
University of Southern California
Los Angeles, CA 90007

Director
Microwave Research Institute
Polytechnic Institute of New York
333 Jay Street
Brooklyn, NY 11201

Director
Research Laboratory of Electronics
Massachusetts Institute of Technology
Cambridge, MA 02139

Director
Stanford Electronics Laboratory
Stanford University
Stanford, CA 94305

Director
Edward L. Ginzton Laboratory
Stanford University
Stanford, CA 94305

Dr. Lester Eastman
School of Electrical Engineering
Cornell University
316 Phillips Hall
Ithaca, NY 14850

Dr. Carlton Walter
Electroscience Laboratory
The Ohio State University
Columbus, OH 43212

Dr. Richard Sparks
Department of Electrical Engineering
Texas Tech University
Lubbock, TX 79409

Dr. Ray Jould
Executive Office for Applied Physics
California Institute of Technology
Pasadena, CA 91125

Director
School of Electrical Engineering
Georgia Institute of Technology
Atlanta, GA 30332

Prof. J. F. Gallup
Department of Electrical Engineering
Texas Tech University
Lubbock, TX 79409

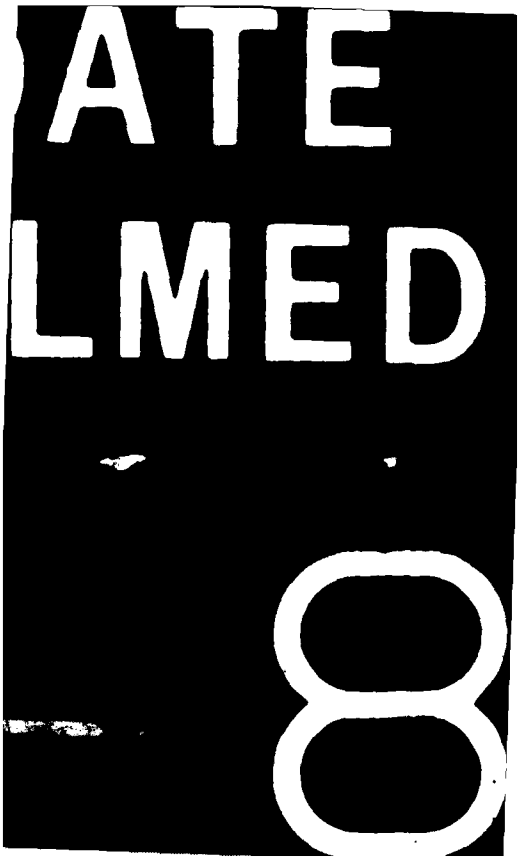
ATE
LMED
8